UNCLASSIFIED

AD NUMBER	
ADB805288	
CLASSIFICATION CHANGES	
TO:	**unclassified**
FROM:	**restricted**
LIMITATION CHANGES	
TO: **Approved for public release; distribution is unlimited.**	
FROM: **Distribution authorized to DoD only; Administrative/Operational Use; JUL 1943. Other requests shall be referred to National Aeronautics and Space Administration, Washington, DC. Pre-dates formal DoD distribution statements. Treat as DoD only.**	
AUTHORITY	
NACA list dtd 28 Sep 1945; NASA TR Server website	

THIS PAGE IS UNCLASSIFIED

CLASSIFICATION CANCELED

RESTRICTED

TECHNICAL NOTES

NATIONAL ADVISORY COMMITTEE FOR AERONAUTICS

No. 906

FOR REFERENCE

NOT TO BE TAKEN FROM THIS ROOM

SOME INVESTIGATIONS OF THE GENERAL INSTABILITY OF STIFFENED METAL CYLINDERS

II - PRELIMINARY TESTS OF WIRE-BRACED SPECIMENS AND THEORETICAL STUDIES

Guggenheim Aeronautical Laboratory
California Institute of Technology

CLASSIFIED DOCUMENT

This document contains classified information affecting the National Defense of the United States within the meaning of the Espionage Act, USC 50:31 and 32. Its transmission or the revelation of its contents in any manner to an unauthorized person is prohibited by law. Information so classified may be imparted only to persons in the military and naval Services of the United States, appropriate civilian officers and employees of the Federal Government who have a legitimate interest therein, and to United States citizens of known loyalty and discretion who of necessity must be informed thereof.

Washington
July 1943

FILE COPY
To be returned to
the files of the Langley
Memorial Aeronautical
Laboratory

NATIONAL ADVISORY COMMITTEE FOR AERONAUTICS

TECHNICAL NOTE NO. 906

SOME INVESTIGATIONS OF THE GENERAL INSTABILITY OF STIFFENED METAL CYLINDERS

II - PRELIMINARY TESTS OF WIRE-BRACED SPECIMENS AND THEORETICAL STUDIES

Guggenheim Aeronautical Laboratory
California Institute of Technology

This is the second of a series of reports covering an investigation of the general instability problem by the California Institute of Technology. The first five reports of this series cover investigations of the general instability problem under the loading conditions of pure bending and were prepared under the sponsorship of the Civil Aeronautics Administration. The succeeding reports of this series cover the work done on other loading conditions under the sponsorship of the National Advisory Committee for Aeronautics.

INTRODUCTION

The first report of this series (reference 1) was primarily concerned with the present state of the theoretical and the experimental knowledge regarding the general instability failure of stiffened metal cylinders. Three important conclusions were arrived at during this study. They were as follows:

(a) That several methods have been advanced by different investigators for the calculation of the critical stresses for such stiffened cylinders

(b) That available experimental data were insufficient to prove the validity or usefulness of any of the proposed methods

(c) That some of the basic problems concerning the failure of thin shells have not been satisfactorily treated theoretically as evidenced by the large discrepancies between the theoretically predicted and the experimentally obtained failing stresses

The recent research, therefore, has been concentrated along two major lines: first, to obtain sufficient experimental data on the failure of stiffened cylinders so that the proposed methods of analysis could be checked; second, to endeavor to develop a more sound theoretical background for the study of the failure of thin shell structures. The body of this report will, therefore, consist of three parts: namely,

(a) Preliminary experimental investigations on the failure of stiffened metal cylinders

(b) Theoretical investigations into the principles underlying the theory of failure of thin shells

(c) Experimental investigations on the compressive failing stress of unstiffened circular cylinders

PRELIMINARY EXPERIMENTAL INVESTIGATIONS ON THE FAILURE OF STIFFENED METAL CYLINDERS

Type of Test

Inasmuch as bending is one of the critical loading conditions for airplane structures, the problem of the failure of stiffened metal cylinders when subjected to a pure bending moment, was attacked first. From observations of the stress and the deflection patterns produced under this simple loading condition, it was hoped a correlation with the simple beam equations could be obtained. Although no airplane structure is subjected to bending moments without a certain amount of attendant direct shear, it was felt that a rather complete study of the pure bending phenomenon would form a desirable background for the more complicated problem of bending plus shear and for the more general combined loading conditions.

In view of the above, all of the tests on stiffened cylinders which have been conducted to date have been made

with pure bending as the only externally applied loading. Stress readings were taken on representative parts of the structure during loading; Huggenberger type extensometers with a magnification factor of approximately 300 being used for this purpose. In addition to the observations of the stress in the structure, the deflection patterns of both frames and longitudinals were taken as a function of the applied moment. From the above observations the stress pattern and the mode of failure were determined for each specimen tested, as well as the maximum bending moment that carried by the specimen.

Testing Equipment

The testing machine used is shown schematically in figure 1 and by photographs in figures 2 and 3. This machine is adapted to the application of bending moments, torsional moments, or any combination of bending and torsion to specimens up to 3 feet in diameter and 20 feet long. It has a capacity of 500,000 inch-pounds in both bending and torsion.

For the present tests it was desired to apply a uniform moment over the entire specimen; so the bending-moment arms of the testing machine were connected by an extra-flexible aircraft cable as shown. A loading screw (fig. 4) and load dynamometer (fig. 5) were placed at one end of the cable. If, at any time, it is desired to find the effect of a bending moment with a linear variation in magnitude over the length of the specimen, the cable will be replaced by a separate loading screw and a dynamometer at the end of each of the bending-moment arms.

The entire machine is supported on ball-bearing joints similar to the one shown in figure 6, these joints also being present at the ends of the loading arms as shown in figure 1. One head of the testing machine is free to move horizontally, thus eliminating the possibility of any direct tensile or compressive forces being applied to the cylinder.

A rod is freely supported at the center of the two ends of the specimen, this rod carrying a device making it possible to obtain the radial and angular position of any point on a cross-sectional plane through the specimen. This device can be shifted lengthwise and thus it is possible to obtain a complete deflection pattern of the

longitudinals and frames at any given applied moment. This deflection-measuring instrument can be seen in several of the attached photographs.

Specimens

In order to eliminate as many variables as possible, the specimens were made up of frames and longitudinals only, without skin covering. The longitudinals and frames used for this first series of tests are shown with their section properties in figure 7. The material used for the longitudinals was 3/8- by 0.028-inch 17S-T dural tubing drawn to the shape shown and the frames were cut from 17S-T dural-sheet stock and rolled to the proper radius. The longitudinals and frames were joined at all intersections by one 4-40 machine screw and nut. The station numbers for frames and longitudinals are shown in figure 8.

The specimens were all 32 inches in diameter and 64 inches long, the length being measured from the edge of the outstanding leg of the end angle. The ends of all longitudinals were rigidly attached to an end angle by means of U-bolts as shown in figures 9 and 10. This angle, which was in the form of a ring with an internal diameter equal to that of the specimen, was then solidly bolted to the face plates of the testing machine.

Inasmuch as there was no sheet covering and only one type of frame and longitudinal was used in this first series of tests, the two important variables remaining were the frame spacing and the longitudinal spacing. Table I shows the variations in these two parameters as related to the assigned specimen numbers.

It was first thought that it might be possible to obtain a true bending failure without the use of any shear bracing in the specimen. Upon testing the first specimen it was found that shear bracing would be necessary in order to prevent a torsional form of failure in which the frames tended to rotate about the top or tension longitudinal. Therefore, a network of steel wire 0.016 inch in diameter was used to provide shear stiffness. A preliminary discussion of the effect that these wires may have is given in appendix B.

Experimental Results

The early part of the program was devoted to accumulating data on this first series of specimens. The results obtained have so far been analyzed only in a preliminary manner in order to study trends which would influence the choice of data desired on succeeding specimens.

Tables I, II, and III give a summary of the experimental failure bending moments obtained on the specimens tested to date. Figures 11 to 34, inclusive, are photographs taken of the specimens which show the method of testing and the failure pattern of the longitudinals and frames. Figures 35 and 36 give, in curve form, the relationship between failure bending moment and the frame and longitudinal spacing, respectively. Figures 37 to 53 inclusive, show a representative group of frame and longitudinal deflection patterns. These deflection patterns were taken at or near to the failure bending moment, primarily so that the deflections would be large enough to give an accurate picture of the failure wave form. In nearly every case the wave pattern at failure was the same as that taken earlier in the loading. Figure 54 indicates the relationship between the maximum radial deflection of the center frame (taken on the compression side) and the applied bending moment.

At the beginning of the test program it was desired to know if the vertical stress distribution in the specimen was linear - that is, if the stress distribution followed the simple beam equation of $\sigma = \frac{My}{I}$. In order to check this factor a large number of extensometers were placed on the longitudinals and stress readings were taken as a function of the bending moment. The results are plotted in figures 55 and 56 for three longitudinals on the compression and for three longitudinals on the tension side, respectively. The stresses calculated from the simple beam equation are indicated and show remarkably good agreement. Near failure it was necessary to correct for the bending moment in the longitudinals due to the fact that they were in the wave form and this was done by taking extensometer readings on both sides of the longitudinal simultaneously. This type of stress study was not made on all specimens but checks were made on representative specimens and the linearity of the vertical stress distribution was found to hold in all cases. In all specimens except

1, 9, 10, and 11, sufficient wire shear bracing was used to prevent any torsional deflection of the center of the specimen. In other words, the lower (compression) longitudinal deflected only in a vertical plane. The specimens noted previously are discussed separately in appendix B.

Check of Experimental Results with Current Theories

The various methods of analysis which were discussed in detail in the first report of this series (reference 1) are, with one exception, all based on the assumption that the effect of the longitudinals and frames on the strength of the specimen is relatively small compared to the effect of the skin. Therefore, when the skin thickness goes to zero, as it does in this first set of specimens, the suggested methods of analysis break down for one reason or another.

The methods of Ryder, Dschou, and Hoff might be used for the analysis of the present specimens. However, the parameters of the present specimens lie completely out of the range of Ryder's curves, and as no method of calculating these curves is given in Ryder's paper, it was impossible to make a check of his method with the experimental results.

A check using Dschou's method of analysis gives theoretically predicted failing moments which are very much too high if the torsional rigidity of the longitudinals is taken into account, and which are much too low if this factor is neglected. For this reason no calculations using this method have been included.

In contrast to the other proposed methods, that of Hoff's deals essentially with a structure similar to that of the tested specimens. For this reason, it might be expected that the failing stresses predicted by Hoff might show some agreement with those obtained experimentally. As can be seen in table II, this is not the case, for Hoff's method gives failing stresses which are much too low when the correct wave pattern of one half-wave is used. A change in the assumed wave pattern to two half-waves raises Hoff's predicted failing stresses, but not sufficiently in most cases to give agreement. It is also interesting to note that the failing stress predicted by Hoff increases slightly as the frame spacing is increased; whereas the experimental data show that a decrease occurs.

Conclusions from Experimental Results

As most of the time in the early part of this program was spent in testing, the experimental results have not as yet been analyzed in any great detail. It can be said, however, that failures of the general instability type have been obtained in this first series of specimens and that the dependence of the failing bending moment on the frame and longitudinal spacing has been obtained. It is expected that a study of the deflection patterns and the variables involved will lead to a method of analysis of this type of structure which will enable a designer to predict the allowable bending moment to a satisfactory degree of accuracy.

An interesting result of this first set of experiments was the discovery that specimens of the type tested do not fail suddenly but tend to approach a maximum allowable bending moment in an asymptotic manner. This is clearly indicated by the curves of bending moment against radial deflection of the frames which are plotted in figure 54. Preliminary investigation seems to indicate that it might be possible to use Southwell's method of predicting the critical instability load of columns on curves of this type and obtain the maximum allowable bending moment on the structure without actually failing the specimen. If this method proves to be applicable, deflections taken on a fuselage structure during proof test could be used to determine the maximum load which could be carried by the structure.

In all present methods of analysis of this problem, it has been assumed that certain stiffness factors of the longitudinals and frames are constant quantities independent of the load. However, observations have shown that if the specimens are loaded by a bending moment and if, for example, an additional radial force is applied to a point on the surface of the structure, then the resistance of the structure to radial deflection is dependent upon the applied bending moment. Preliminary tests indicate that the stiffness of the structure on the compression side may drop to as little as half of its original value as the failing bending moment is approached, and that a definite decrease in value is found even for very small applied moments. This factor may explain some of the discrepancies between Hoff's predicted failing stresses and those obtained experimentally. This phenomenon is being carefully investigated at present, as this factor will certainly be important in the development of a satisfactory theoretical solution to the problem.

THEORETICAL INVESTIGATIONS INTO THE PRINCIPLES UNDERLYING THE FAILURE OF THIN SHELLS

As was pointed out in the first report of this series (reference 1), the classical theory of thin shells as given in Love's "Elasticity," gives a critical buckling stress far above that obtained experimentally. It was also suggested in the first report that this failure of the classical theory accurately to predict buckling stresses might be due to the linearization of the differential equations and that an attempt should be made to generalize the theory so that second-order terms could be taken into account. This has been done for the case of a thin spherical shell under uniform external pressure, and it is hoped that the method used can be extended to the case of the thin cylindrical shell under axial compression.

The necessity for the development of a nonlinear theory of deflection can best be shown by considering a very thin spherical shell as illustrated in figure 57. If the shell is sufficiently thin, the bending stiffness (which is proportional to t^3) can be neglected and, under this assumption, the strain energy of the shell is the same in the deflected position (3) as it was in the undeflected position (1), figure 57. In other words, neglecting the bending energy in the region A-A, the shell will be in equilibrium in the reflected position (3) without the aid of any external pressure applied to the shell surface.

On the other hand, the intermediate positions between (1) and (3) do involve compression of the shell elements and, therefore, the shell can be in equilibrium in these positions only with the aid of an external pressure. Deforming the shell between positions (1) and (2) involves compression of the shell elements and thus a positive external pressure is necessary to maintain equilibrium. When δ is greater than δ_o (between positions (2) and (3)), a negative external pressure is necessary to maintain equilibrium as the compressed elements are trying to force the shell to take up the equilibrium position (3). The pressure-deflection curve (under the assumption of no-bending stiffness) is, therefore, of the form shown in figure 58a.

The effect of the bending stiffness is to increase the positive external pressure necessary to hold the shell

in equilibrium. Thus, for increasing values of the bending stiffness of the shell, the curve in figure 58a will take the form of those shown in figure 58b. Any linear theory which does not take into account the higher-order terms of the deflection will give a linear relationship between the pressure and the deflection. This linear relationship is a good approximation at the initial stage of the deformation; but when the deformation becomes equal to, or greater than, the sheet thickness, erroneous results are obtained.

The investigation of this type of problem has been limited in extent (references 2, 3, and 4) and has never been, to the authors' knowledge, applied to the problem of the buckling of thin shells. The following discussion will, therefore, consider the problem of the buckling of a thin spherical shell under uniform external pressure and will be based on the following simplifying assumptions:

1. The deflection is rotationally symmetric.

2. The deflection of any element of the shell is vertical.

3. The shell is very thin so that t/R is small.

4. The effect of lateral contraction is neglected - that is, Poisson's ratio is assumed equal to zero.

5. The buckling is restricted to a small portion of the shell and the edges of this region are fixed - that is, the deflection of the edges is zero and the slope remains a constant equal to the initial slope.

Figure 59 indicates the element discussed and the parameters involved.

As can be seen from this figure, for a linear element of the section of the shell,

$dr/\cos\alpha$ the original length

$dr/\cos\theta$ the length after deflection

and the strain is, therefore,

$$\epsilon = \frac{\dfrac{dr}{\cos\theta} - \dfrac{dr}{\cos\alpha}}{\dfrac{dr}{\cos\alpha}} = \frac{\cos\alpha}{\cos\theta} - 1$$

Hence, the strain energy due to the extension of the elements of the shell is:

$$\frac{Et}{2}\int_0^a \left(\frac{\cos\alpha}{\cos\theta} - 1\right)^2 2\pi r \frac{dr}{\cos\alpha}$$

$$= \frac{Et}{2}\int_0^\beta \left(\frac{\cos\alpha}{\cos\theta} - 1\right)^2 2\pi R \sin\alpha R\, d\alpha$$

$$= \frac{ER^3}{2}\left(\frac{t}{R}\right) 2\pi \int_0^\beta \left(\frac{\cos\alpha}{\cos\theta} - 1\right)^2 \sin\alpha\, d\alpha \qquad (1)$$

The two curvatures of the shell at the point P before buckling are both equal to $1/R$. After deflection, the curvature in the YZ plane is equal to:

$$\frac{d\theta}{ds} = \frac{d\theta}{d\alpha}\Big/\frac{ds}{d\alpha}$$

But

$$ds = \frac{dr}{\cos\theta} = \frac{R\cos\alpha\, d\alpha}{\cos\theta}$$

Hence,

$$\frac{d\theta}{ds} = \frac{d\theta}{d\alpha}\Big/\frac{R\cos\alpha}{\cos\theta}$$

The change in curvature in the YZ plane is then:

$$\frac{\dfrac{d\theta}{d\alpha}}{\dfrac{R\cos\alpha}{\cos\theta}} - \frac{1}{R} = \frac{1}{R}\left[\frac{\cos\theta}{\cos\alpha}\frac{d\theta}{d\alpha} - 1\right]$$

The change in the second principal curvature can be shown to be:

$$\frac{1}{R}\left[\frac{\sin\theta}{\sin\alpha} - 1\right]$$

The total bending energy is then:

$$\frac{Et^3}{24}\int_0^\beta 2\pi R^2 \sin\alpha\, d\alpha \frac{1}{R^2}\left[\left(\frac{\cos\theta}{\cos\alpha}\frac{d\theta}{d\alpha} - 1\right)^2 + \left(\frac{\sin\theta}{\sin\alpha} - 1\right)^2\right]$$

$$= \frac{ER^3}{2}\left(\frac{t}{R}\right)^3 \frac{2\pi}{12}\int_0^\beta \sin\alpha\left[\left(\frac{\cos\theta}{\cos\alpha}\frac{d\theta}{d\alpha} - 1\right)^2 + \left(\frac{\sin\theta}{\sin\alpha} - 1\right)^2\right] d\alpha \quad (2)$$

The potential energy of the external pressure is equal to the pressure times the volume covered under the shell. Thus, the potential energy is:

$$p\int_0^a 2\pi\, r\, z dr = p\left[2\pi \frac{r^2}{2} z\right]_0^a - p\int_0^a \pi r^2 \frac{dz}{dr} dr$$

$$= p\pi\int_0^\beta R^2 \sin^2\alpha \tan\theta\, R\cos\alpha\, d\alpha$$

$$= pR^3\pi\int_0^\beta \sin^2\alpha \tan\theta \cos\alpha\, d\alpha \quad (3)$$

The total energy W of the system is the sum of the strain energy and the potential energy of the external pressure. Thus, from equations (1), (2), and (3):

$$\frac{W}{R^3\pi} = E\left(\frac{t}{R}\right)\int_0^\beta\left(\frac{\cos\alpha}{\cos\theta} - 1\right)^2 \sin\alpha\, d\alpha + \frac{E\left(\frac{t}{R}\right)^3}{12}\int_0^\beta\left[\left(\frac{\cos\theta}{\cos\alpha}\frac{d\theta}{d\alpha} - 1\right)^2\right.$$

$$\left. + \left(\frac{\sin\theta}{\sin\alpha} - 1\right)^2\right]\sin\alpha\, d\alpha + p\int_0^\beta \sin^2\alpha \cos\alpha \tan\theta\, d\alpha \quad (4)$$

At the equilibrium position, the total energy must be a minimum; therefore, the equation of equilibrium can be obtained by minimizing the expression (4). If the calculus of variations is used, the Euler-Lagrange equation is:

$$2E\left(\frac{t}{R}\right)\left[\frac{\sin\alpha\cos\alpha}{\cos\theta}\tan\theta\left(\frac{\cos\alpha}{\cos\theta}-1\right)\right]+\frac{E\left(\frac{t}{R}\right)^3}{6}\left[\cos\theta\left(\frac{\sin\theta}{\sin\alpha}+\tan^2\alpha\right)\right.$$

$$\left.-\frac{\cos^2\theta}{\cos\alpha}\left(2\tan^2\alpha+1\right)\frac{d\theta}{d\alpha}+\frac{\sin\theta\cos\theta\tan\alpha}{\cos\alpha}\left(\frac{d\theta}{d\alpha}\right)^2-\frac{\cos^2\theta\tan\alpha}{\cos\alpha}\frac{d^2\theta}{d\alpha^2}\right]$$

$$+\sin^2\alpha\cos\alpha\sec^2\theta\,p=0 \qquad (5)$$

with the boundary conditions

$$\begin{aligned}\theta &= 0 \quad \text{at} \quad \alpha = 0\\ \theta &= \beta \quad \text{at} \quad \alpha = \beta\end{aligned} \qquad (5a)$$

Since experiments show that the buckling area extends usually only a few degrees, β is assumed very small. In this case equations (4) and (5) can be simplified to:

$$\frac{W}{R^3\pi}=\frac{E\left(\frac{t}{R}\right)}{4}\int_0^\beta\left(\theta^2-\alpha^2\right)^2\alpha\,d\alpha+\frac{E\left(\frac{t}{R}\right)^3}{12}\int_0^\beta\left[\left(\frac{d\theta}{d\alpha}-1\right)^2\right.$$

$$\left.+\left(\frac{\theta}{\alpha}-1\right)^2\right]\alpha\,d\alpha+p\int_0^\beta\alpha^2\theta\,d\alpha \qquad (6)$$

and

$$\alpha\frac{d^2\theta}{d\alpha^2}+\frac{d\theta}{d\alpha}-\frac{\theta}{\alpha}=\frac{6}{\left(\frac{t}{R}\right)^2}\alpha\theta\left(\theta^2-\alpha^2\right)+\frac{6p}{E\left(\frac{t}{R}\right)^3}\alpha^2 \qquad (7)$$

The differential equations (5) and (7) are nonlinear, as expected, and it is difficult, if not impossible, to solve them analytically. However, useful information about the character of the relation between θ and α can be obtained by attempting a solution of the form:

$$\theta = \sum_{n=1}^{\infty} C_n \alpha^n \tag{8}$$

which starts as $C_1\alpha$ owing to the boundary condition:

$$\theta = 0 \quad \text{at} \quad \alpha = 0$$

Substituting equations (8) and (7), and equating coefficients of equal powers of α, it can be seen that all even powers of α in equation (8) drop out. Therefore, θ must be of the form:

$$\theta = \sum_{m=0}^{\infty} C_{2m+1} \alpha^{2m+1} \tag{9}$$

The analytical method of solving the problem can hardly proceed any farther. To solve the problem, it is necessary to use the Rayleigh-Ritz approximate method - that is, assume a plausible form of θ with arbitrary constants but satisfying the boundary conditions; substitute this equation into (6), and then determine the constants by minimizing the resulting expression. From a consideration of equation (9), the first approximation will be:

$$\theta = C\alpha \left[1 + \left(\frac{1}{C} - 1\right)\left(\frac{\alpha}{\beta}\right)^2\right] \tag{10}$$

which satisfies the boundary conditions (5a). The constant C is a measure of the deflection at the center. Substituting equation (10) into equation (6) and carrying out the integration, yields:

$$\frac{W}{R^3\pi} = \frac{E\left(\frac{t}{R}\right)}{4}\left[\frac{(C^2 - 1)^2}{6} + \frac{1}{2}C(1 - C)(C^2 - 1) + \frac{1}{5}(3C^2 - 1)(1 - C)^2 + \frac{1}{3}C(1 - C)^3 + \frac{(1 - C)^4}{14}\right]\beta^6 + \frac{E\left(\frac{t}{R}\right)^3}{12}\frac{2}{3}(C - 1)^2\beta^2 + pC\left[\frac{1}{4} + \frac{1}{6}\left(\frac{1}{C} - 1\right)\right]\beta^4 \tag{11}$$

To find the equilibrium condition, equation (11) is differentiated with respect to C, and the resultant expression set to zero. This gives

$$\frac{p}{E\left(\frac{t}{R}\right)} = 3(1 - C)\,\beta^2\left[\frac{2}{3}\,C(C + 1) - \frac{1}{2}\,(4C^2 + C - 1)\right.$$

$$\left. + \frac{2}{5}\,(6C^2 - 3C - 1) - \frac{1}{3}\,(4C^2 - 5C + 1) + \frac{2}{7}\,(C - 1)^2\right]$$

$$+ \left(\frac{t}{R}\right)^2 \frac{4}{3}\,(1 - C)\,\frac{1}{\beta^2} \qquad (12)$$

This equation gives the value of p as a function of the region of buckling β and the amplitude of the deflection, which is proportional to C. For the buckling problem of the sphere, β is a free variable. It is then evident that the shell must adjust itself so that p is a minimum for each value of C. In other words, the expression for p with respect to β can be minimized and solved for the size of the region which corresponds to the minimum buckling pressure. This gives:

$$\beta^2 = \frac{2}{3}\left(\frac{t}{R}\right)(4C^2 + 13C + 11)^{-\frac{1}{2}} \qquad (13)$$

If equation (13) is substituted into equation (12), the following relation is obtained:

$$\frac{\sigma}{E\left(\frac{t}{R}\right)} = \frac{p}{2E\left(\frac{t}{R}\right)^2} = k = \frac{2}{\sqrt{210}}\,(1 - C)(4C^2 + 13C + 11)^{\frac{1}{2}} \qquad (14)$$

where σ is the average stress in the shell due to p and

$$\sigma = \frac{p}{2\left(\frac{t}{R}\right)}$$

Equation (14) is plotted in figure 60, the maximum and the minimum values of k being 0.4911 and 0.2378, respectively.

The maximum value of k is of less practical significance than the minimum value because, as shown by Marguerre in his investigation of the collapse of curved bars under side load, the symmetrical collapse is usually precipitated

by an unsymmetrical type of buckling. Also, any imperfection in the shell will tend to cause failure to occur at the minimum, rather than the maximum value of p. Therefore, it would be expected that, although carefully machined specimens tested with all precautions to avoid eccentricities might lead to higher values, the specimens made and tested with accuracies corresponding to practical design would give experimental values of k lying close to the minimum value given by the theoretical analysis.

In order to calculate the maximum deflection δ_m at the center, the ordinate z_o at the center has to be first computed (fig. 59). By means of the boundary condition that $z = 0$ at $\alpha = \beta$ the following relation is obtained:

$$z_o + \int_0^\beta \frac{dz}{dr}\, dr = 0$$

or

$$z_o = R \int_0^\beta \tan\theta \cos\alpha \, d\alpha$$

$$\cong R \int_0^\beta \theta \, d\alpha \tag{15}$$

Substituting equation (16) into equation (15), and integrating, z_o can be expressed as:

$$z_o = R \frac{1 + C}{4} \beta^2 \tag{16}$$

Before deformation,

$$z_{o_{original}} = R (1 - \cos\beta) \cong R \frac{\beta^2}{2}$$

Using equation (16), the deflection δ_m is calculated as

$$\delta_m = z_{o_{original}} - z_o = R\beta^2 \frac{1 - C}{4}$$

When this value is substituted into equation (13), the following expression for δ_m/t is obtained:

$$\frac{\delta_m}{t} = \frac{\sqrt{210}}{6} \frac{(1 - C)}{(4C^2 + 13C + 11)^{\frac{1}{2}}} \tag{17}$$

Using equations (13) and (17), $\frac{\sigma}{E\left(\frac{t}{R}\right)}$ can be plotted as a function of δ_m/t. This has been done in figure 61, and the curve indicates that at the buckling pressure corresponding to the minimum $\sigma/E\left(\frac{t}{R}\right)$, the center deflection is of the order of ten times the sheet thickness.

Very few experimental data are available to check the above theoretical values; however, a number of investigators have stated that the previously accepted theoretical value of $k = 0.605$ obtained by Zoelly, Schwerin, and Van der Neut, and as quoted by Timoshenko (reference 5), was much too high. A test made at GALCIT on a thin copper hemisphere indicates that the theoretical values obtained by this new treatment of the problem agree surprisingly well with the experimental results. The experimental values were:

$$E = 14.5 \times 10^6 \text{ pounds per square inch}$$

$$R = 18 \text{ inches}; \quad t = 0.020 \text{ inch}; \quad t/R = 1/900$$

$$\frac{\sigma}{E\left(\frac{t}{R}\right)} = 0.154; \quad \frac{\delta_m}{t} = 12.5; \quad \beta = 0.139 \text{ radian} = 8^\circ$$

Comparing these values with those predicted theoretically, which are:

$$\frac{\sigma}{E\left(\frac{t}{R}\right)} = 0.2378; \quad \frac{\delta_m}{t} = 9.4$$

$$\beta = 0.1330 \sqrt{1000\ t/R} \text{ radians} = 7.63\sqrt{1000\ t/R} \text{ degrees} = 7.2^\circ$$

a very good agreement is found when due consideration is given to the simplifying assumptions that have been made and to the fact that an approximate energy method of solution has been used.

Recalling the fact that the theoretical value of k at buckling is 0.605, the present calculation shows, at least, that the method of attack on the problem is correct. Another indication of the correctness of the method lies in the fact that the theoretical wavelength of the buckles corresponds closely to that found experimentally, which is not the case for the earlier theoretical solutions. The investigation will be continued, and it is hoped that in the near future, the treatment can be extended to the case of the thin cylindrical shell under axial compression. The results of some experimental investigations on the compressive failing stress at unstiffened circular cylinders are given in appendix A.

APPENDIX A

EXPERIMENTAL INVESTIGATIONS ON COMPRESSIVE FAILING STRESS OF UNSTIFFENED CIRCULAR CYLINDERS

In order to clarify the problem of the thin circular cylinder under axial compression, a systematic series of experiments were made on a number of steel cylinders. The parameters which are involved in this problem are:

1. The radius-thickness ratio, R/t
2. The length-radius ratio, L/R
3. The elastic properties of the material
4. The total axial load that can be carried by the specimen

The specimens tested were all made from steel shim stock, which was formed into specimens 12.75 inches in diameter. The ends of the cylinder were rigidly clamped into steel end plates, giving fixed end support to the axial fibers of the cylinder. The variables used were the thickness of the material and the length of the specimen.

The test results are shown in figures 62 to 67, and the faired experimental curves are replotted in figures 68 and 69. The curves are plotted against the ratio $\sigma_{act}/\sigma_{theo}$

where

σ_{act} actual failing stress obtained in the test

σ_{theo} theoretical failing stress which is equal to $0.605\ E\ (t/R)$

As can be seen by figures 68 and 69, there is a continuous decrease in the experimentally obtained failing stress as the R/t ratio increases, this decrease occurring for all values of L/R. For all values of L/R greater than 1.0, it is seen that the failing stress remains practically constant with increasing L/R for any given value of R/t. Thus, for any cylinder with an L/R ratio greater than approximately 1.0, no length effect would have to be considered in an analysis, and a correction of any appreciable magnitude would not be necessary until the L/R value fell below approximately 0.75.

In order to facilitate the theoretical work on this problem, it was desired to determine the exact shape of the initial waves which appeared in the test cylinders. This has been done in a preliminary manner by restraining the loading mechanism during buckling, and it has been found that the initial waves which occur are of an elliptical form and are scattered at random through the specimen. This wave pattern does not agree with the uniformly distributed, sinusoidal type of wave which has been previously assumed for the theoretical solution, and this discrepancy in assumed wave pattern may account for the large difference between the theoretically predicted and the experimentally obtained buckling loads.

Work is now in progress to obtain a more exact knowledge regarding this initial wave pattern and to obtain a more exact picture of the sequence of wave patterns during buckling. A theoretical solution of the problem will then be attempted following a procedure similar to that given in the body of this report for the case of the spherical shell.

APPENDIX B

A PRELIMINARY DISCUSSION ON THE USE OF A WIRE NETWORK TO PROVIDE SHEAR STIFFNESS

The addition of sheet covering, or any form of peripheral wire network, to a skeleton cylinder made up of frames and longitudinals, will have two effects on the bending properties of the cylinder. First, it will increase the moment of inertia of the section; second, it may change the mode of failure due to an increase in shear stiffness. Fine wire bracing and extremely thin sheet covering will have the same general type of action because neither can take compression and, therefore, only the portion on the tension side need be considered in the calculation of the moment of inertia of the section. Furthermore, under shearing forces the sheet will buckle and carry the shear stresses by means of a diagonal tension field corresponding to the effect of diagonal wiring.

In order to approximate the case of a cylinder covered with a sheet of zero thickness, it was necessary to provide sufficient shear stiffness without appreciably changing the moment of inertia or the position of the neutral axis of the specimen. In the present series of tests this was done by building up a rectangular network of steel wires, 0.016 inch in diameter on the periphery of the cylinder. It was found that the primary effect of these wires was to prevent a type of failure, which has been called torsional failure, in which the longitudinals tended to fail in a circumferential rather than in a radial direction.

Experiments showed that if circumferential failing was entirely prevented, the cylinder would carry its maximum bending moment and that the addition of more wires would not raise the allowable bending moment that could be supported by the specimen. This is shown by specimens 9, 10, 11, and 12 of table I. These specimens were identical with the exception that the amount of wire bracing was changed. Specimen 9 had no wire bracing and carried a bending moment of 60,000 inch-pounds. Failure of the specimen was definitely of a torsional nature, the frames tending to rotate about the tension longitudinal and showing very little radial deflection.

A wire network constituting the diagonals of rectangles measuring 5 inches in the frame direction and 8 inches in the longitudinal direction was then added and this new specimen was tested, failure taking place at 90,000 inch-pounds of applied moment - an increase of 50 percent. The wire bracing was then doubled, giving a network of diagonally braced rectangles 2.5 inches by 4 inches. This change increased the shear stiffness of the section by a factor of 2.0; however, the specimen failed at an applied moment of only 102,000 inch-pounds - an increase of 13 percent. The longitudinals in this last specimen showed very little tendency to fail in the circumferential direction, the deflection being almost entirely radial in nature.

Further increase in shear stiffness raised the failure bending moment to 114,000 inch-pounds, beyond which no increase could be obtained. The specimen carrying the maximum moment showed no tendency for torsional failure. From this series of specimens, and from numerous other observations, it was concluded that if sufficient shear stiffness was used so that there was no circumferential deflection of the longitudinals, then the maximum allowable bending moment for the specimen would be obtained. Furthermore, it was felt that the type of failure would closely correspond to that which would occur in a specimen covered with an infinitely thin sheet.

The wire bracing used on the specimens had a negligible effect on the section properties of the cylinder. Considering a representative cylinder after converting the steel wire to its equivalent duralumin area, it was found that the neutral axis shift was equal to:

$$y' = 0.07 \text{ inch}$$

in a diameter of 32.0 inches, and that the moment of inertia changed from

$$I_0 = 160.95 \text{ inches}^4$$

without wires to

$$I' = 162.03 \text{ inches}^4$$

with wires, a change of less than 1 percent. Similar results were obtained with the wire bracing used on the other specimens tested.

Guggenheim Aeronautical Laboratory,
California Institute of Technology,
Pasadena, Calif., February 1939.

REFERENCES

1. Guggenheim Aeronautical Laboratory, California Institute of Technology: Some Investigations of the General Instability of Stiffened Metal Cylinders. I - Review of Theory and Bibliography. T.N. No. 905, NACA, 1943.

2. Biezeno, C. B.: Über die Bestimmung der Durchschlagkraft einer schwach gekrümmten kreisförmigen Platte. Z.f.a.M.M., vol. 15, 1935, p. 13.

3. Anon.: Über eine Stabilitätsfrage beim gelenkig gelargerten schwach gekrümmten Stab. Proc., Kon. Akad. van Wetenschappen te Amsterdam, vol. 32, no. 7, 1929.

4. Marguerre, K.: Die Durchschlagskraft eines schwach gekrümmten Balkens. Sitzungsberichte der Berliner Mathematischen Gesellschaft, vol. 37, 1938, pp. 22-40.

5. Timoshenko, S.: The Theory of Elastic Stability. McGraw-Hill Book Co., Inc., New York, N. Y., 1936, pp. 491-497.

TABLE I.-PURE BENDING TESTS OF LONGITUDINAL-FRAME COMBINATIONS WITHOUT SHEET COVERING

Experimental Data - Set I

[All longitudinals S_1; All frames F_5]

Specimen	Longitudinal		Frame		Failing moment (lb)	Description of test	Remarks
	Spacing (in.)	Number	Spacing (in.)	Number			
1	2.53	40	4	15	33,300	No wire bracing	Longitudinals failed in circumferential direction.
2	2.53	40	4	15	90,000	Wire bracing	Longitudinals failed in radial direction; 1/2 wave complete length of specimen.
3	2.53	40	4	15	87,000	——do——	General instability same as specimen 2.
4	2.53	40	8	7	60,800	——do——	General instability; 1/2 wave complete length of specimen.
5	2.53	40	16	3	49,000	——do——	General instability; however, specimen looked like combination of small waves between frames and one long half-wave.
6	2.53	40	32	2	40,000	——do——	Similar to specimen 5. General instability.
7	2.53	40	32	1	36,300	——do——	Specimens started to fail between frames; however, as deflection increased, frame failed.
8	2.53	40	[1]64	0	18,000	——do——	Longitudinals failed in one long half-wave in radial direction.
9	2.53	40	2	31	60,000	No wire bracing	Longitudinals failed in circumferential direction.
10	2.53	40	2	31	90,000	Some wire bracing	Bottom longitudinal failed partly in radial and partly in circumferential direction.
11	2.53	40	2	31	102,000	Wire bracing	General instability; one long half-wave. Bottom longitudinal failed little in circumferential direction.
12	2.53	40	2	31	114,000	——do——	General instability; one long half-wave; longitudinals failed in radial direction.
13	5.06	20	2	31	65,000	——do——	General instability; length of buckle was less than length of specimen; about 23 frames failed.
14	[2]10.12	10	2	31	33,000	——do——	General instability; 1 to $1\frac{1}{2}$ complete waves in lengthwise direction.
15	[3]10.12	10	2	31	31,500	——do——	General instability; $1\frac{1}{2}$ waves in lengthwise direction.

[1]Total length of specimen, distance between supports. [2]Single longitudinal at maximum stress.

[3]Two longitudinals equal distance from

TABLE II.- THE EFFECT OF CHANGING THE FRAME SPACING ON THE BENDING STRENGTH OF THE CYLINDERS

Moment of inertia of complete specimen, $I_{sp} = 161.0$ in.^{4}
Radius to center of stiffener, $R = 15.76$ in.
Number of stiffeners, 40
$\sigma_{cr} = \frac{BM \times R}{I_{sp}} = \frac{BM \times 15.76}{161.0} = 0.0979 \times BM$
Length of specimen, 64 in.

Specimen	Longitudinal					Frame 5						Failing moment, B.M. (in.-lb)	Max. compressive stress failure, σ_{cr}	Type of failure
	Type	Area, A_s (in.^{2})	Moment of inertia, $I_s \times 10^4$ (in.^{4})	Spacing, b (in.)	$\frac{I_s}{b} \times 10^4$ (in.^{3})	Type	Area, A_f (in.^{2})	Moment of inertia, $I_f \times 10^5$ (in.^{4})	Spacing, d (in.)	Number of frames in 64 in.	$\frac{I_f}{d} \times 10^6$ (in.^{3})			
12	S_1	0.0324	3.74	2.53	1.478	F_5	0.0291	1.537	2	31	7.690	114,000	11,160	General instability
2	-do-	.0324	3.74	2.53	1.478	-do-	.0291	1.537	4	15	3.845	90,000	8,810	Do.
3	-do-	.0324	3.74	2.53	1.478	-do-	.0291	1.537	4	15	3.845	87,000	8,500	Do.
4	-do-	.0324	3.74	2.53	1.478	-do-	.0291	1.537	8	7	1.923	60,800	5,950	Do.
5	-do-	.0324	3.74	2.53	1.478	-do-	.0291	1.537	16	3	.962	49,000	4,800	Nearly panel instability.
6	-do-	.0324	3.74	2.53	1.478	-do-	.0291	1.537	32	2	.481	40,000	3,910	Nearly panel instability.
7	-do-	.0324	3.74	2.53	1.478	-do-	.0291	1.537	32	1	.481	36,300	3,555	General instability

TABLE III

THE EFFECT OF CHANGING THE SPACING OF THE LONGITUDINALS ON THE BENDING STRENGTH OF THE CYLINDERS

[Frame spacing = 2.0 in.; Radius to longitudinals, 15.76 in.]

Specimen	Longitudinal		Failing moment (in.-lb)	Moment of inertia of specimen, I_{sp} (in.^{4})	Maximum compressive stress at failure $(\sigma_{cr})_{exp}$	Type of failure
	Spacing	Number				
12	2.53	40	114,000	161.0	11,160	General instability
13	5.06	20	65,000	80.48	12,728	Do.
14	10.12[1]	10	33,000	40.24	12,926	Do.
15	10.12[2]	10	31,500	50.19	9,409	Do.

[1]Single longitudinal at maximum stress

[2]Two longitudinals at equal distance from specimen ℄ (i.e., equal stress)

TABLE IV.- CORRELATION BETWEEN CALCULATED AND EXPERIMENTAL VALUES

Data from Table II

[E taken as 10,000,000 lb/sq in.]

Specimen	Frame spacing, d (in.)	Number of frames in 64 in.	$P_E=\frac{\pi^2 EI}{d^2}$ (lb)	σ_E (lb/sq in.)	Hoff's method					Max. exper. stress	Experimental wave pattern
					Λ	λ ($\frac{1}{2}$ wave)	$\sigma_{cr}=\frac{\sigma_E}{\lambda^2}$ ($\frac{1}{2}$ wave)	λ (1 wave)	$\sigma_{cr}=\frac{\sigma_E}{\lambda^2}$ (1 wave)		
12	2	31	9,275	286,500	72,300	15.5	1,192	7.95	4,530	11,160	1/2 wave
2	4	15	2,319	71,600	9,030	7.72	1,200	3.94	4,610	8,275	Do.
4	8	7	580	17,900	1,130	3.84	1,214	1.95	4,700	5,950	Do.
5	16	3	145	4,485	141.0	1.88	1,267	.97	4,750	4,800	1/2 wave - nearly panel instability
6	32	2	36.2	1,088	17.75	1.32	642	.935	1,278	3,910	Do.
7	32	1	36.2	1,088	17.75	.935	1,283	.500	4,480	3,555	Do.
8	64	0	9.06	280	2.21	.50	1,120	----	----	1,642	1/2 wave

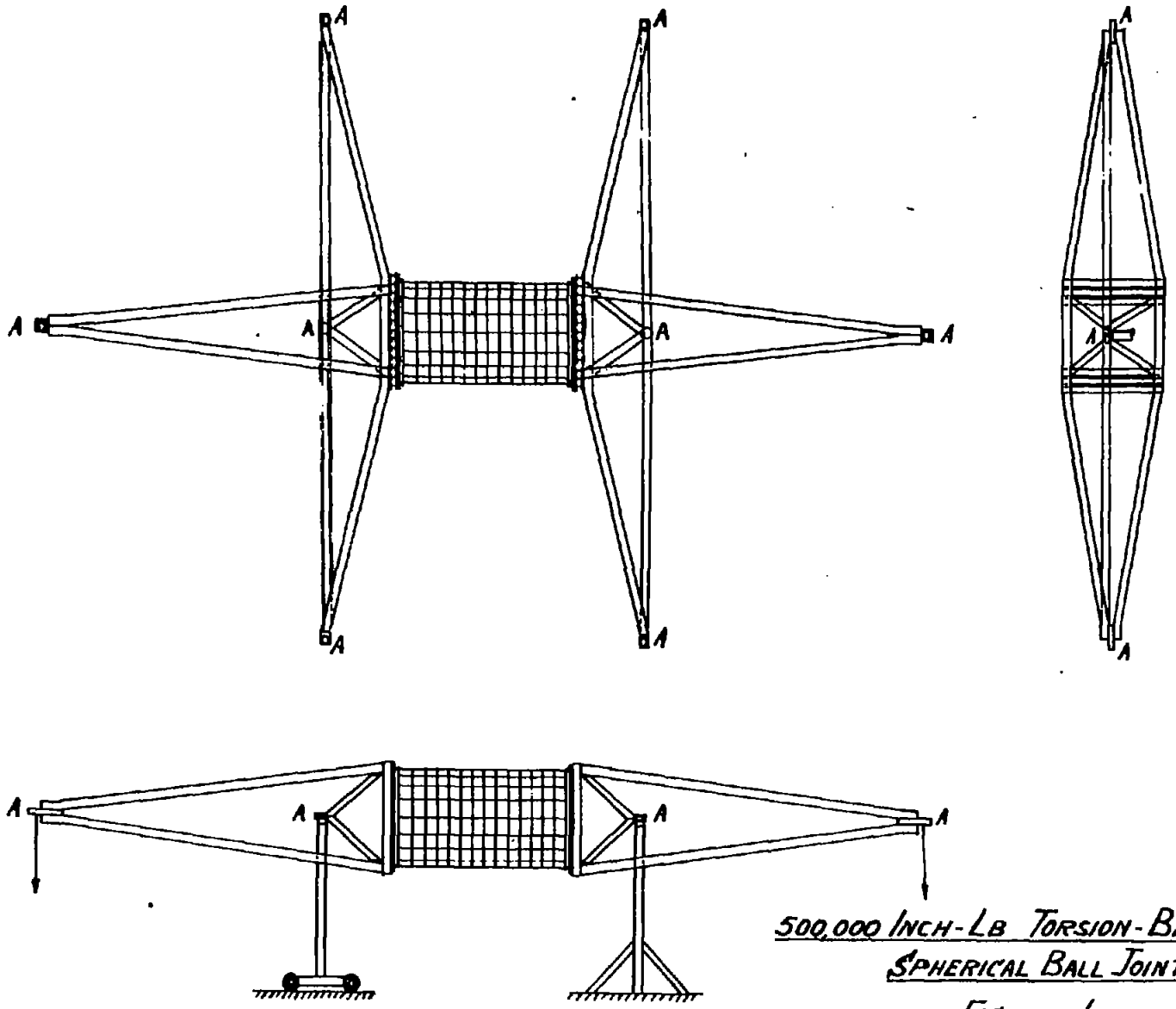

500,000 Inch-Lb Torsion-Bending Test Machine
Spherical Ball Joint at A
Figure 1.

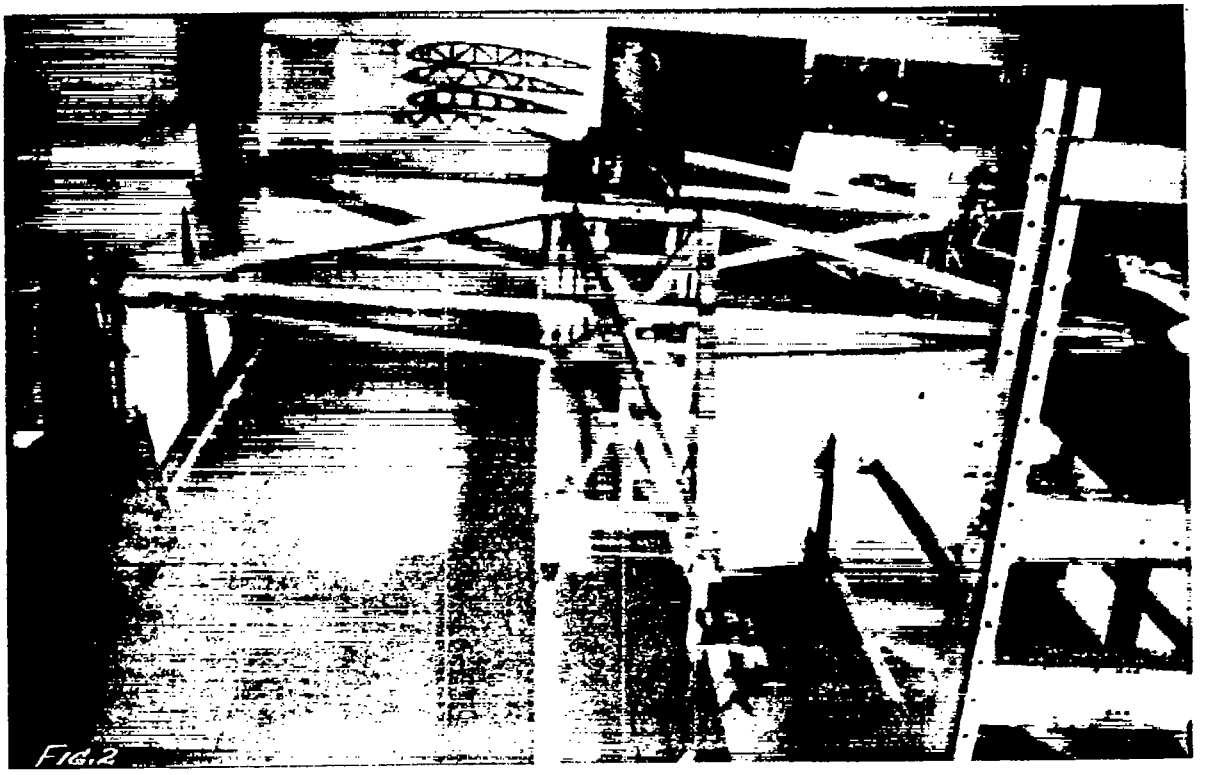

Fig.2

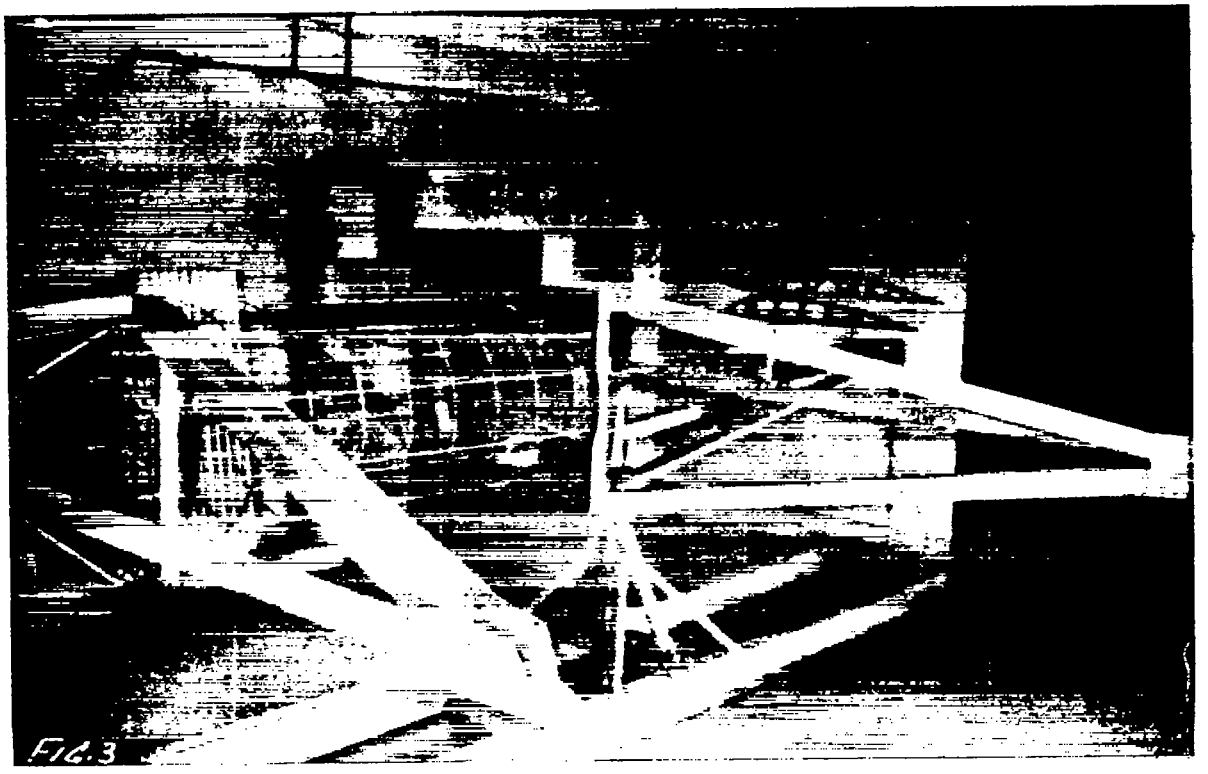

Fig.3

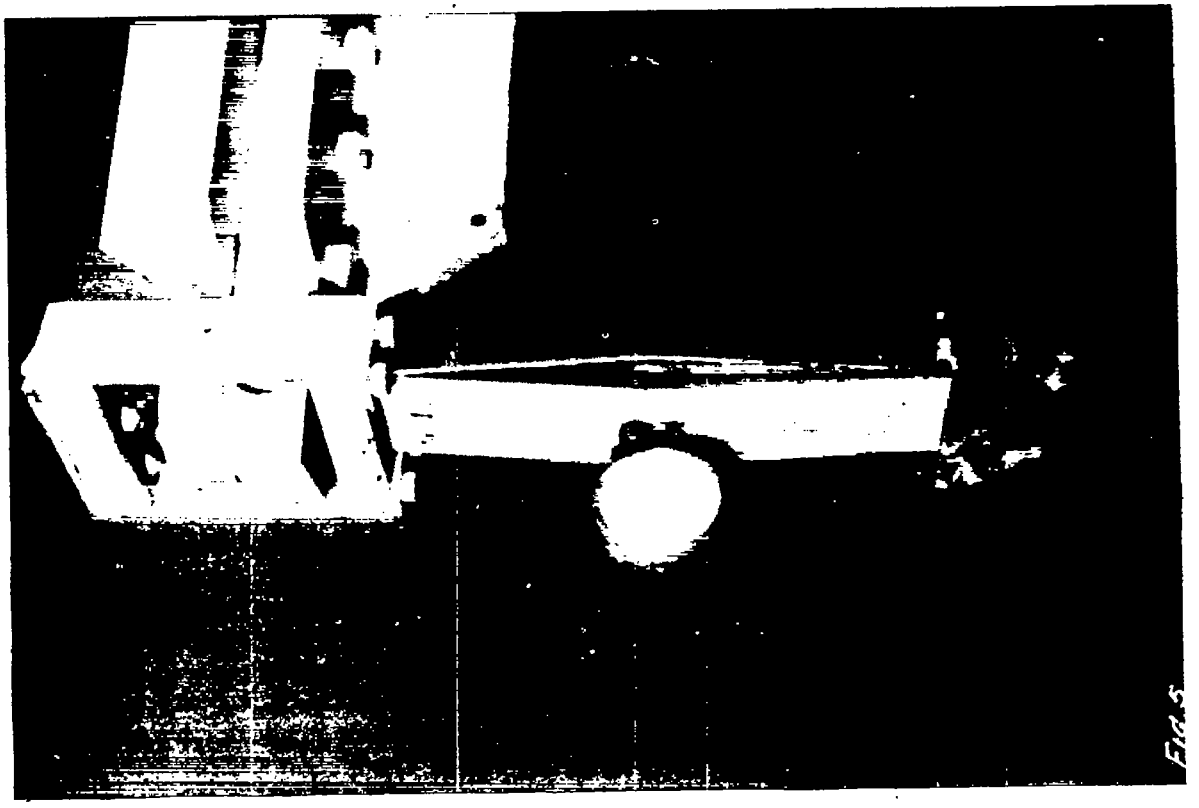

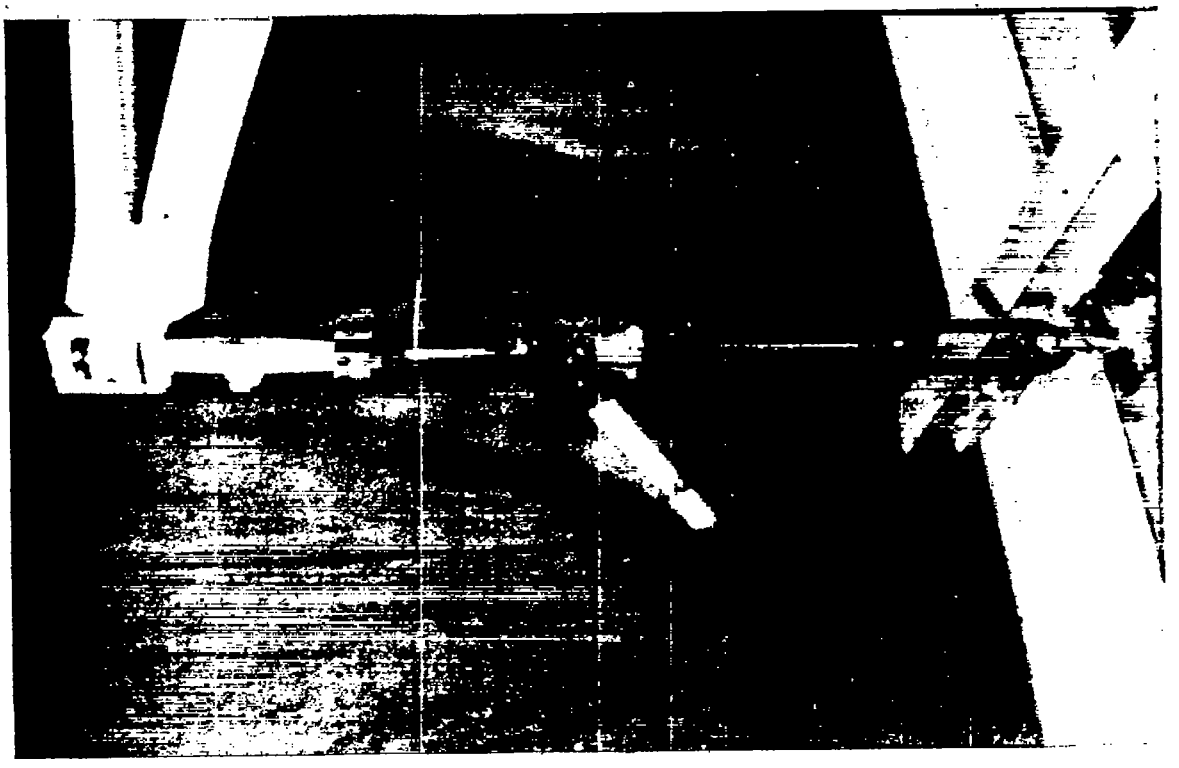

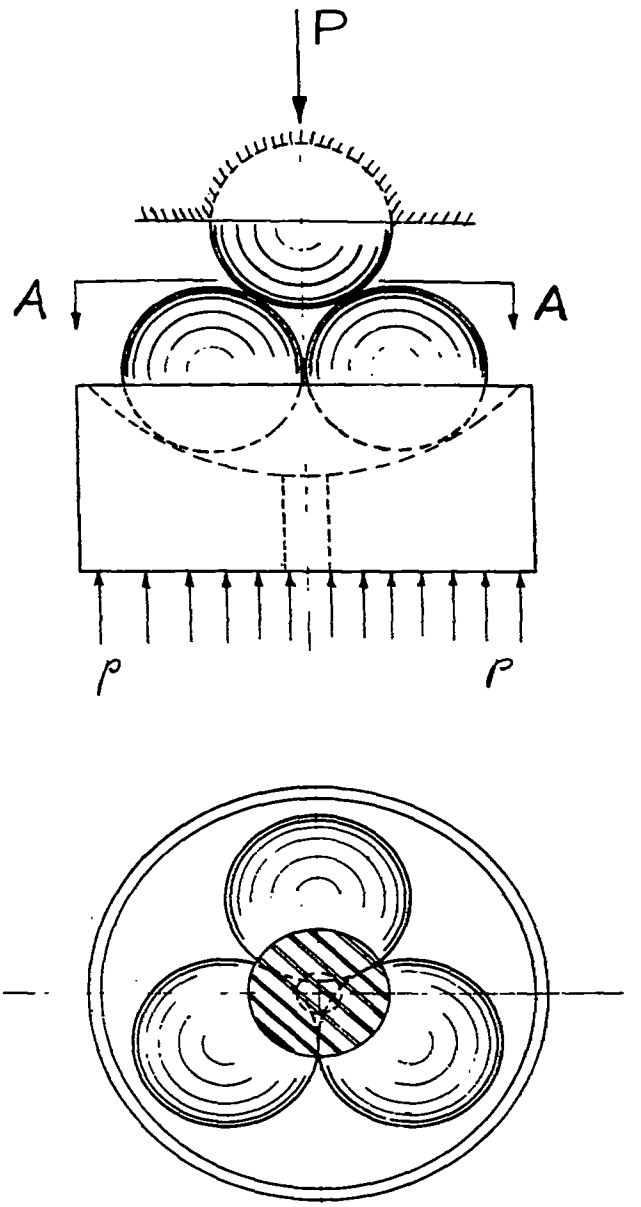

Spherical Ball Joint

Figure 6

Note. All figures are four times actual size

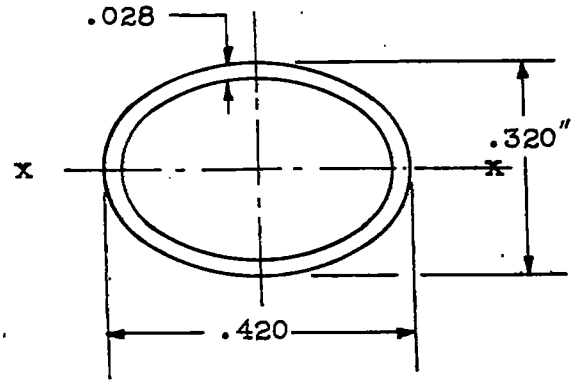

STIFFENER - S_1

AREA = .0324 sq.in. I_{xx} = .000361 $in.^4$

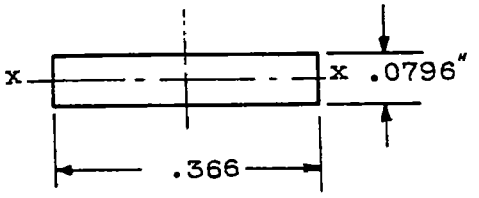

FRAME - F_5

AREA = .0291 sq.in. I_{xx} = .0000407 $in.^4$

FIGURE 7

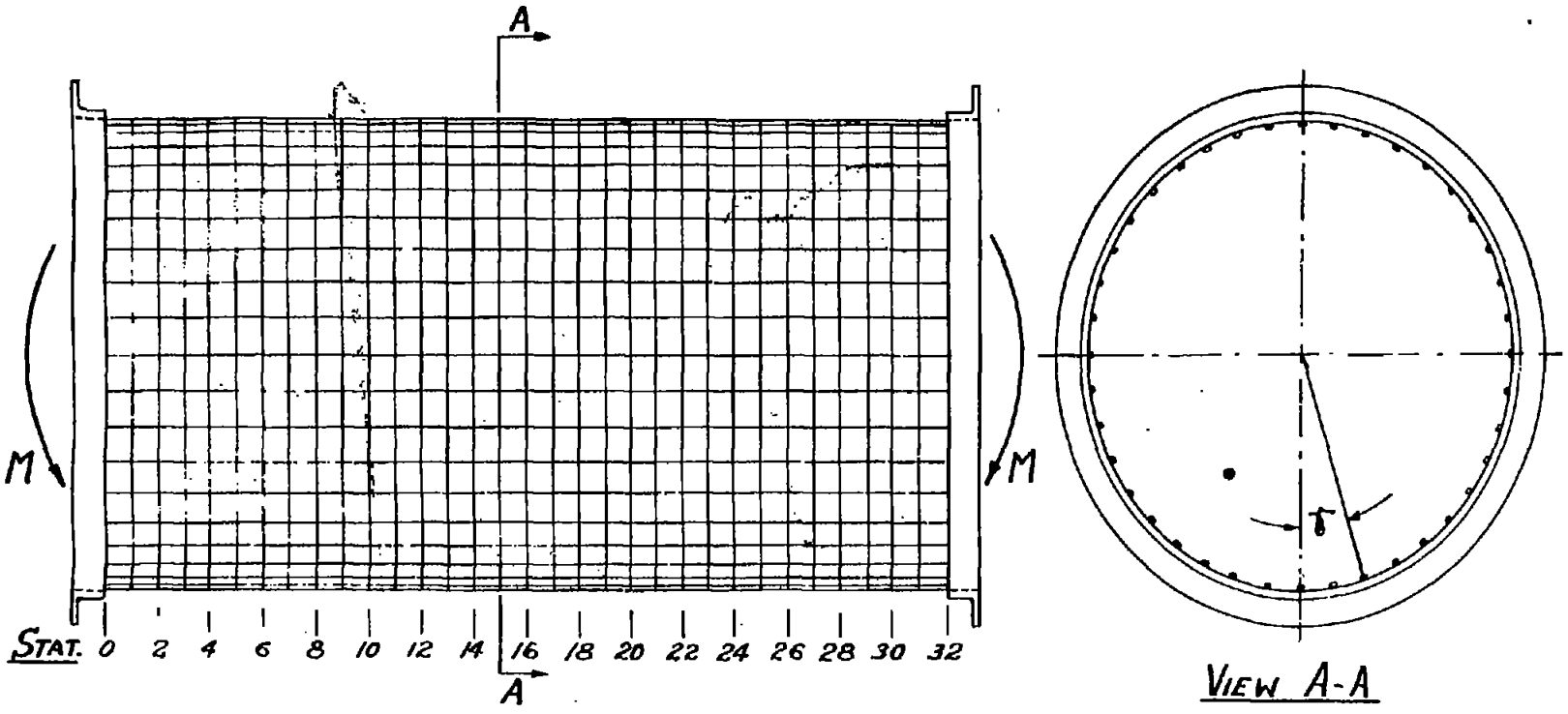

TEST SPECIMEN - FRAME AND LONGITUDINAL LOCATIONS

FIGURE 8

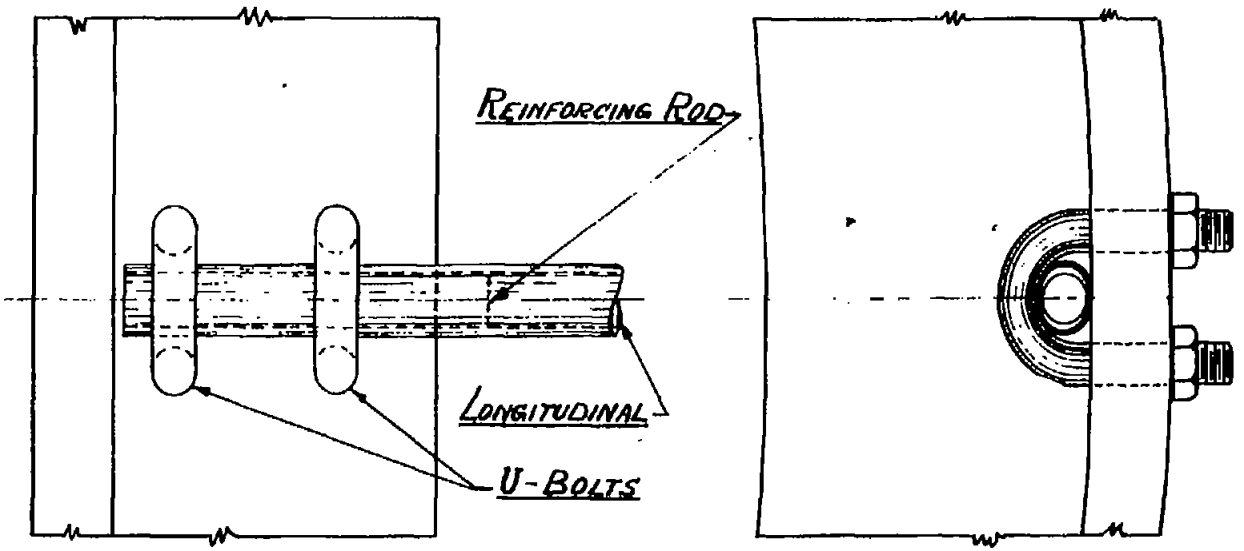

METHOD OF ATTACHING LONGITUDINALS TO END RING

FIGURE 9

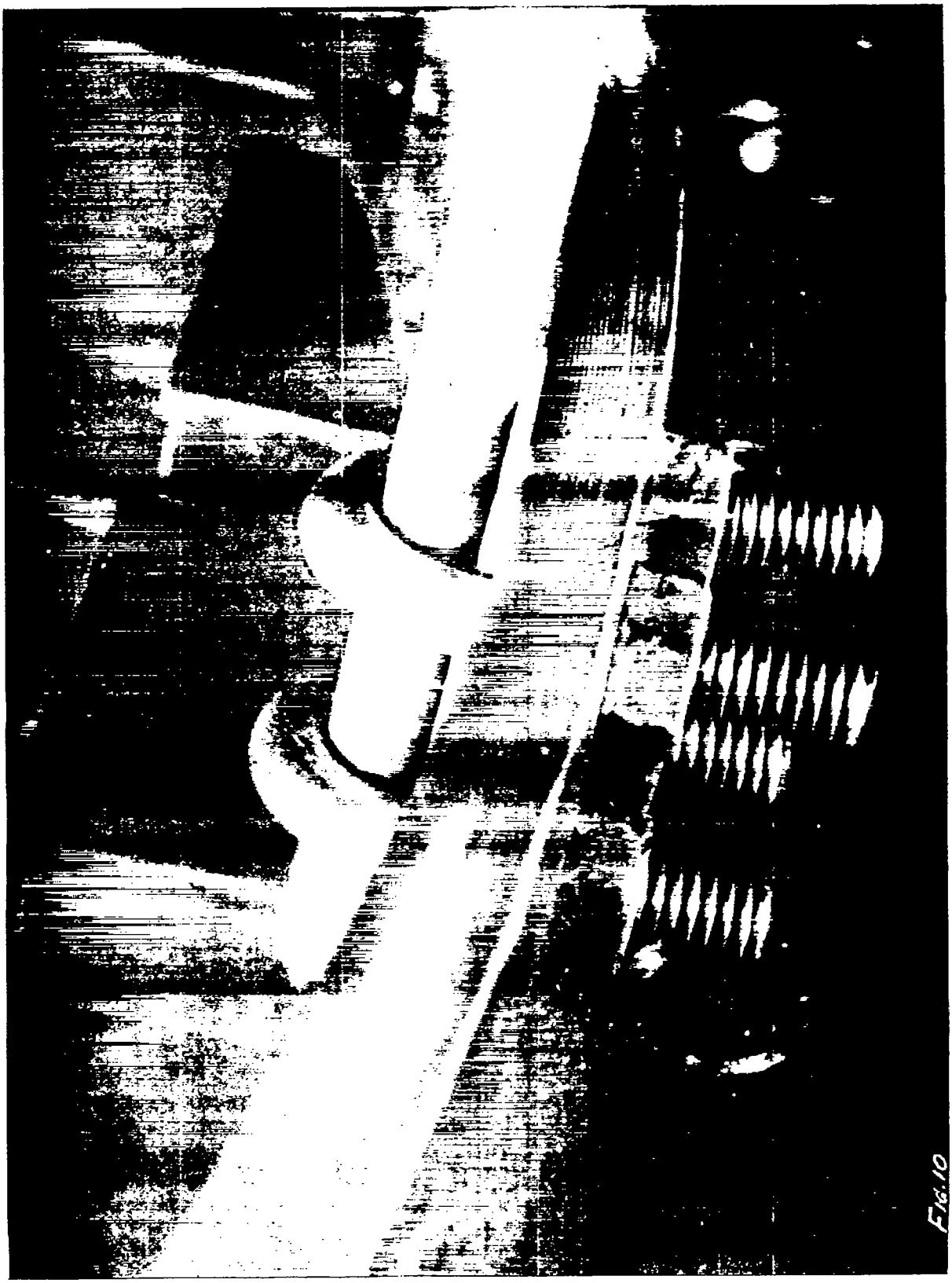
FIG. 10

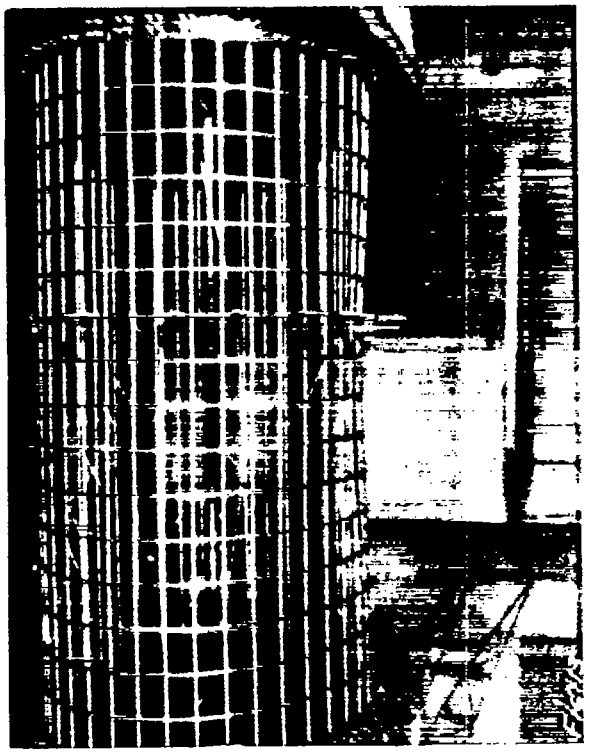

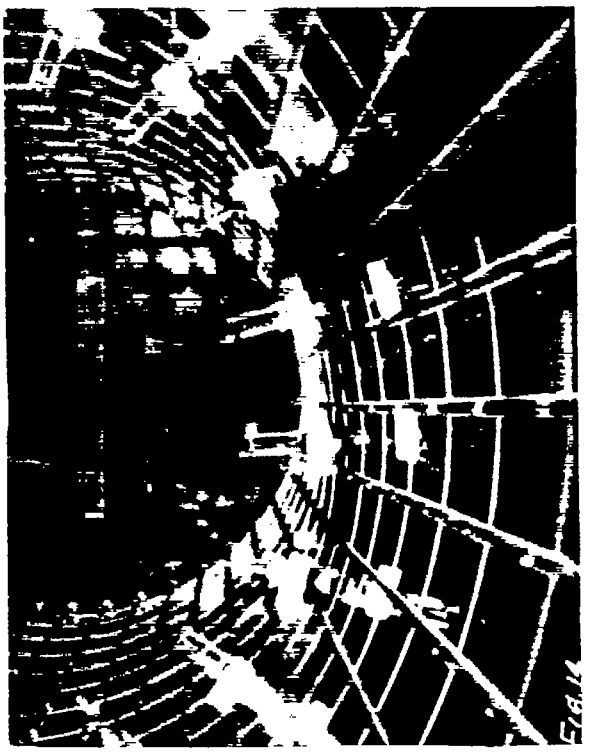

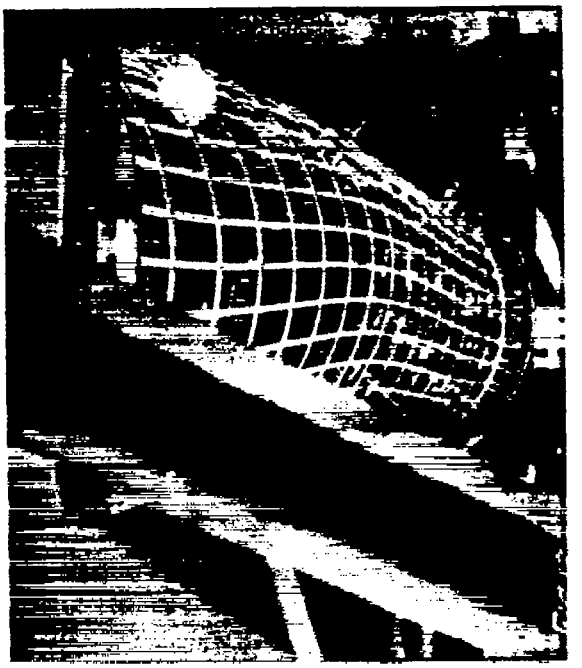

FIG. 17

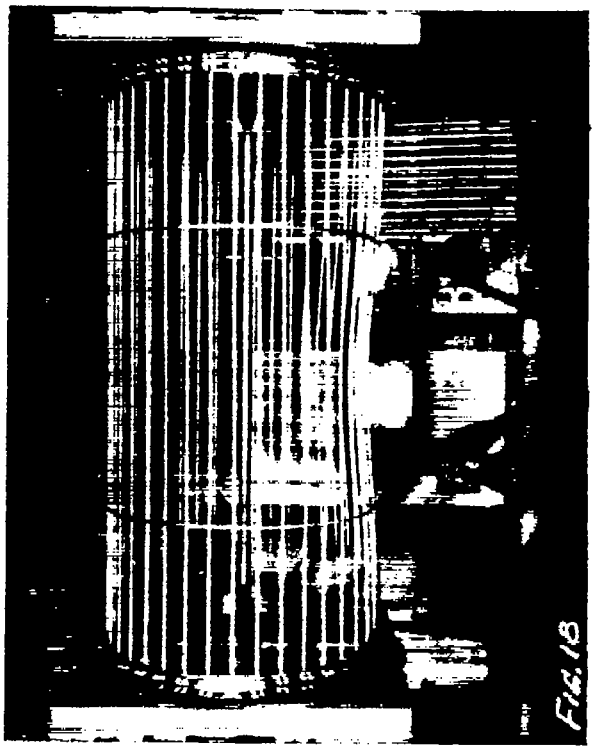

FIG. 18

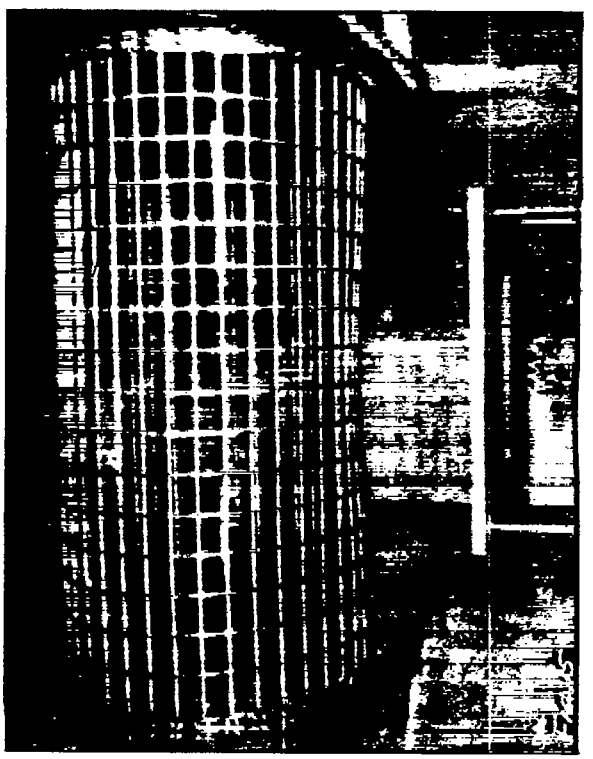

FIG. 15

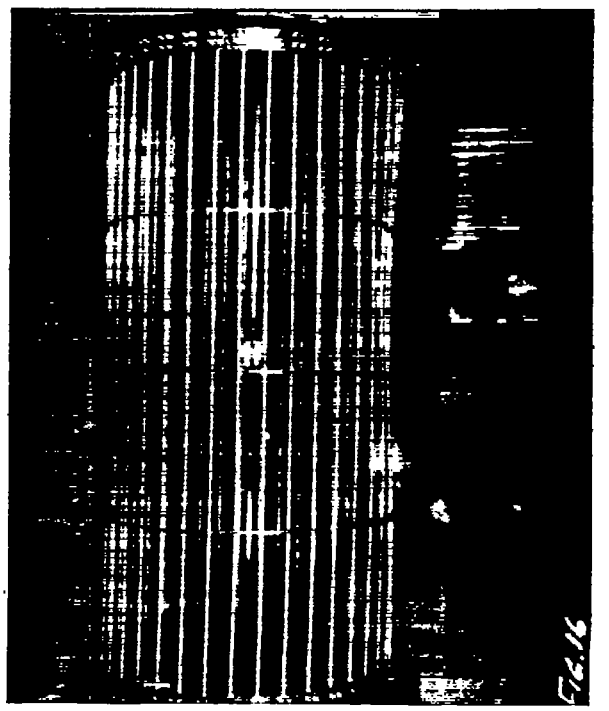

FIG. 16

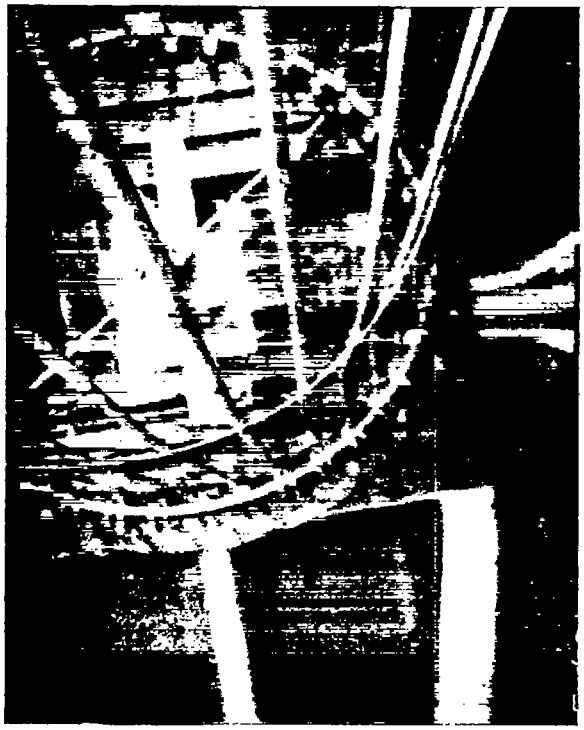

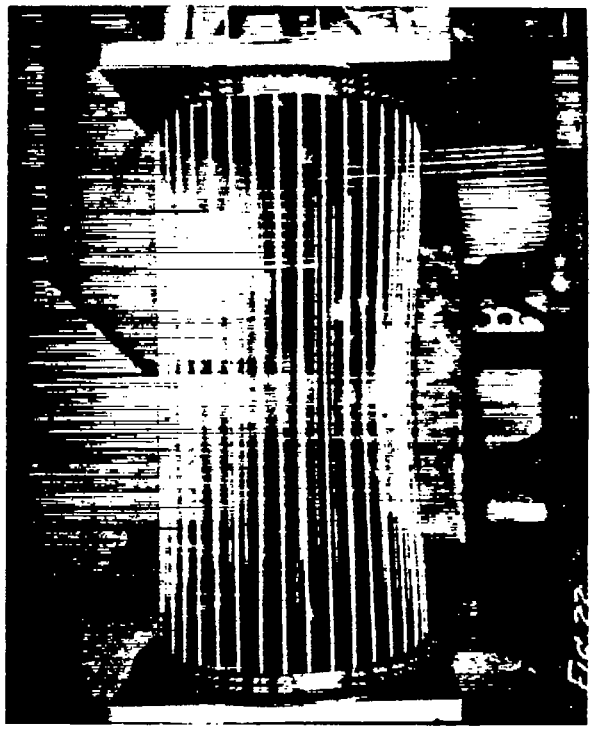

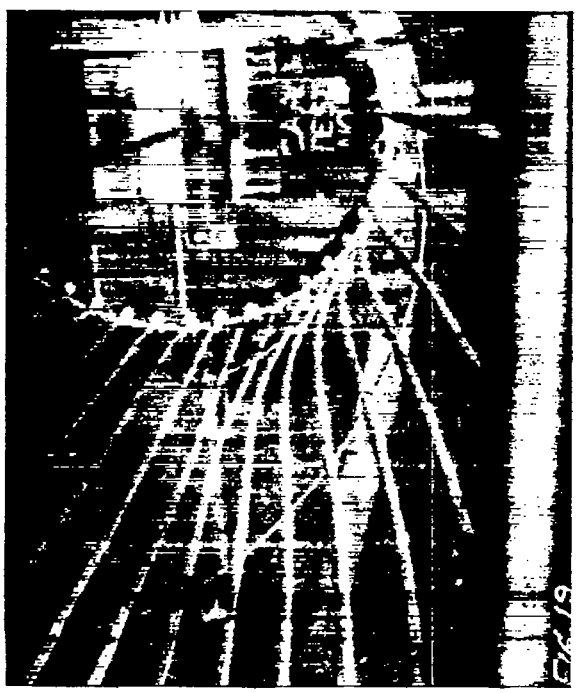

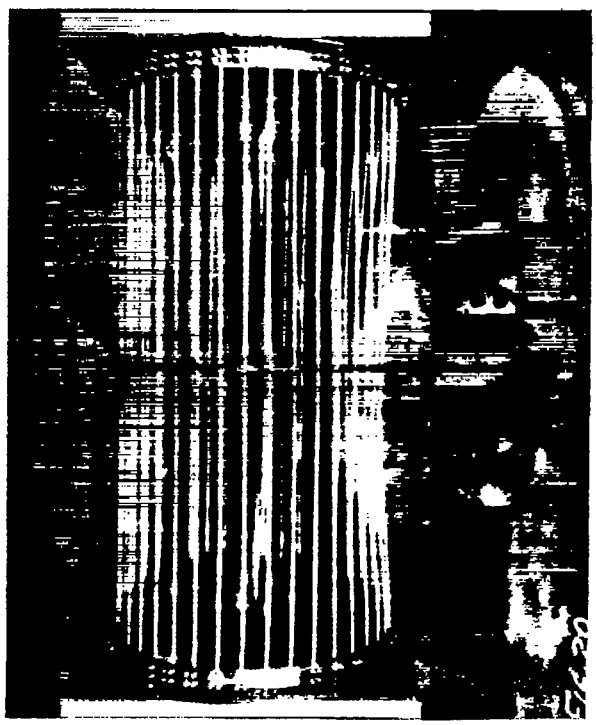

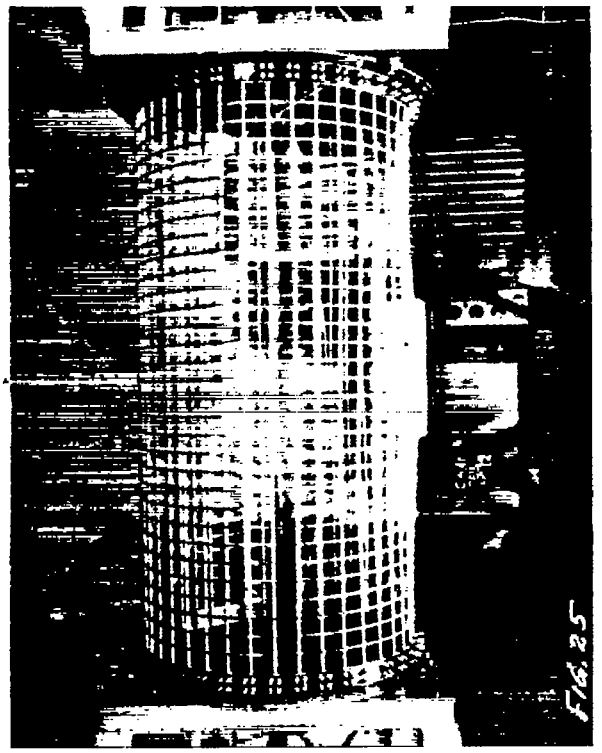

Fig. 25

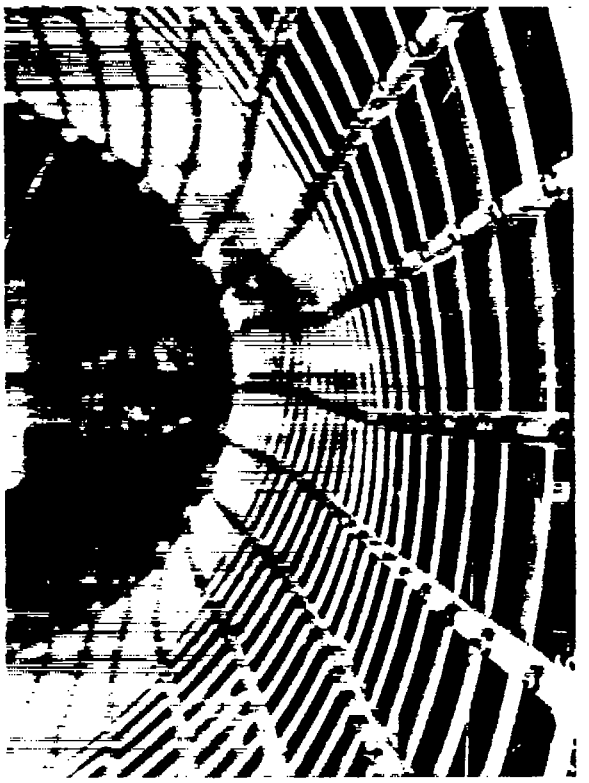

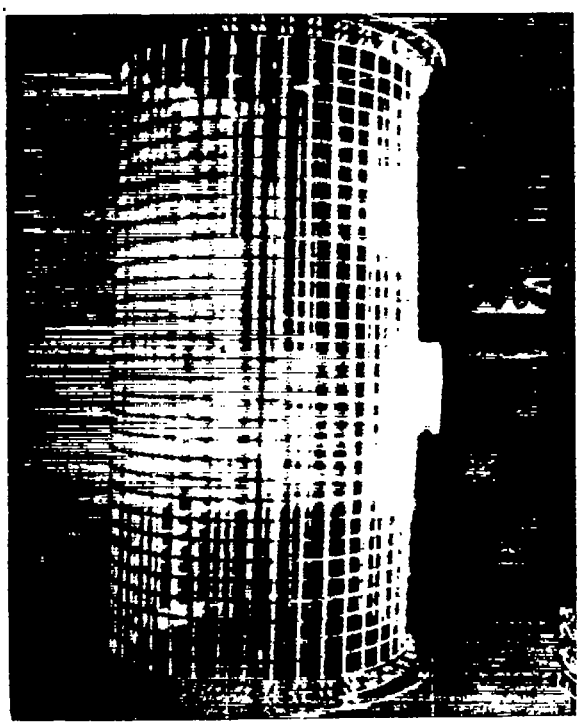

Fig. 23

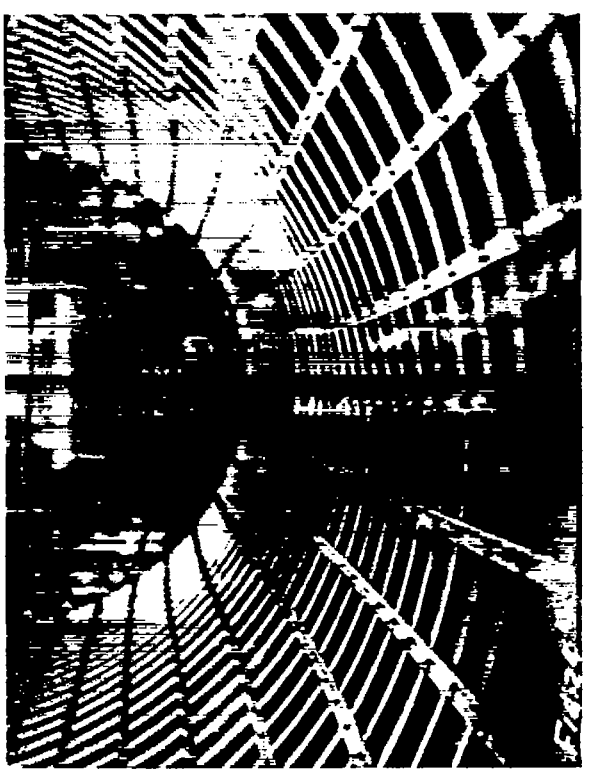

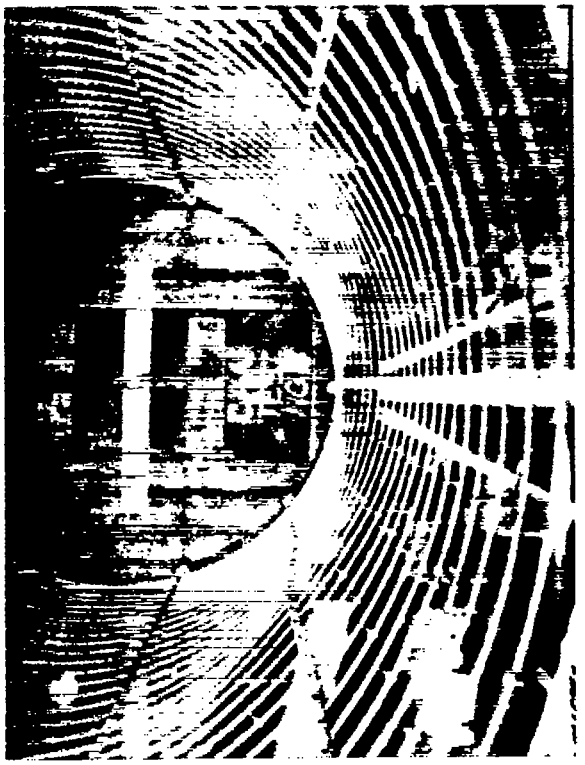

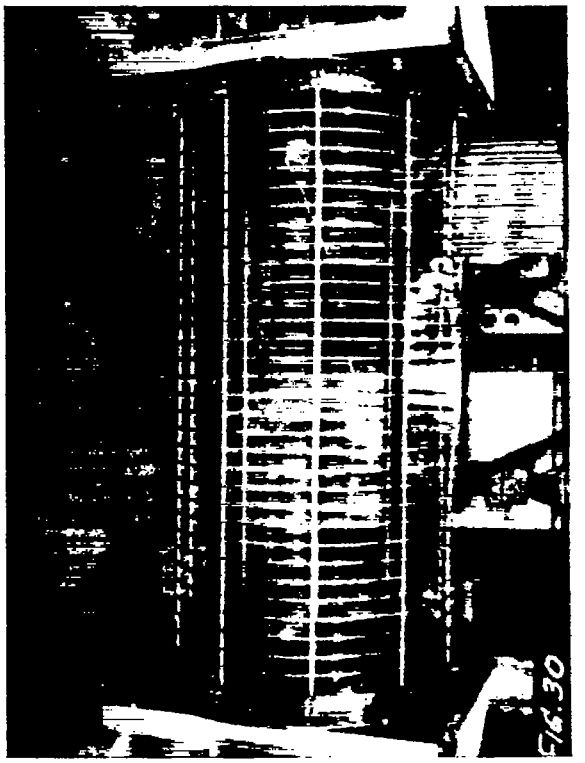
FIG.30

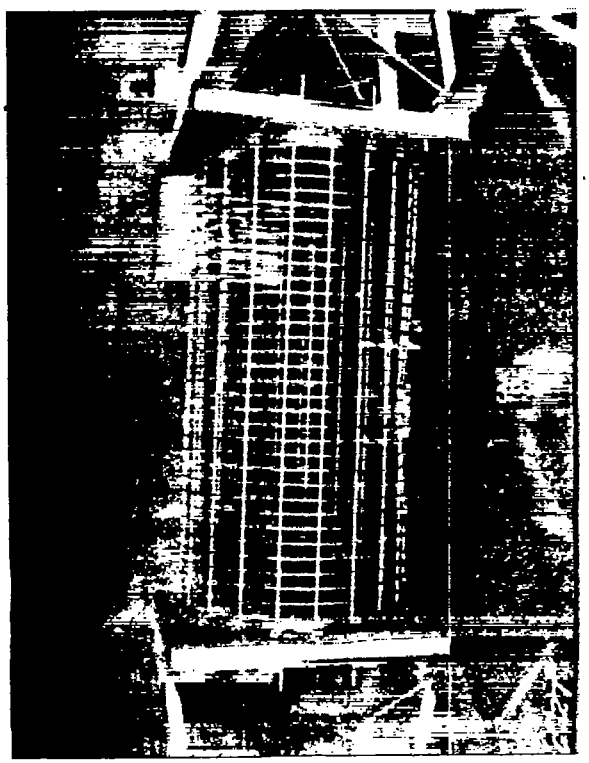

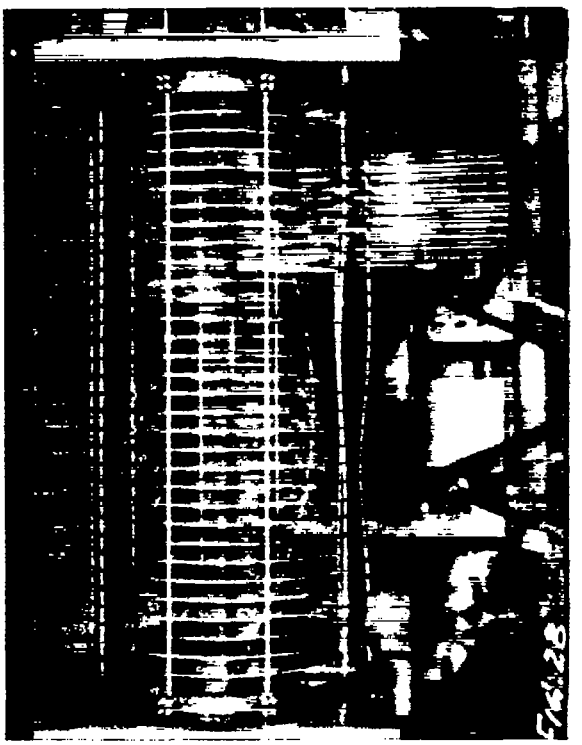
FIG.28

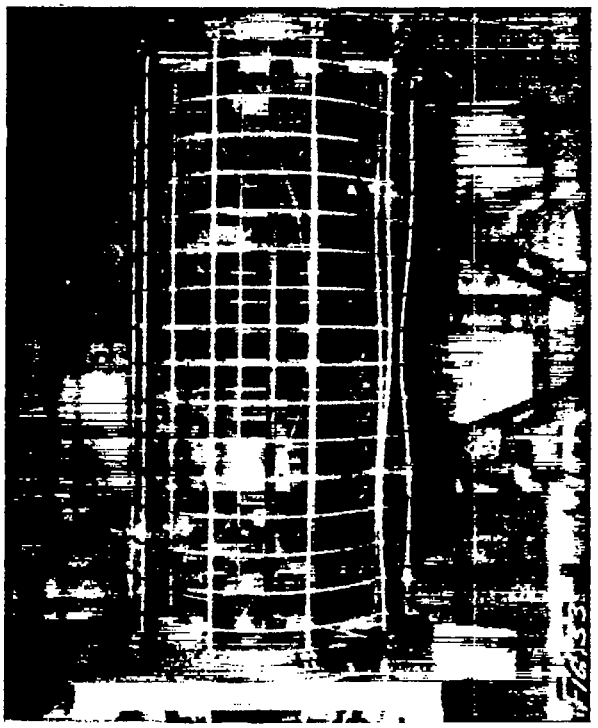

FIG. 33

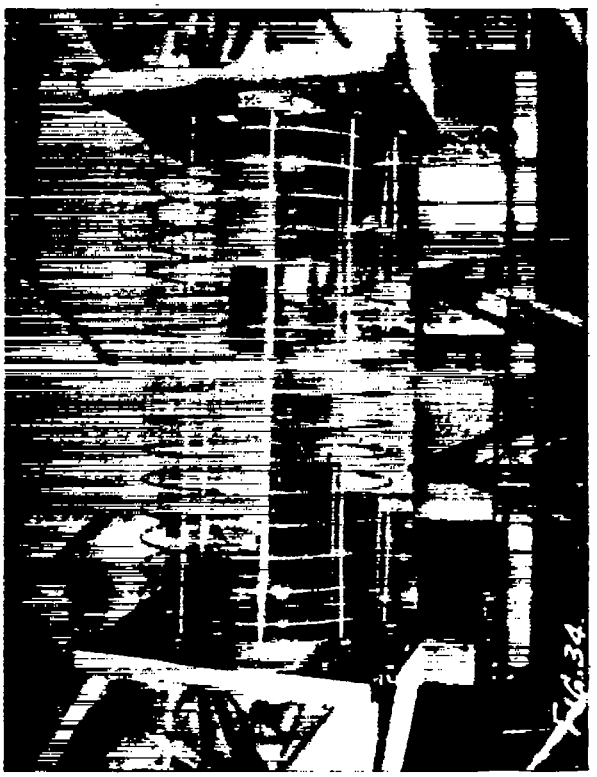

FIG. 34

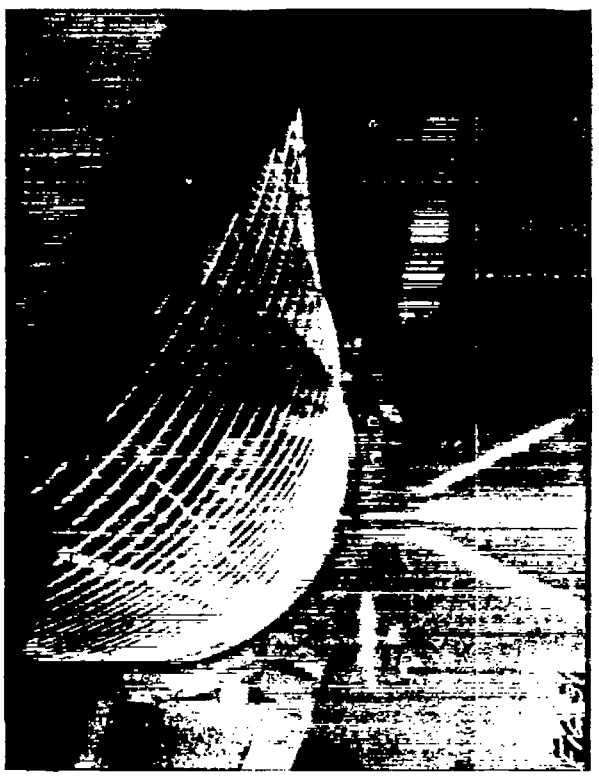

FIG. 31

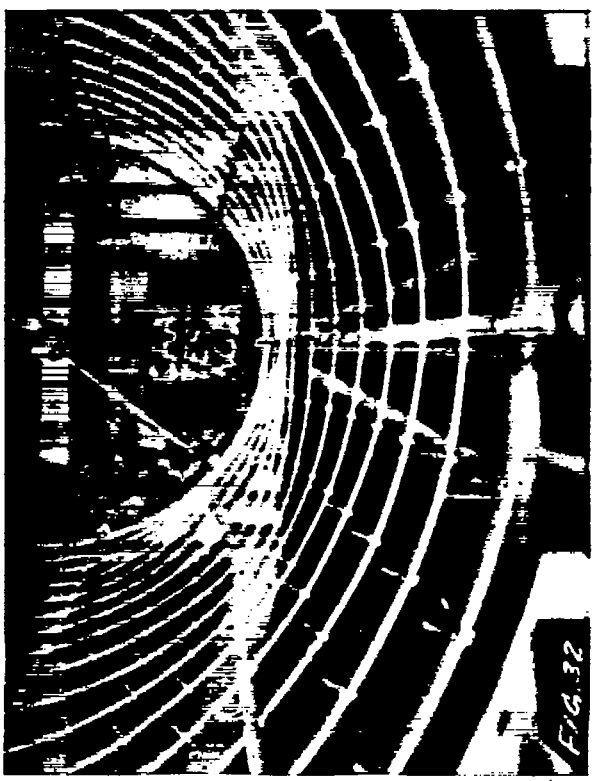

FIG. 32

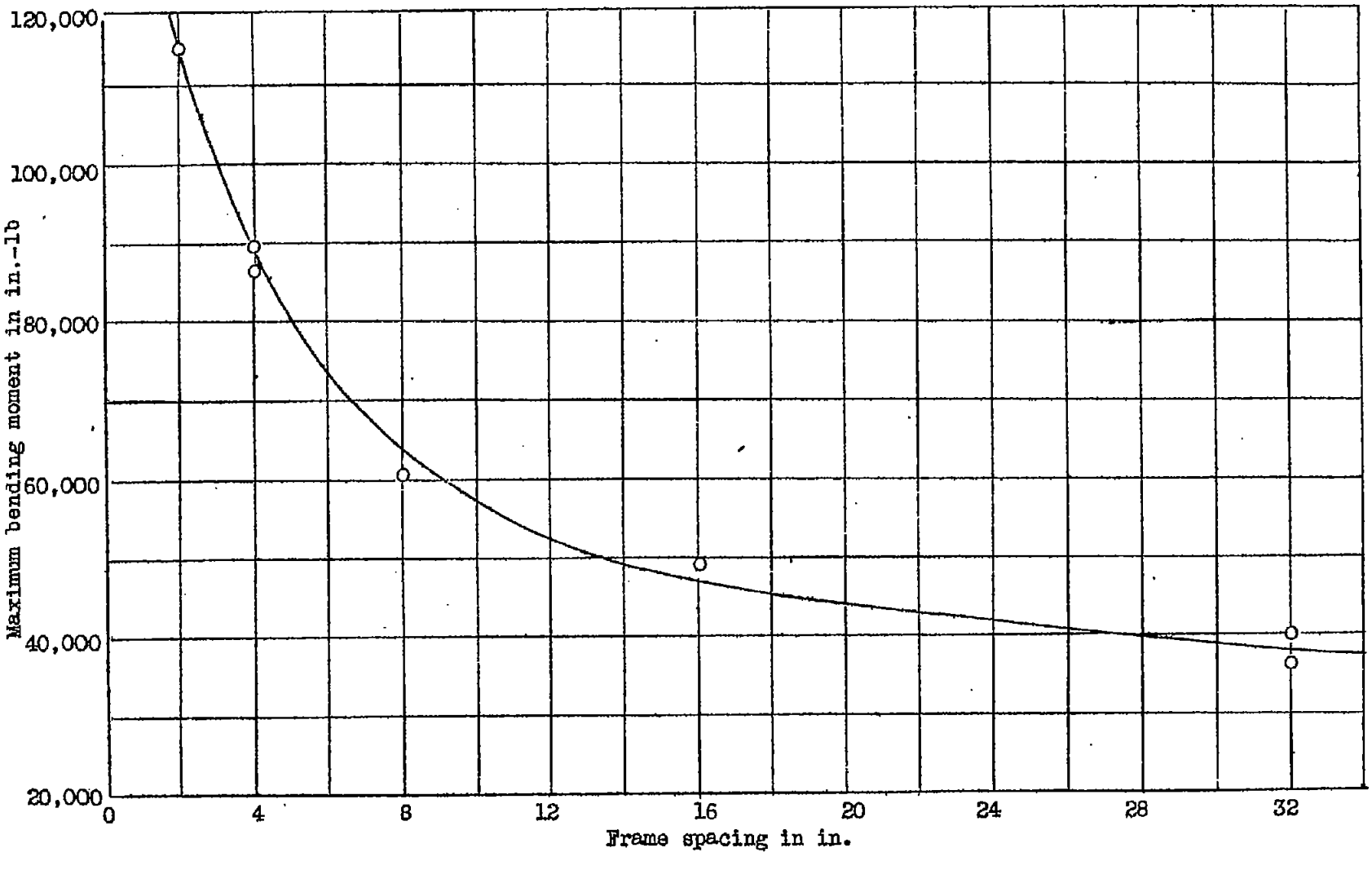

Figure 35.- Relation between bending moment and frame spacing, all specimens - 64" long, 40 longitudinals - S_1, all frames - F_5.

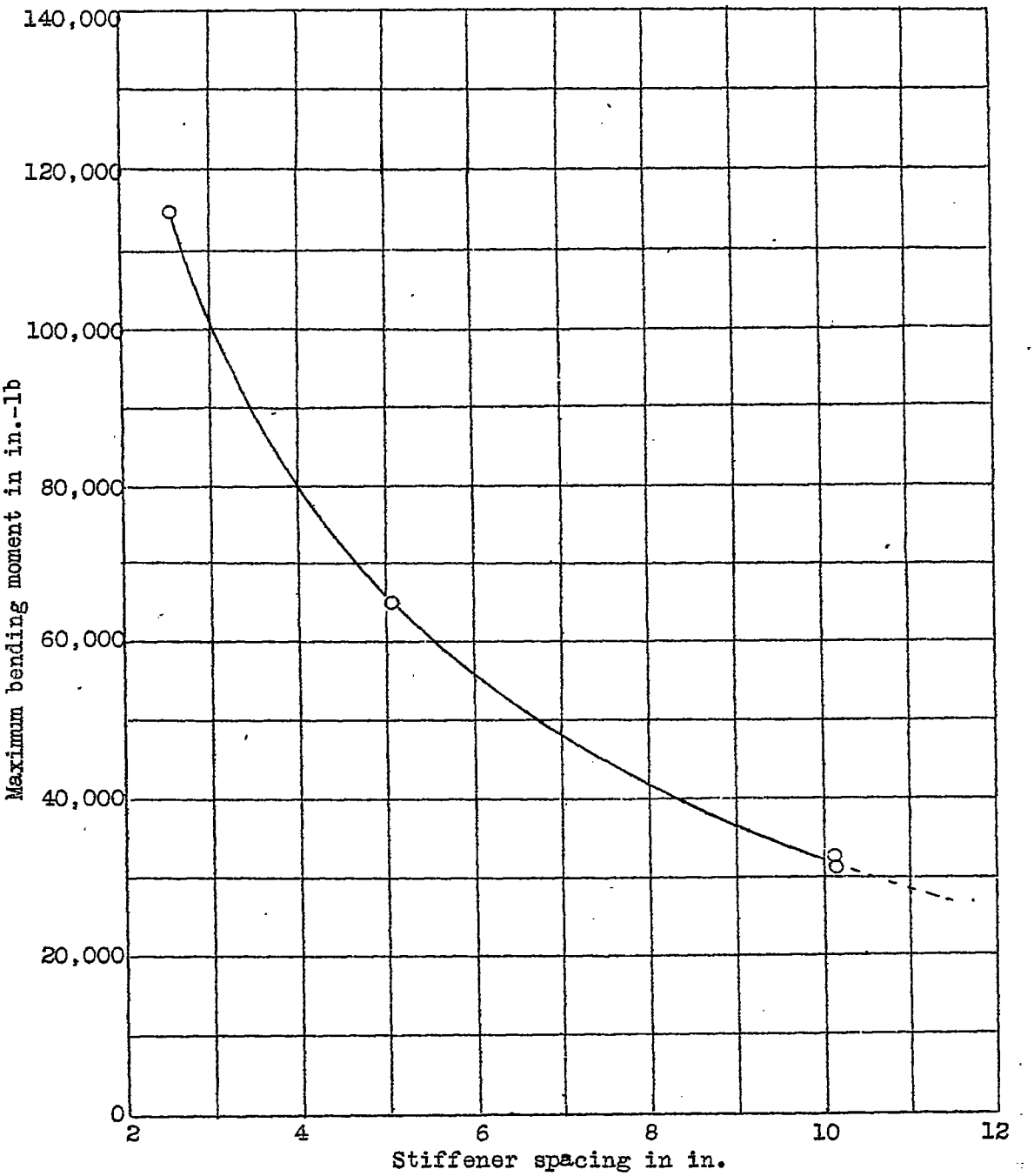

Figure 36.- Relation between bending moment and stiffener spacing, all specimens - 64" long, 31 frames - F_5, all longitudinals - S_1.

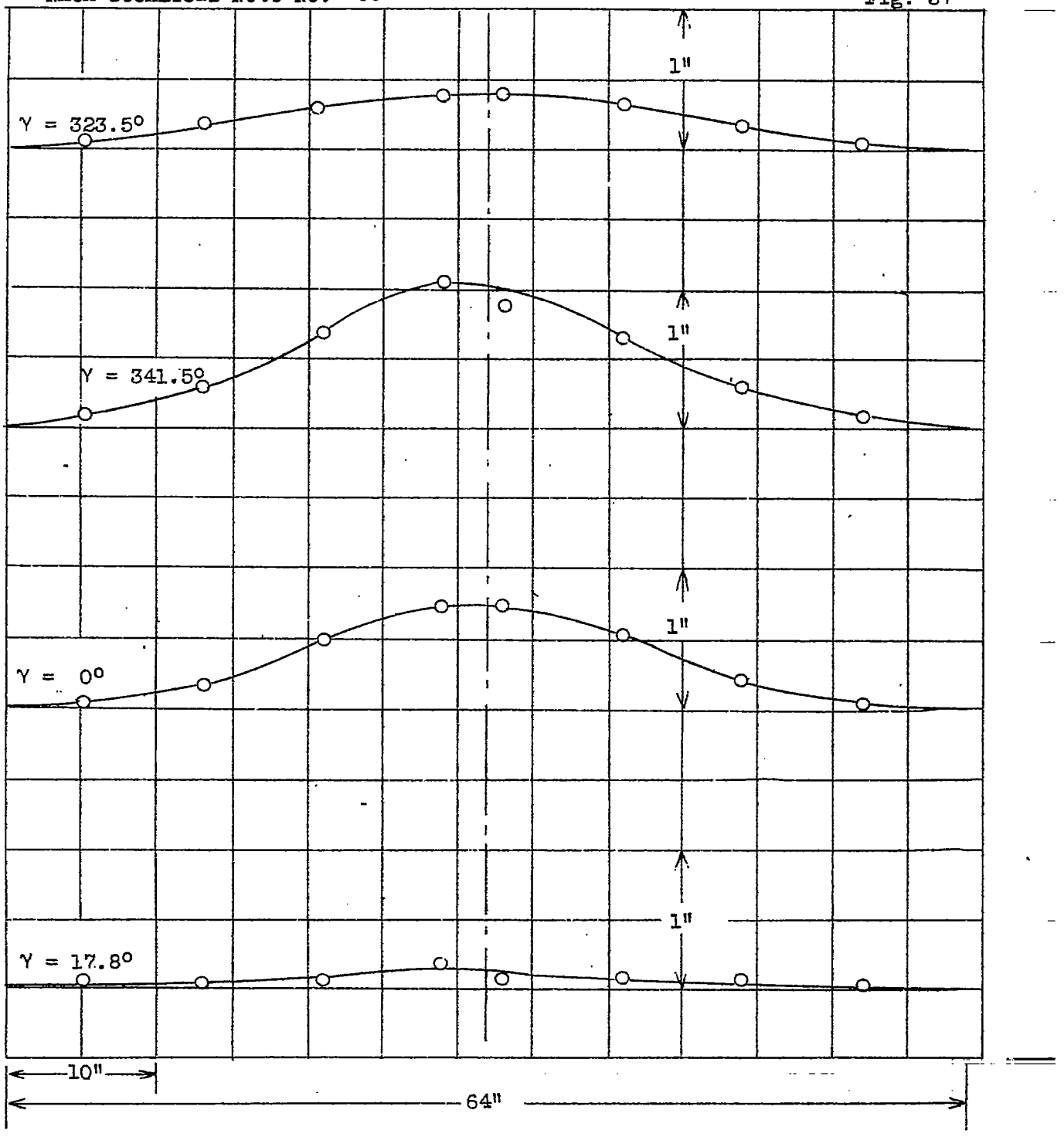

Figure 37.- Test 3, stiffener deflection, 15 frames, frame F_5, 40 stiffener S_1.

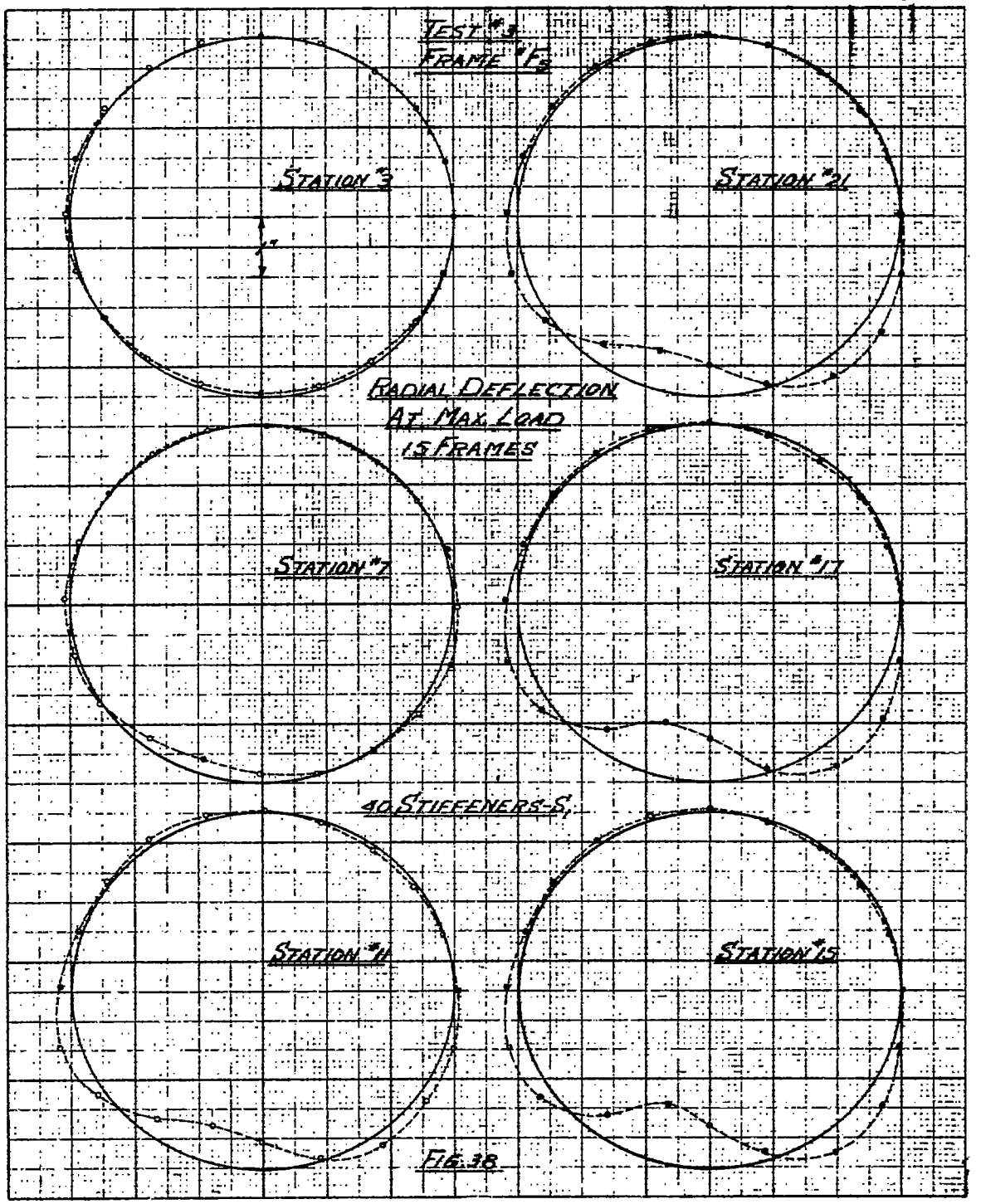
TEST #3
FRAME #F2
STATION #3
STATION #21
RADIAL DEFLECTION
AT MAX. LOAD
15 FRAMES
STATION #7
STATION #17
40 STIFFENERS-S,
STATION #11
STATION #15
FIG. 38

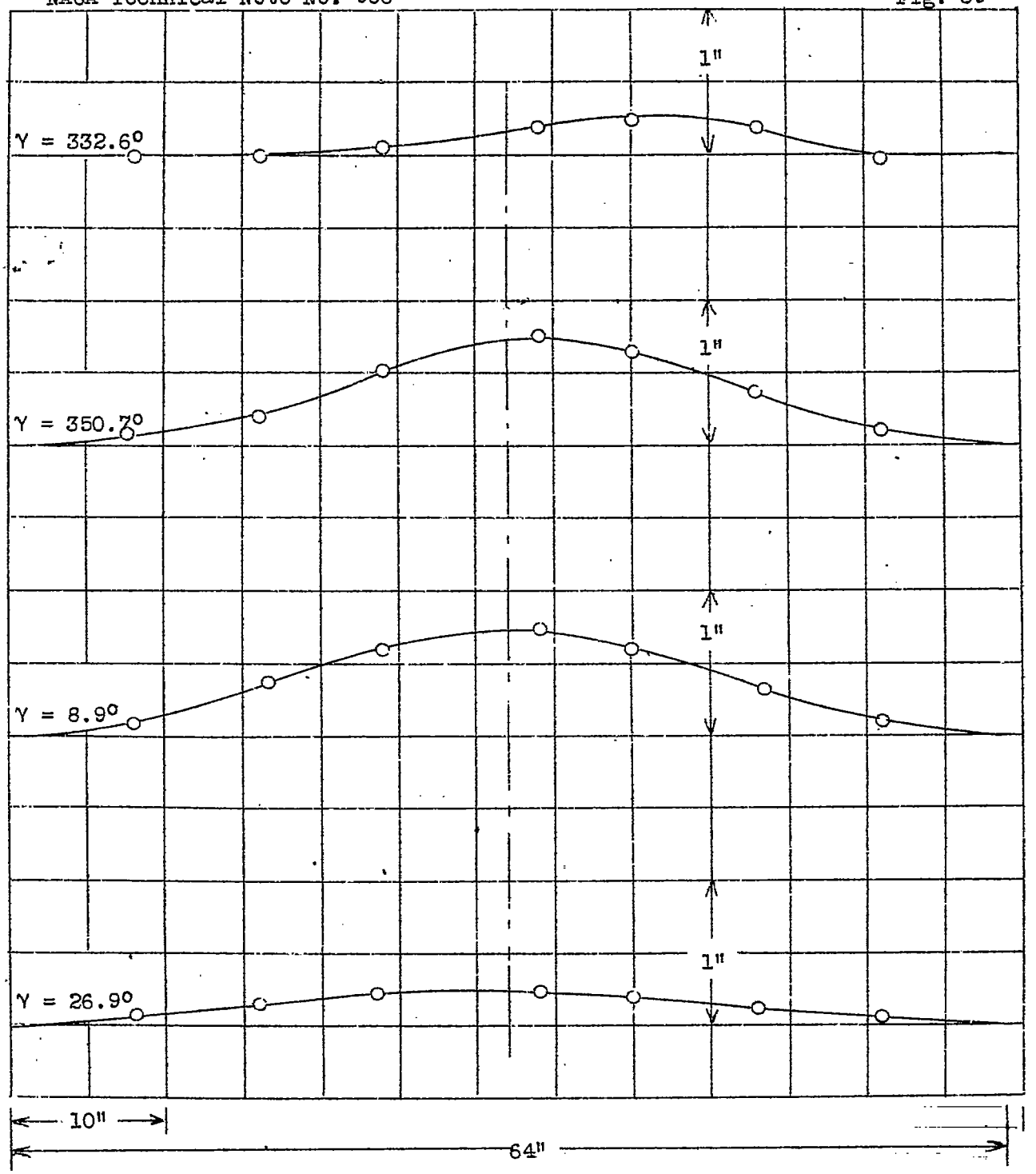

Figure 39.- Test 4, stiffener deflection, 7 frames, frame F_5, 40-stiffener S_1.

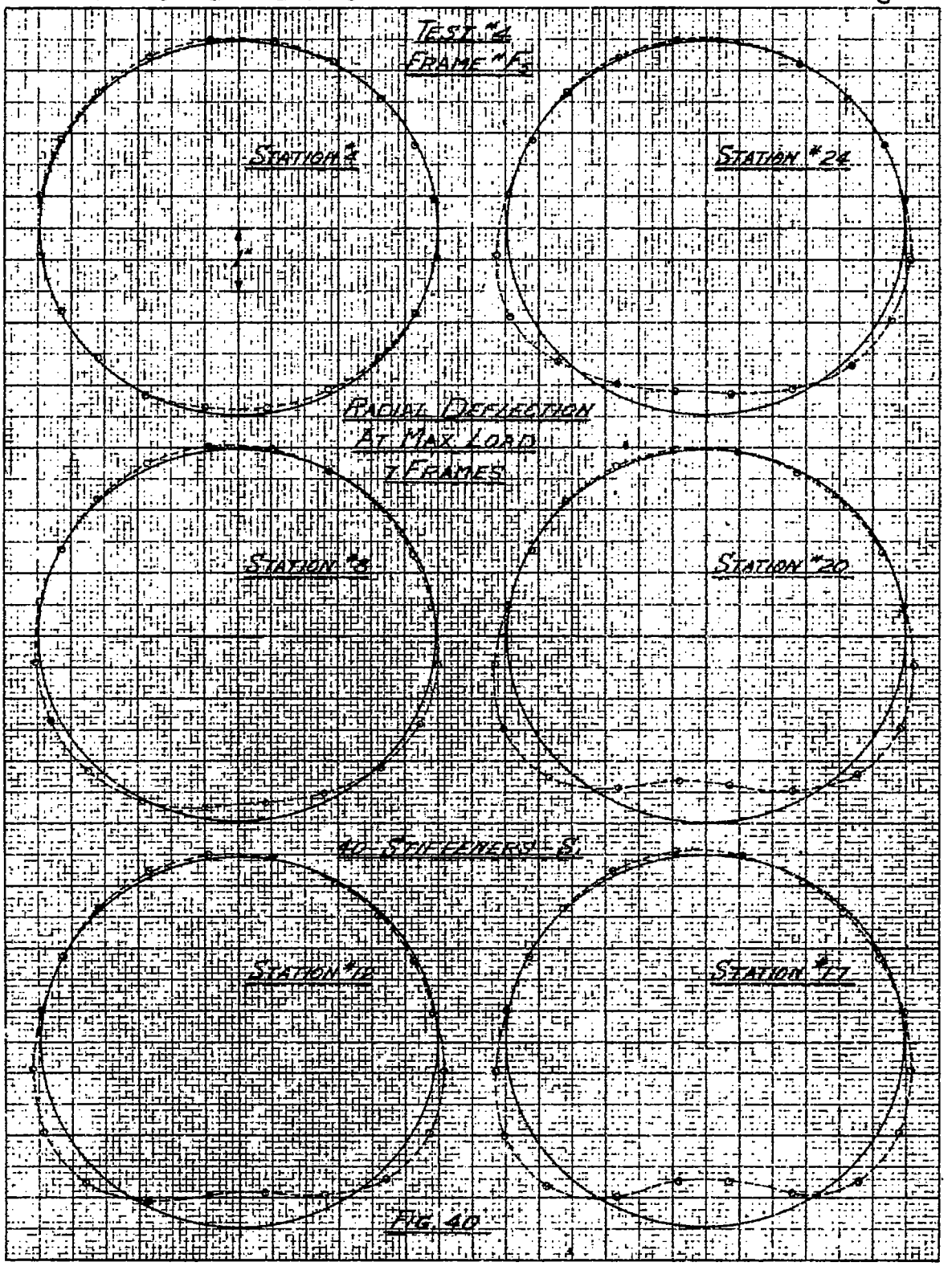
TEST #4
FRAME #F
STATION #4
STATION #24
RADIAL DEFLECTION
AT MAX LOAD
7 FRAMES
STATION #8
STATION #20
40 STIFFENERS
STATION #12
STATION #17
FIG. 40

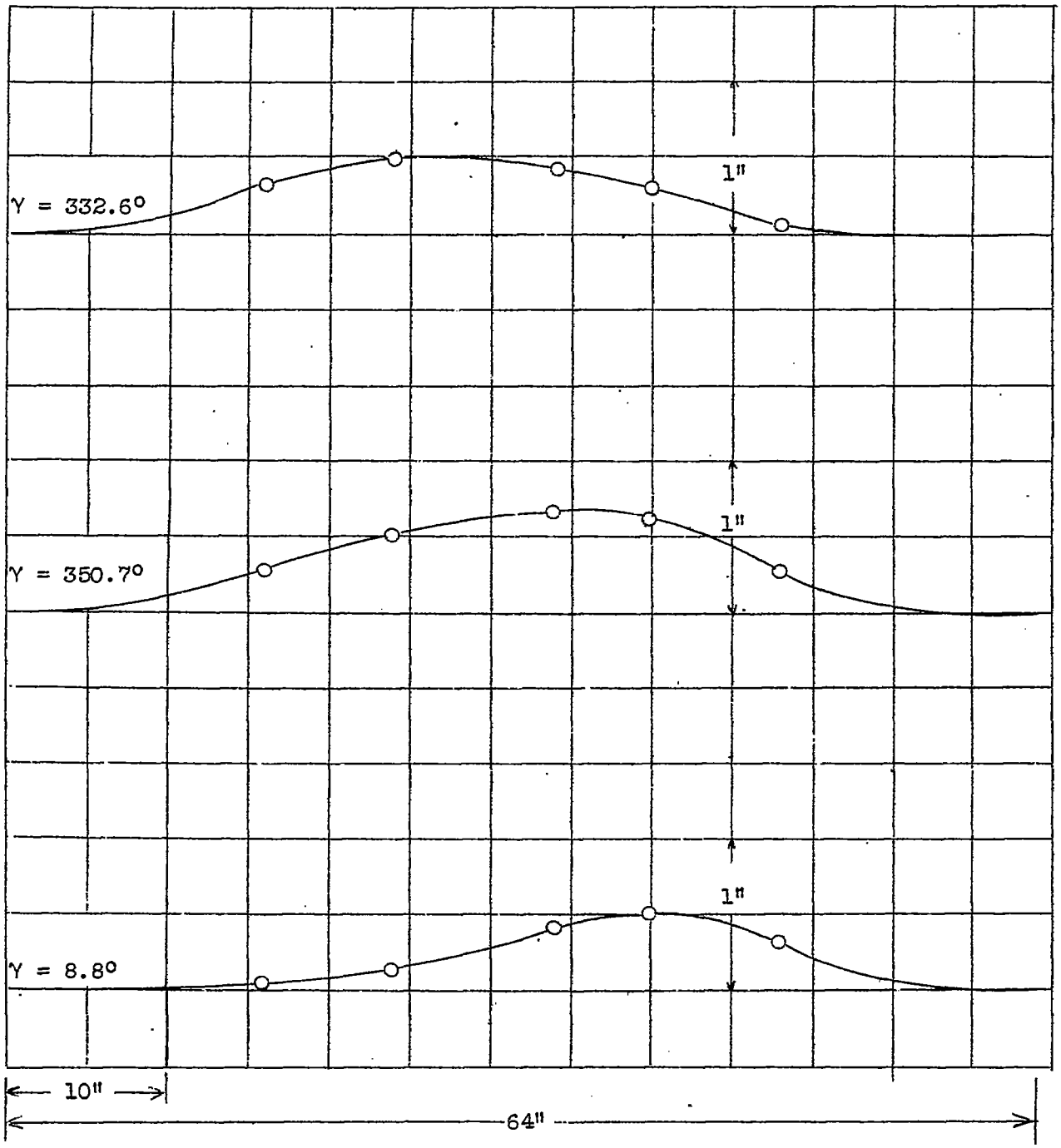

Figure 41.- Test 5, stiffener deflection, 3 frames, frame F_5, stiffener S_1, 40 stiffeners.

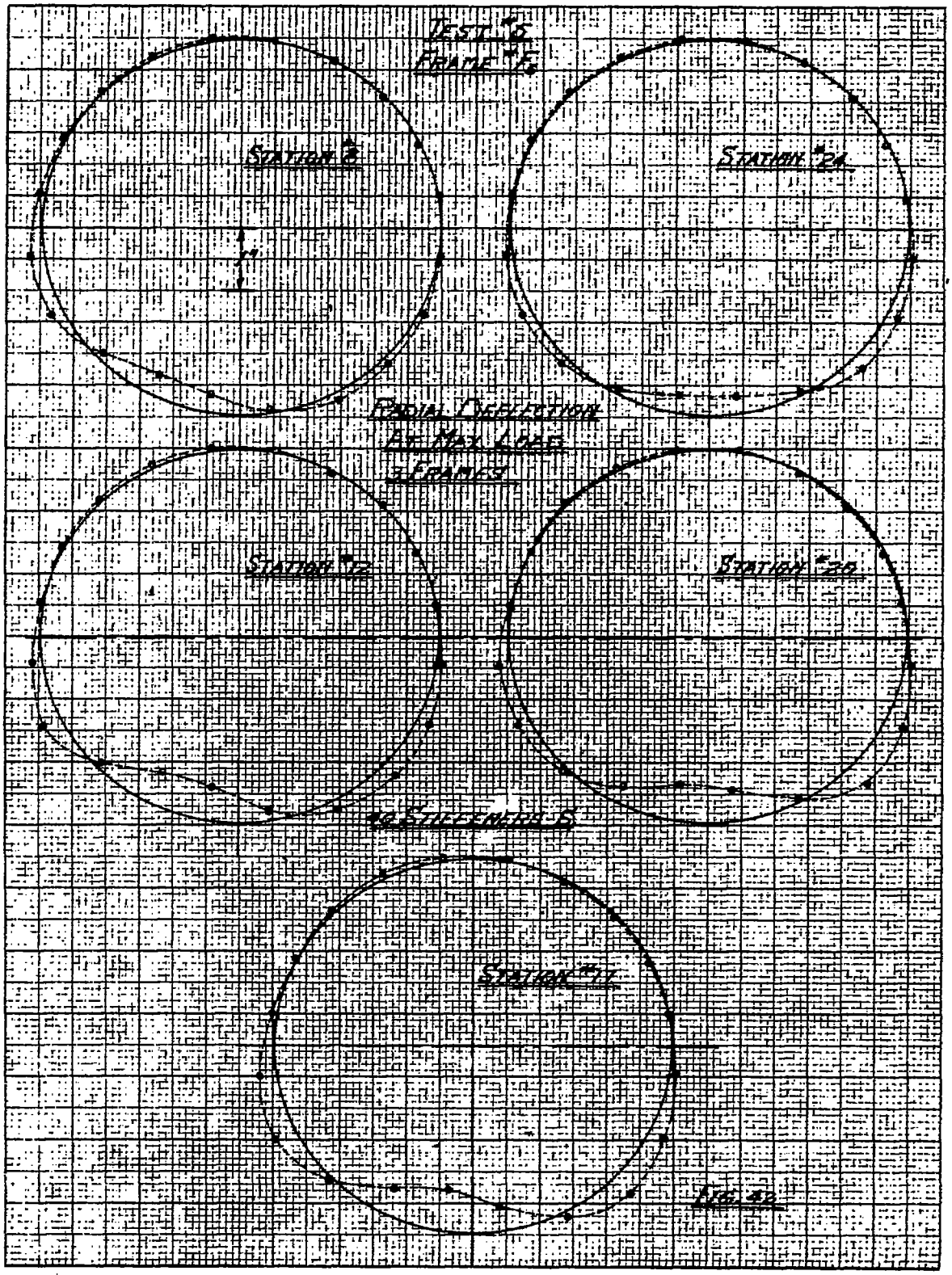
TEST #6
FRAME #6
STATION #8
STATION #24
1"
RADIAL DEFLECTION
AT MAX. LOAD
3 FRAMES
STATION #12
STATION #20
#6 STIFFENERS 5
STATION #16
FIG. 42

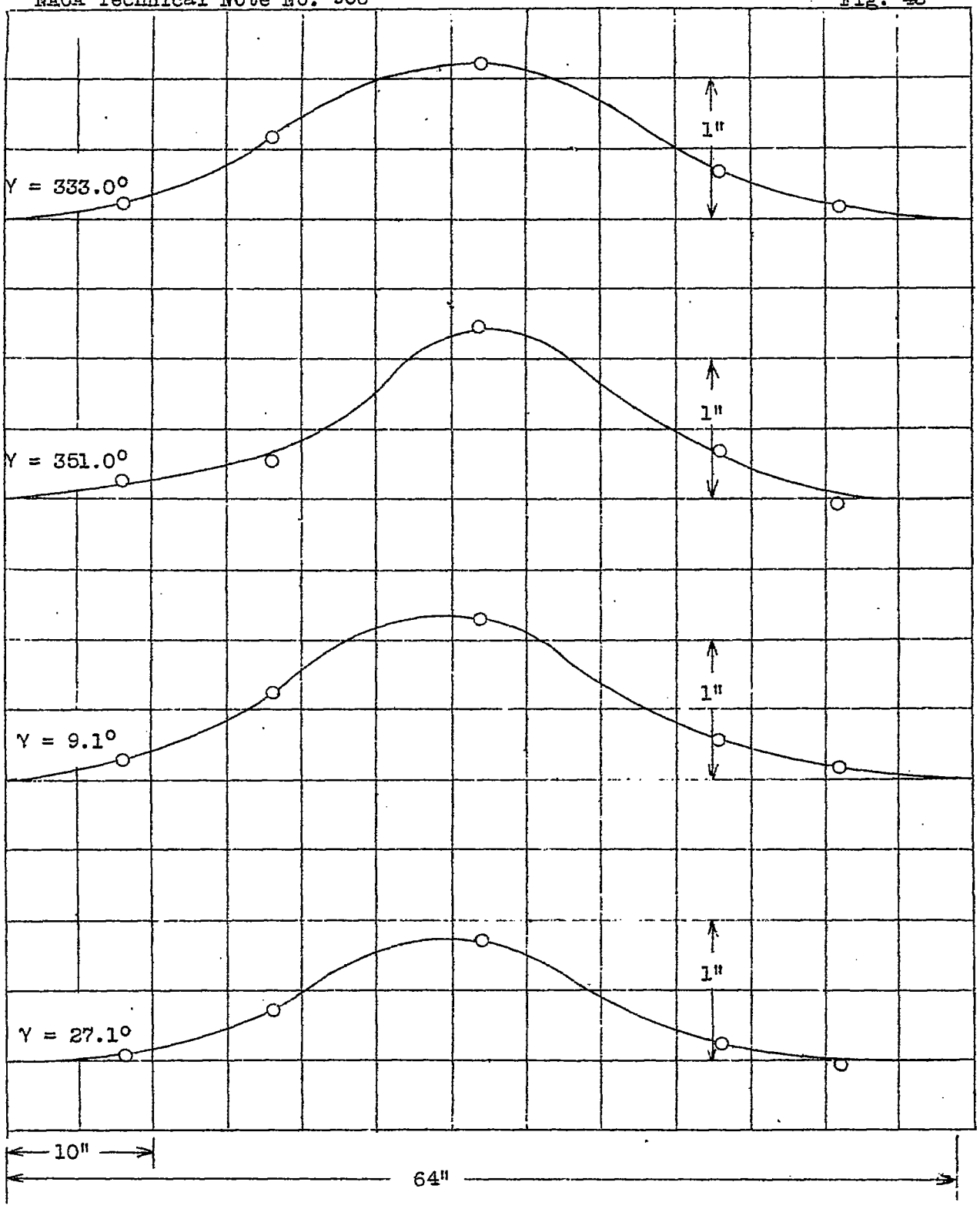

Figure 43.- Test 6, stiffener deflection, 2 frames, frame F_5, stiffener S_1, 40 stiffeners.

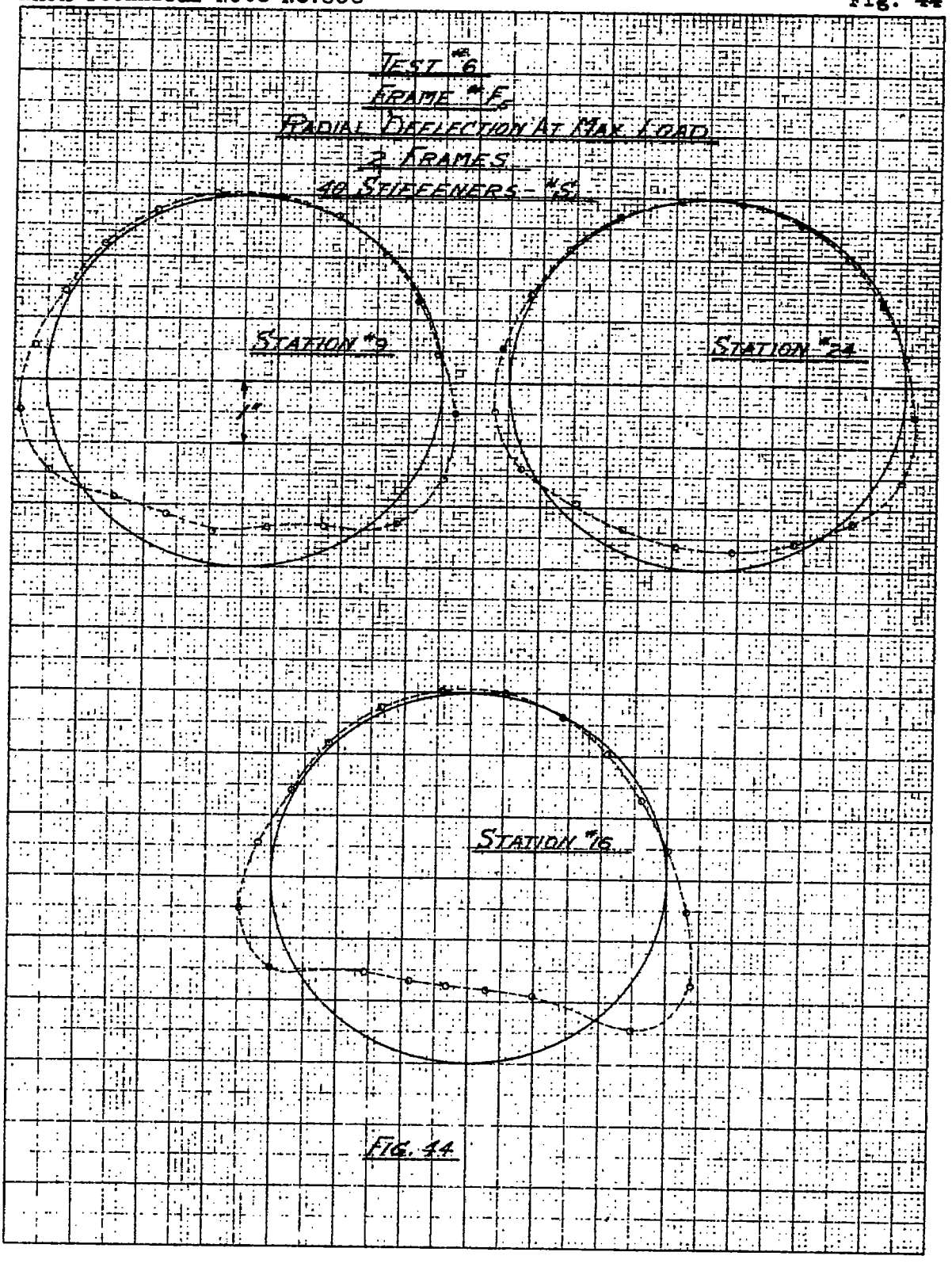
TEST #6
FRAME #F5
RADIAL DEFLECTION AT MAX. LOAD
2 FRAMES
40 STIFFENERS - #S
STATION #9
STATION #24
STATION #16

FIG. 44

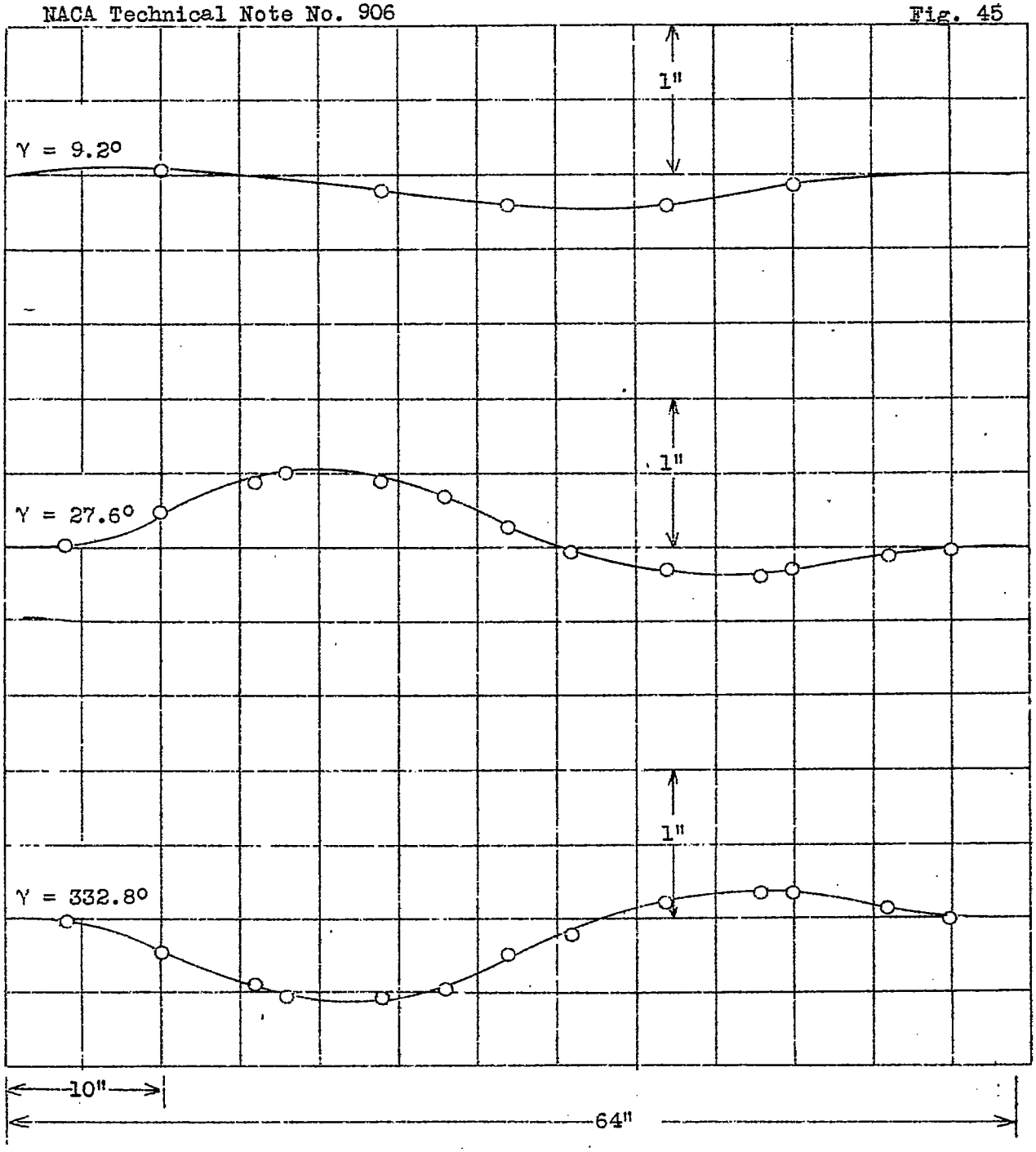

Figure 45.- Test 10, stiffener deflection, 31 frames, frame F_5, stiffener S_1, 40 stiffeners.

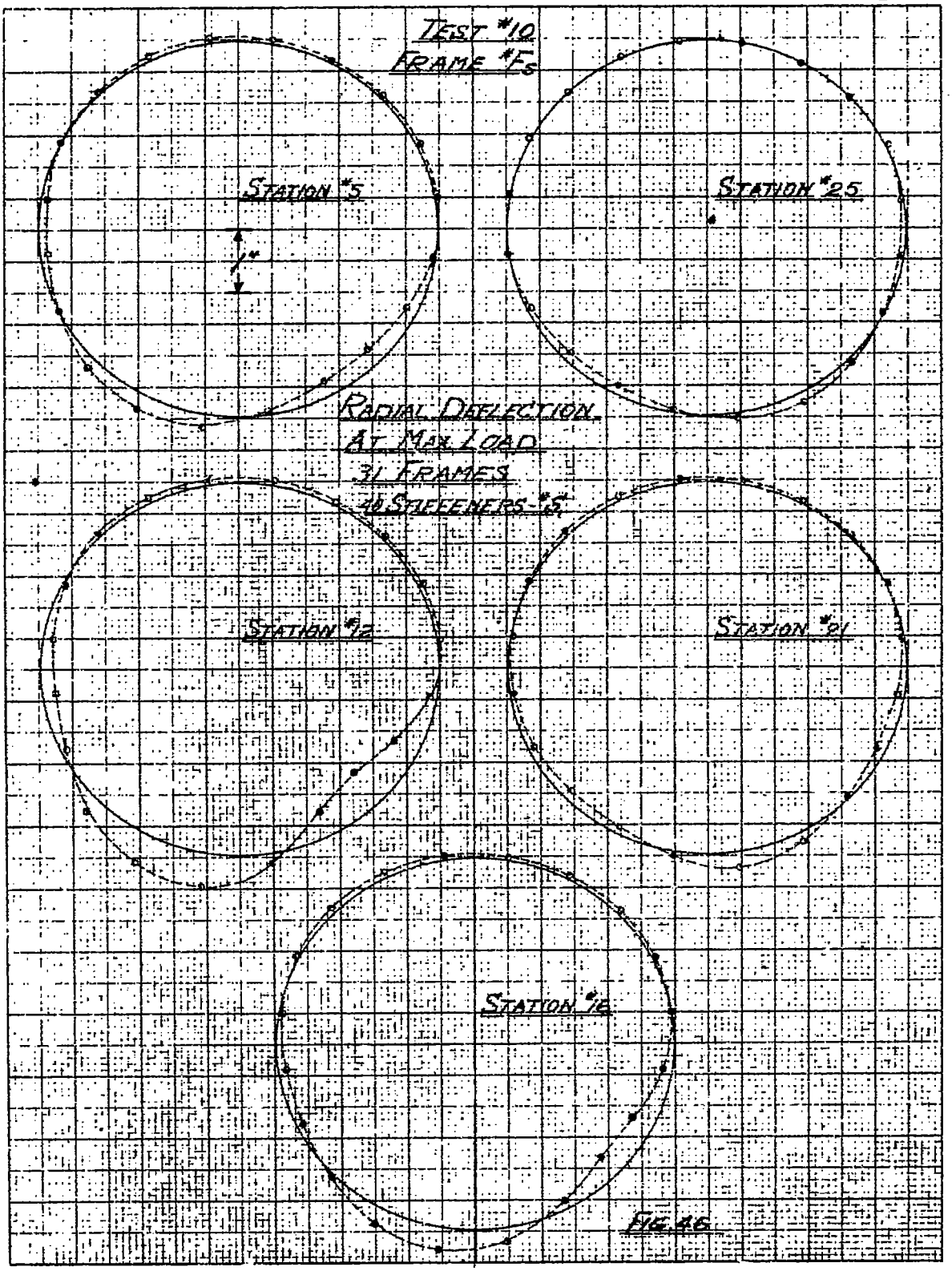
TEST #10
FRAME #F5
STATION #5
1"
STATION #25
RADIAL DEFLECTION
AT MAX LOAD
31 FRAMES
16 STIFFENERS #5
STATION #12
STATION #21
STATION #16
FIG. 46

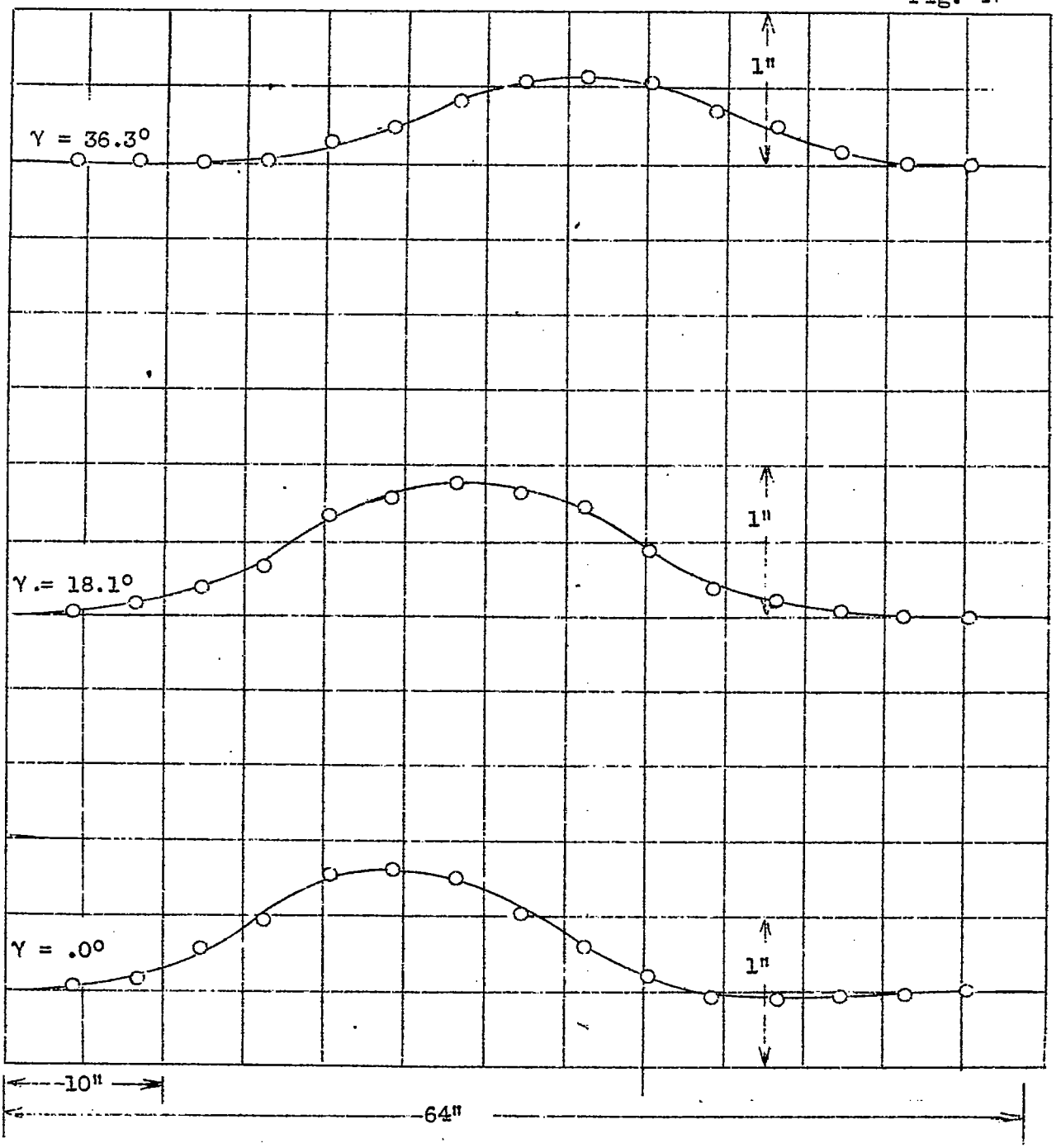

Figure 47.- Test 13, stiffener deflection, 31 frames, frame F_5, stiffener S_1, 20 stiffeners.

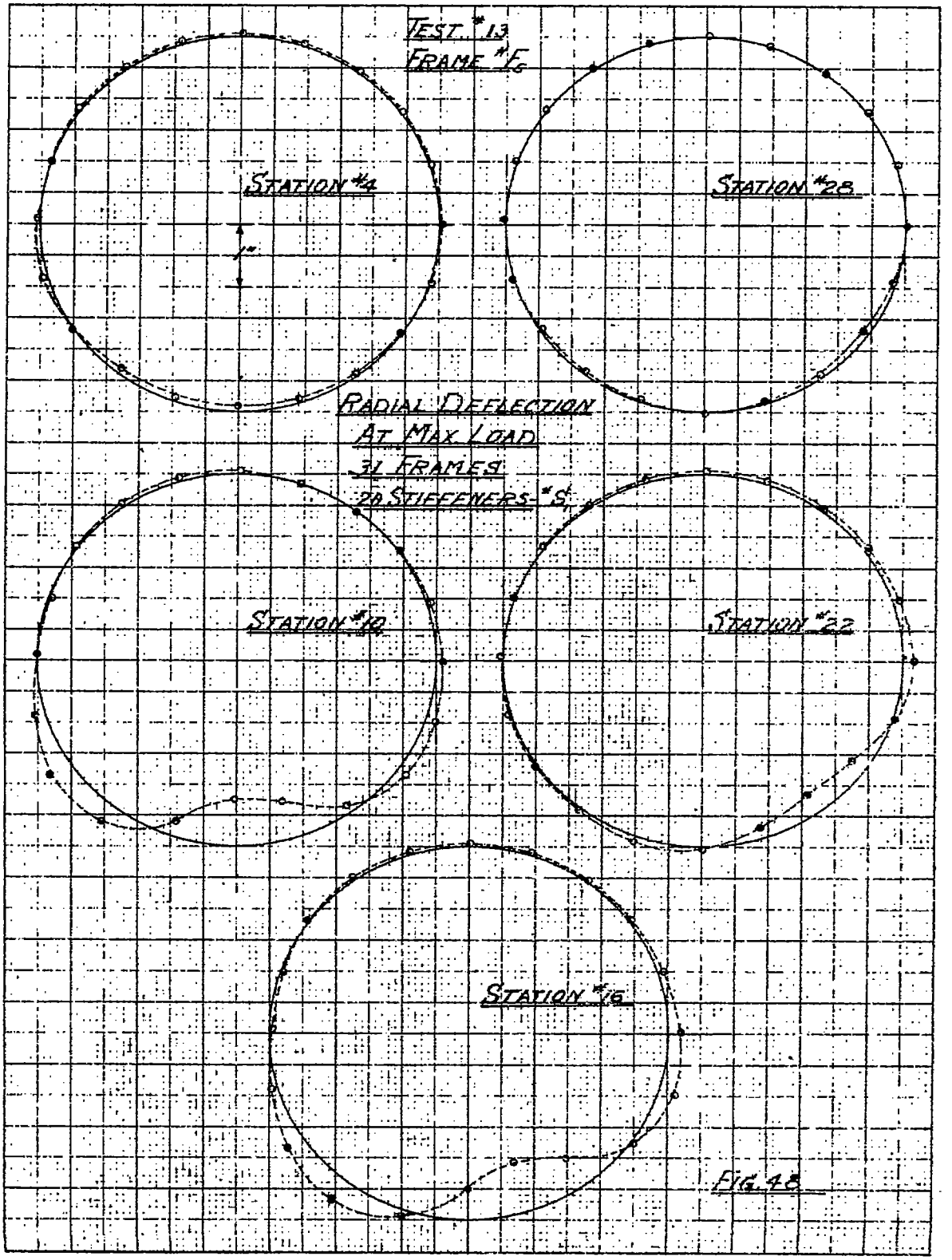
TEST #13
FRAME #F6
STATION #4
STATION #28
1"
RADIAL DEFLECTION
AT MAX LOAD
31 FRAMES
28 STIFFENERS-#S1
STATION #10
STATION #22
STATION #16
FIG. 48

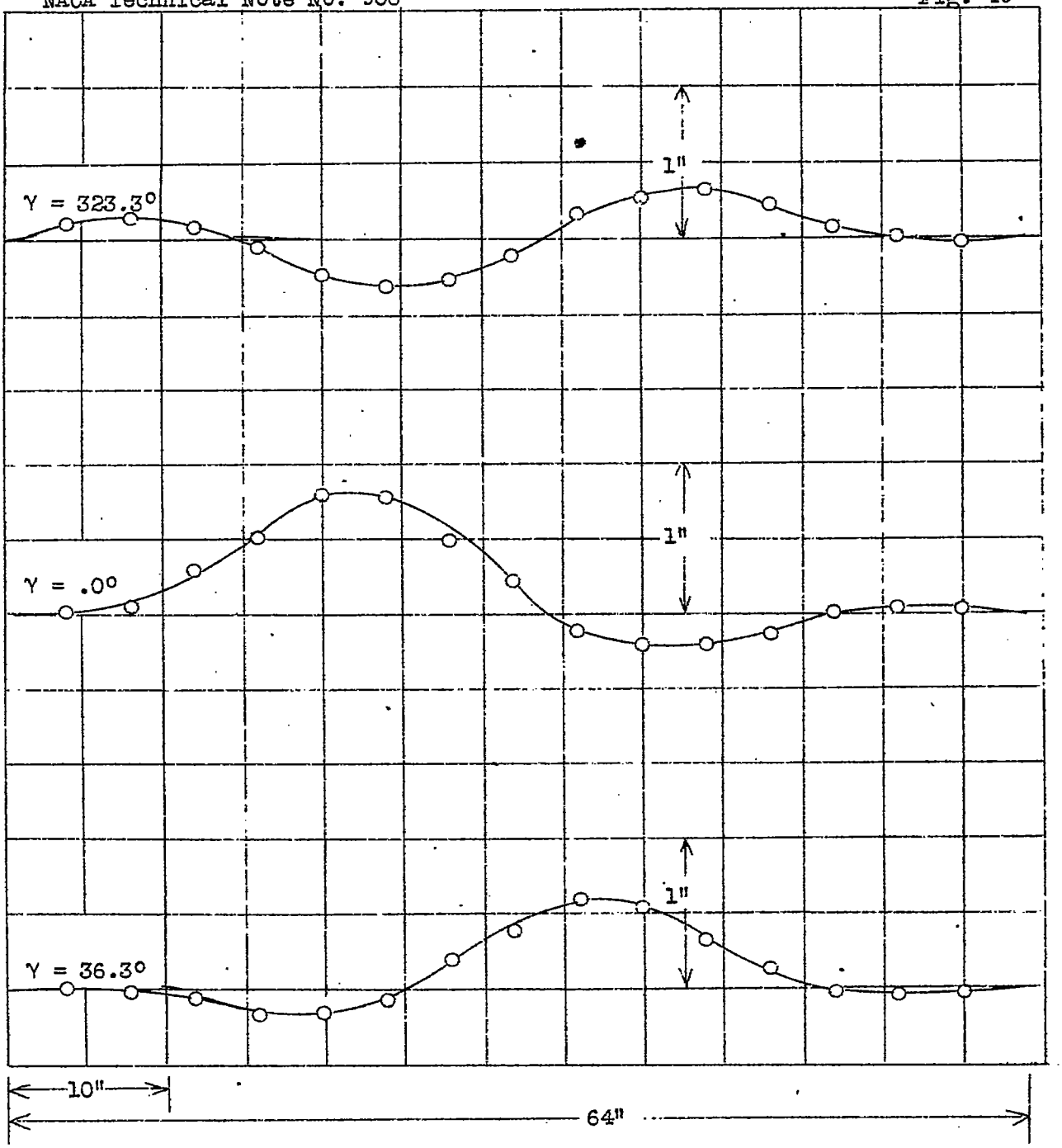

Figure 49.- Test 14, stiffener deflection, 31 frames, frame F_5, stiffener S_1, 10 stiffeners.

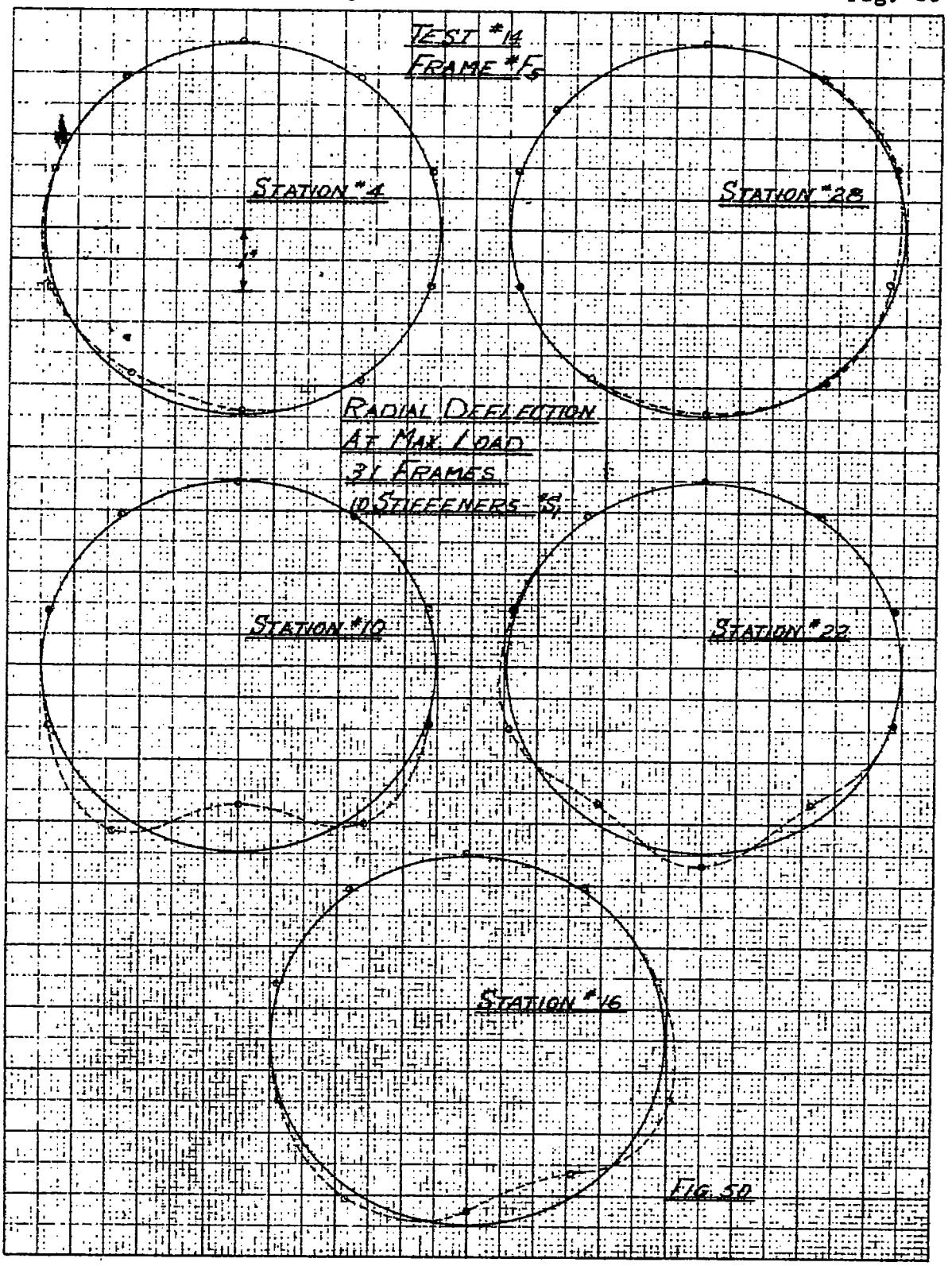
TEST #14
FRAME #F5
STATION #4
STATION #28
RADIAL DEFLECTION
AT MAX. LOAD
31 FRAMES
10 STIFFENERS #S1
STATION #10
STATION #22
STATION #16
FIG. 50

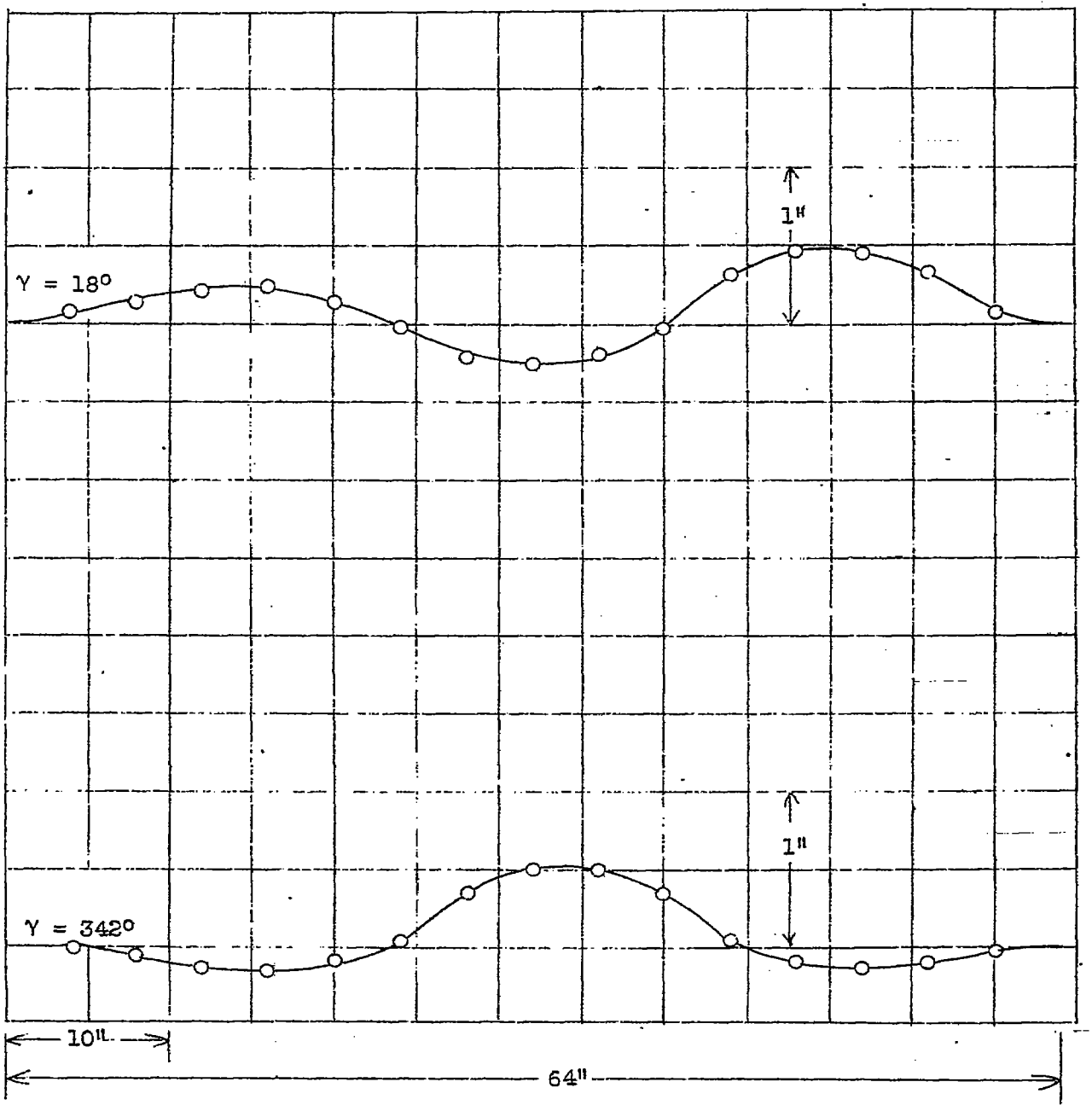

Figure 51.- Test, stiffener deflection, 31 frames, frame F_5, stiffener S_1, 10 stiffeners.

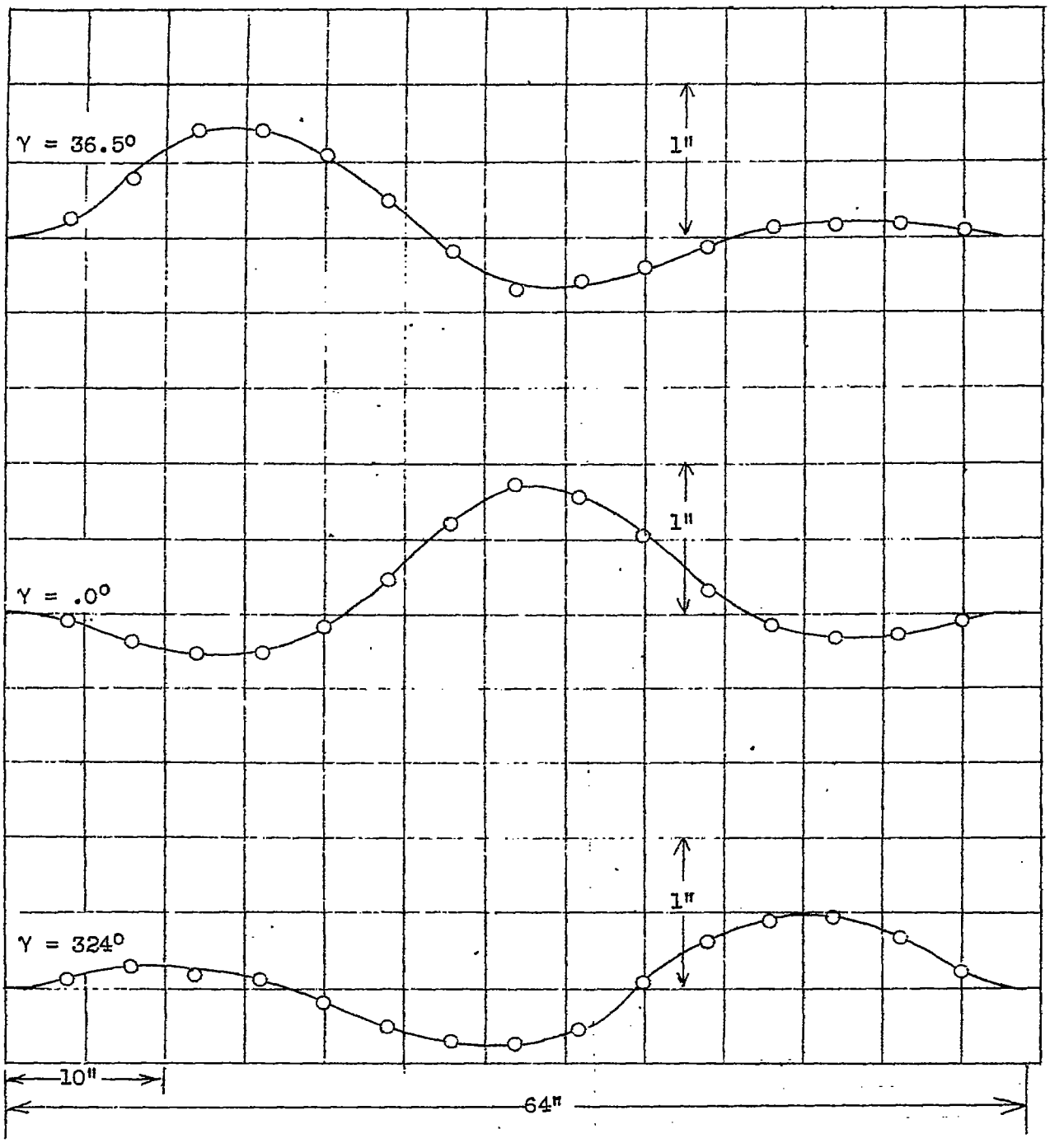

Figure 52.- Test 16, stiffener deflection, 16 frames, frame F_5, stiffener S_1, 10 stiffeners.

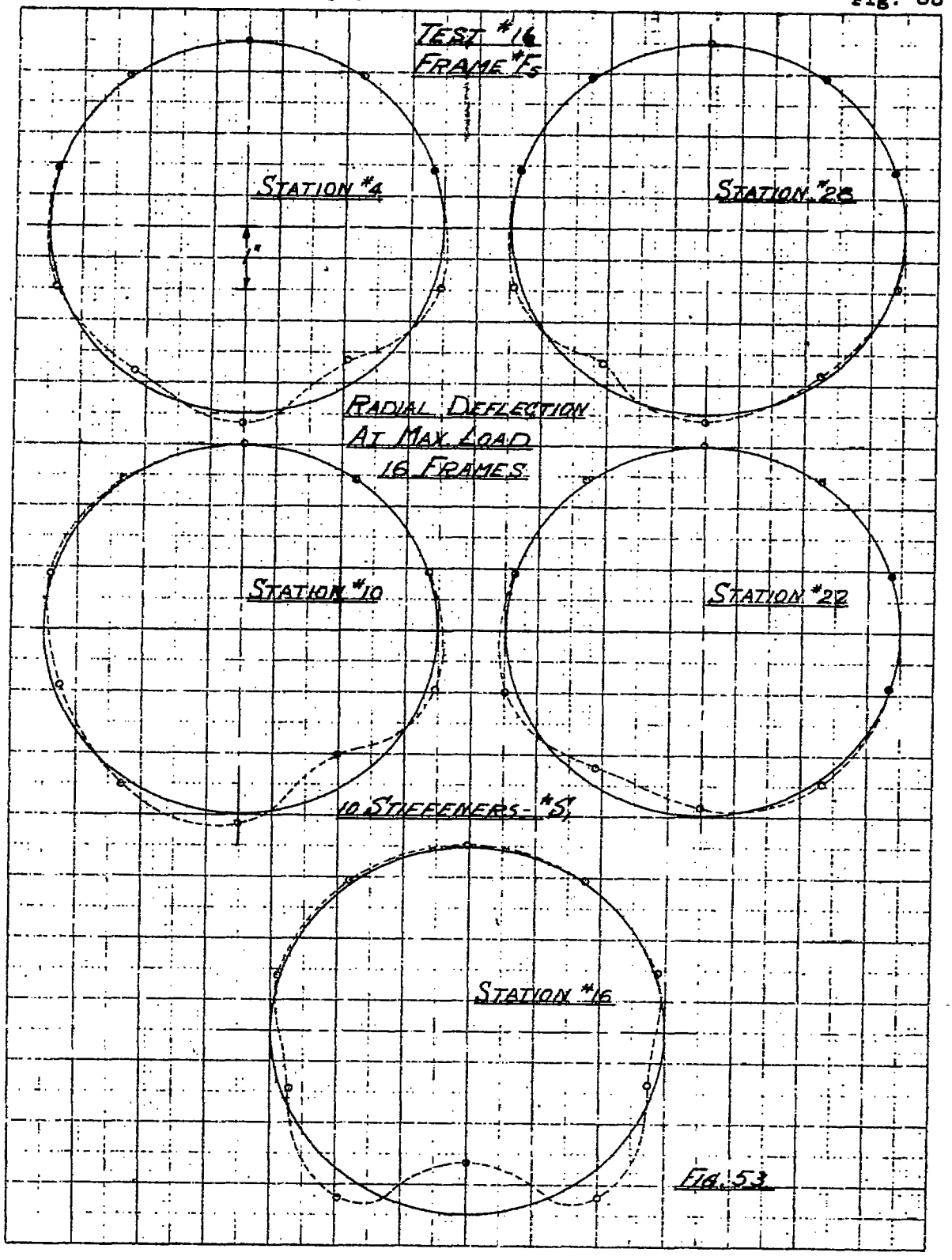
TEST #16
FRAME #F5
STATION #4
STATION #28
1"
RADIAL DEFLECTION
AT MAX. LOAD
16 FRAMES
STATION #10
STATION #22
10 STIFFENERS - #S1
STATION #16

FIG. 53

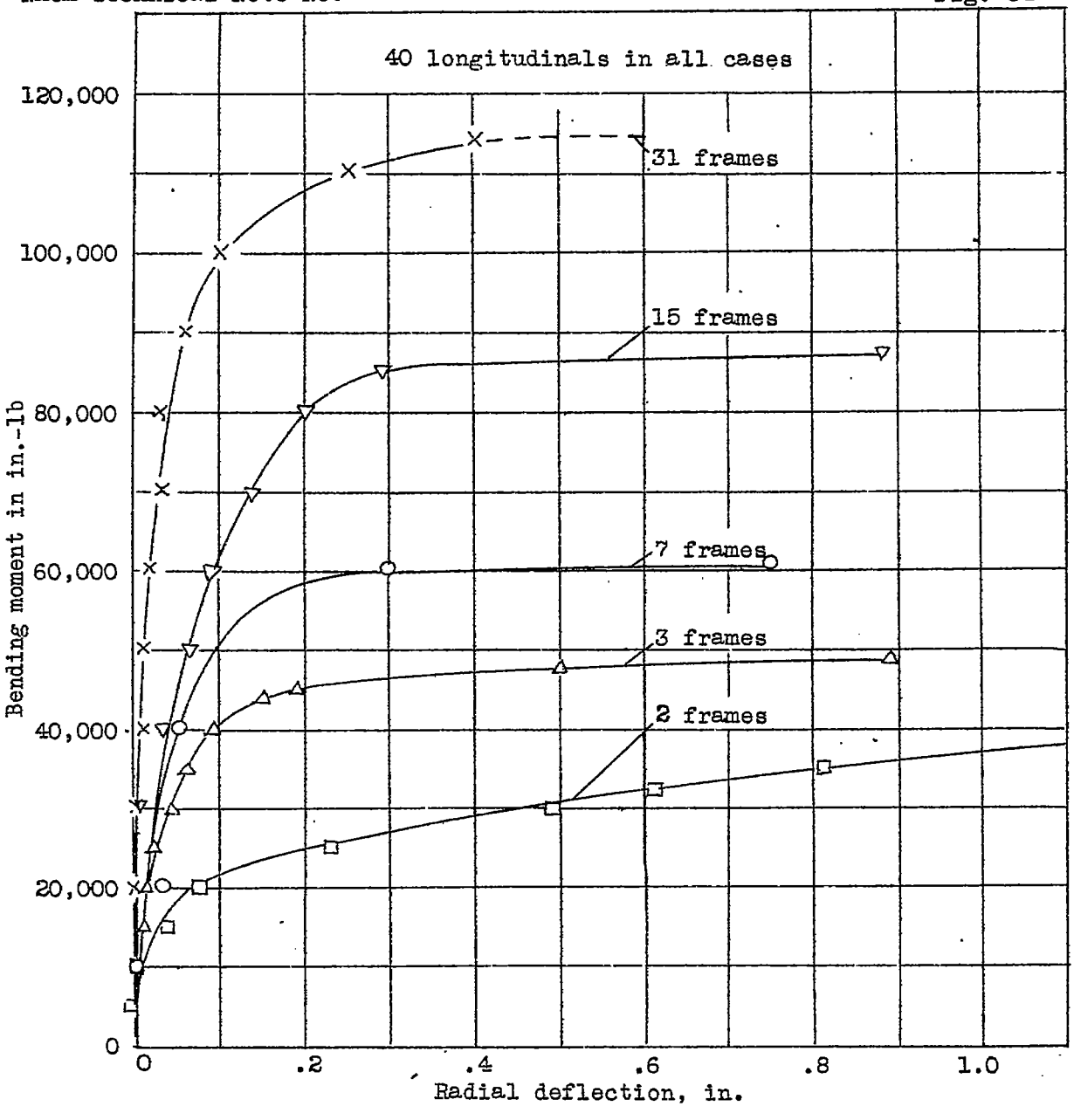

Figure 54.- Maximum radial deflection of frame at station 16 as a function of applied bending moment.

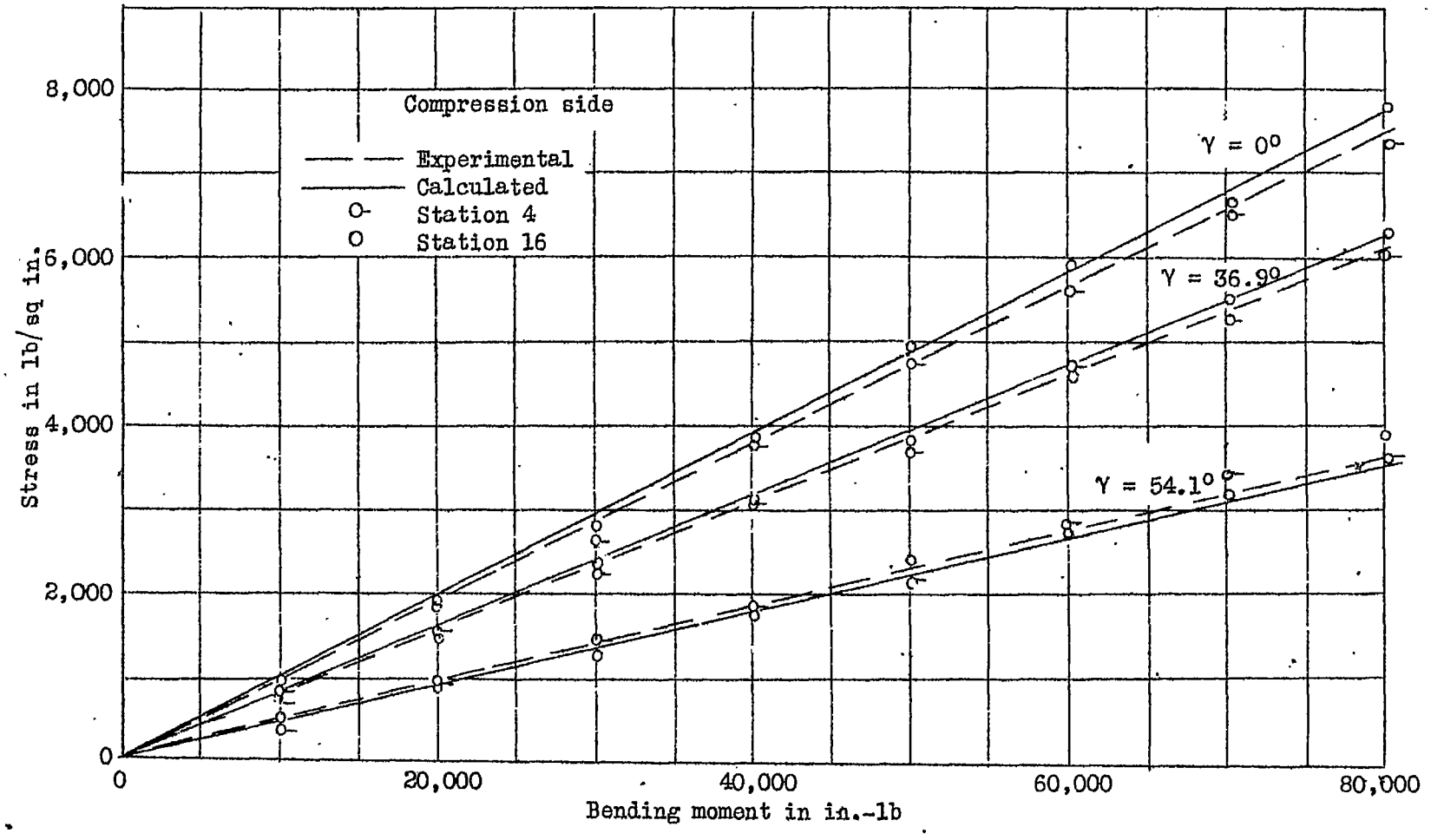
Compression side
Experimental
Calculated
Station 4
Station 16
γ = 0°
γ = 36.9°
γ = 54.1°
Stress in lb/sq in.
8,000
6,000
4,000
2,000
0
0
20,000
40,000
60,000
80,000
Bending moment in in.-lb

Figure 55.-

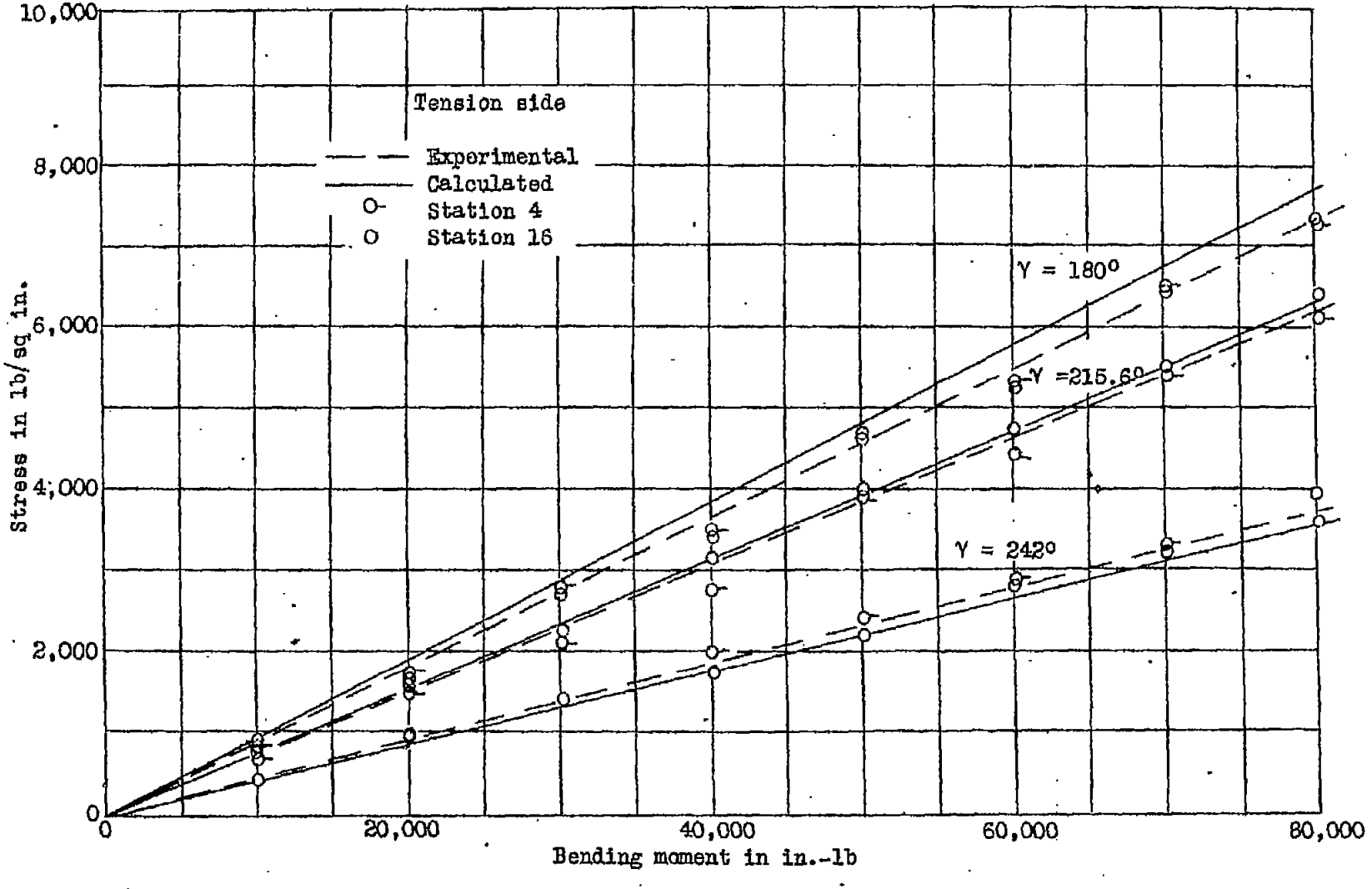
Tension side
Experimental
Calculated
Station 4
Station 16
γ = 180°
γ = 215.6°
γ = 242°
Stress in lb/sq in.
Bending moment in in.-lb
0
2,000
4,000
6,000
8,000
10,000
20,000
40,000
60,000
80,000

Figure 56.-

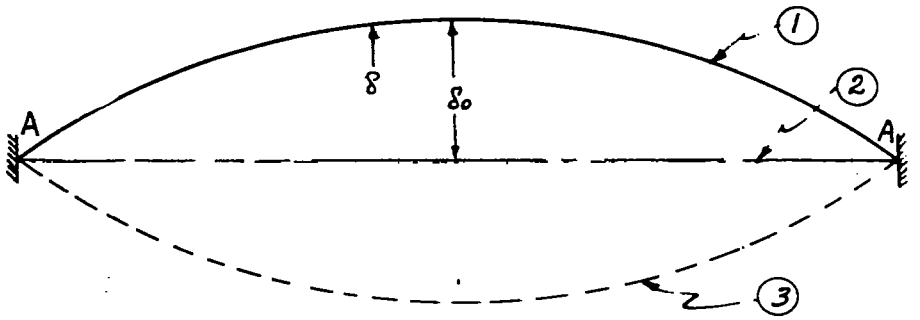

FIG 57

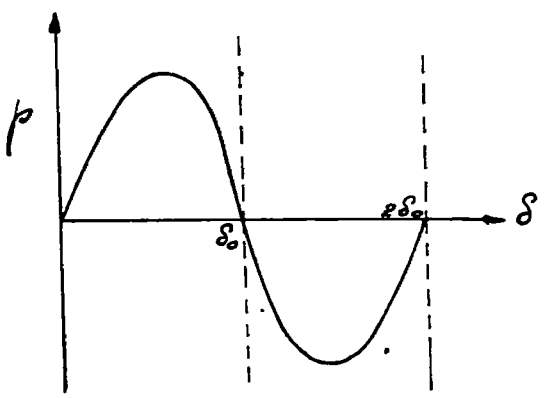

FIG. 58 a

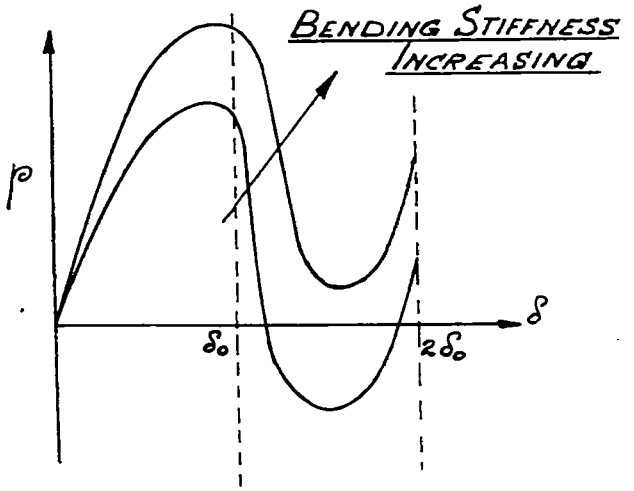

FIG 58 b

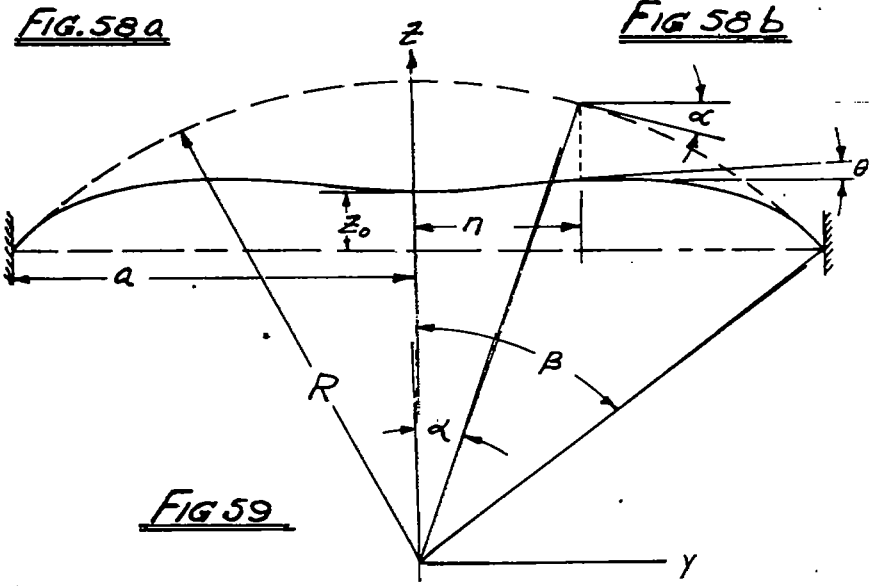

FIG 59

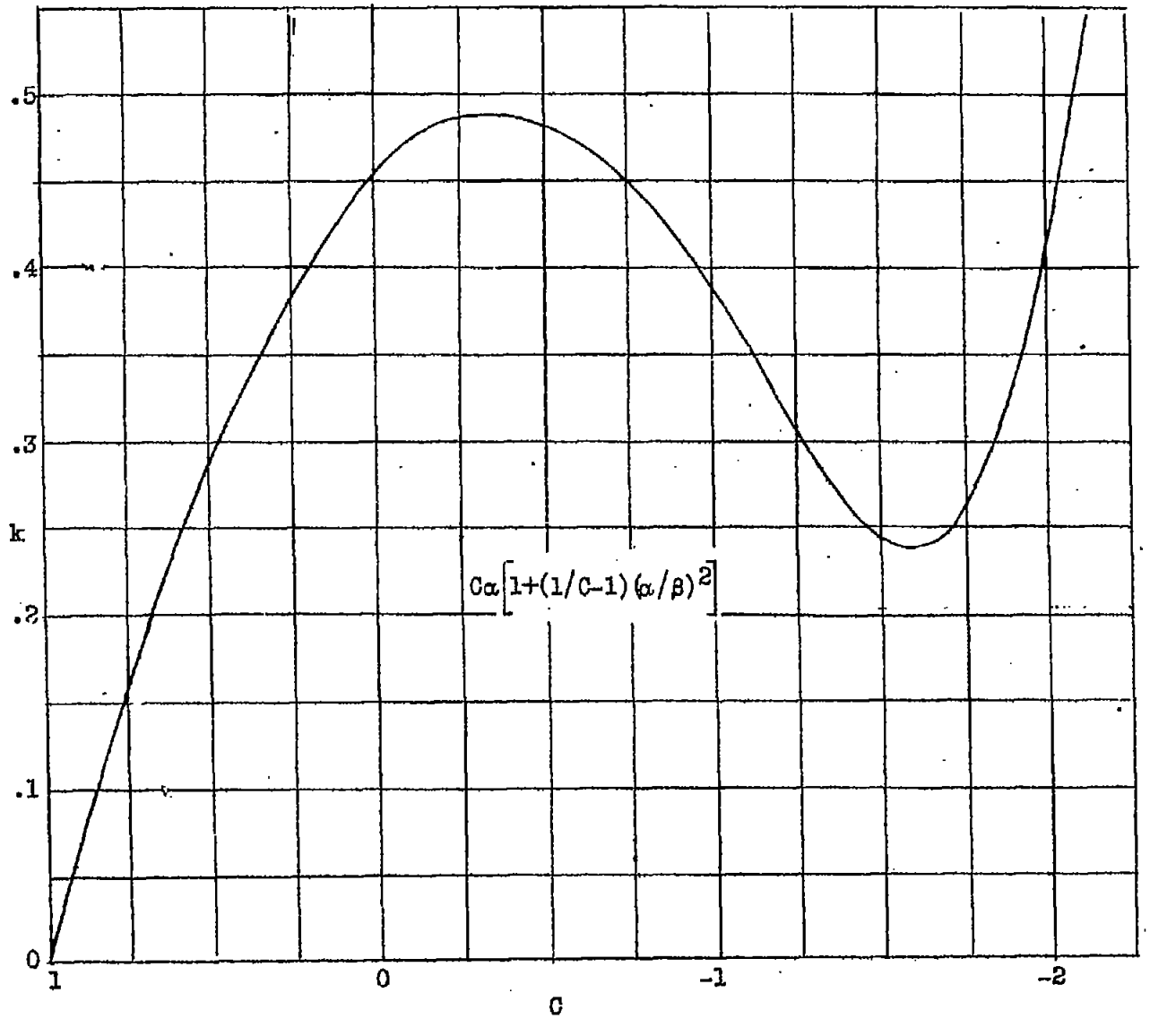

Figure 60.- $\sigma = kE(t/R)$ - clamped ends.

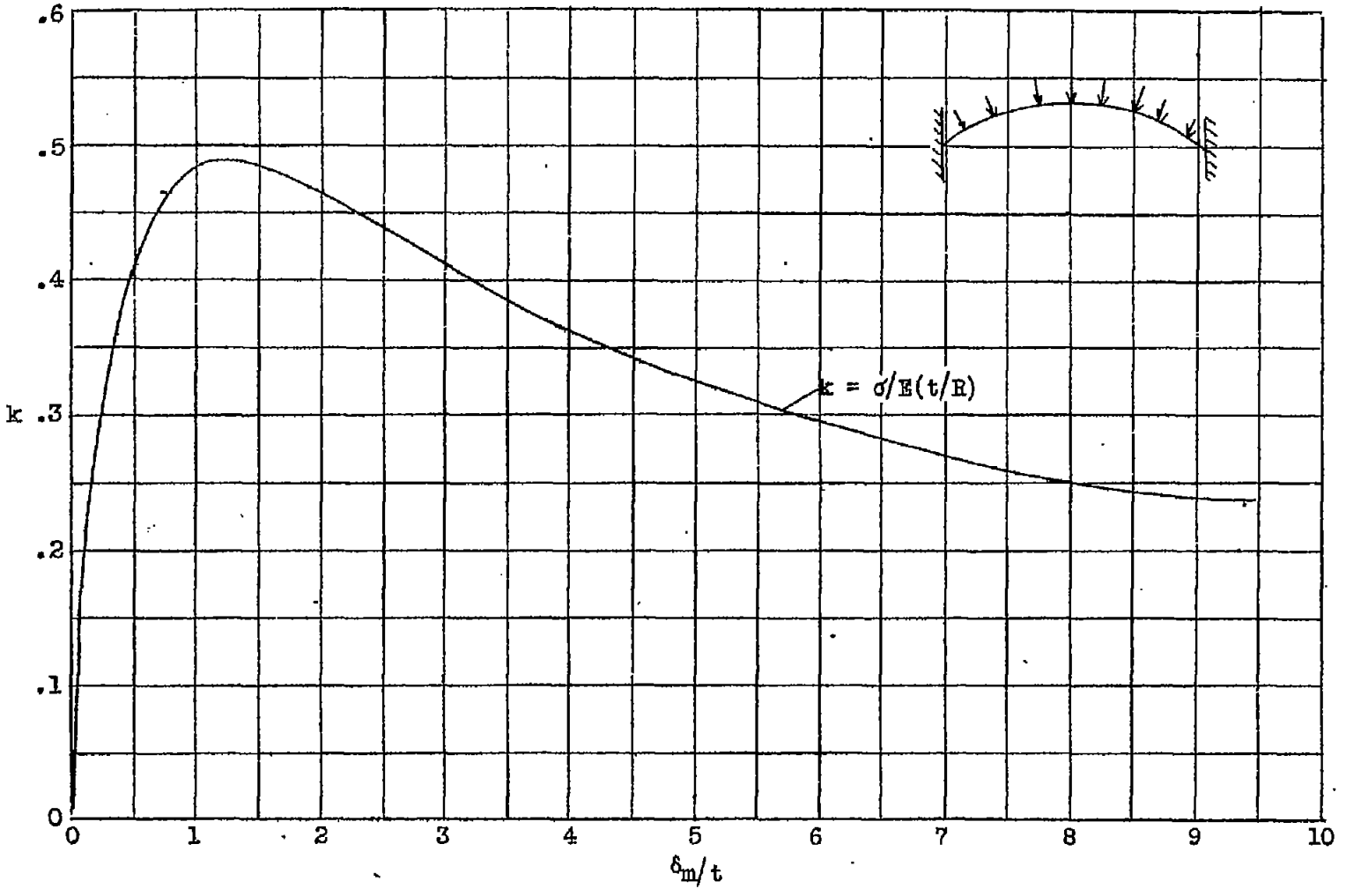

Figure 61.-

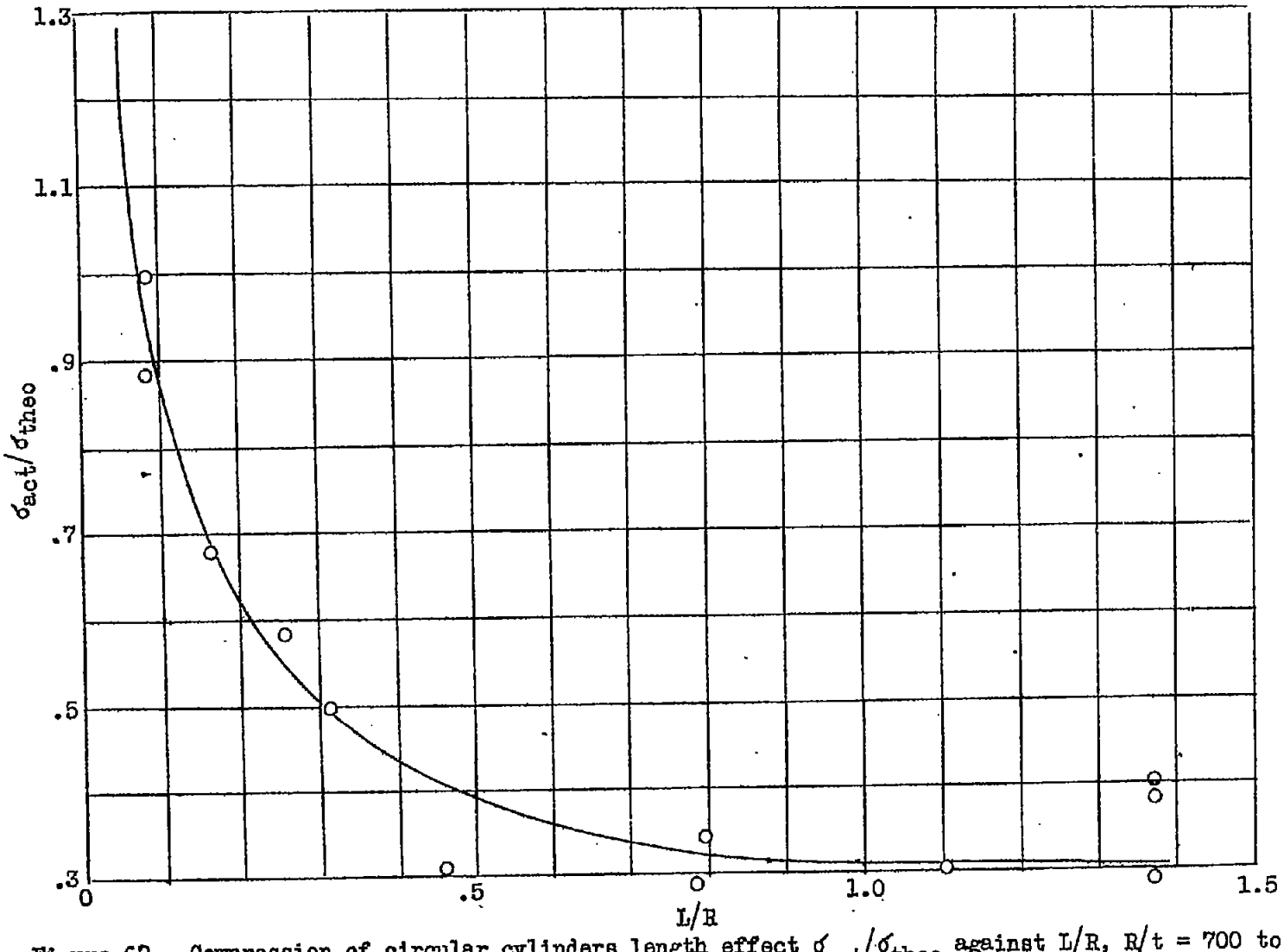

Figure 62.- Compression of circular cylinders length effect $\sigma_{act}/\sigma_{theo}$ against L/R, R/t = 700 to 750, radius 6.375", material steel.

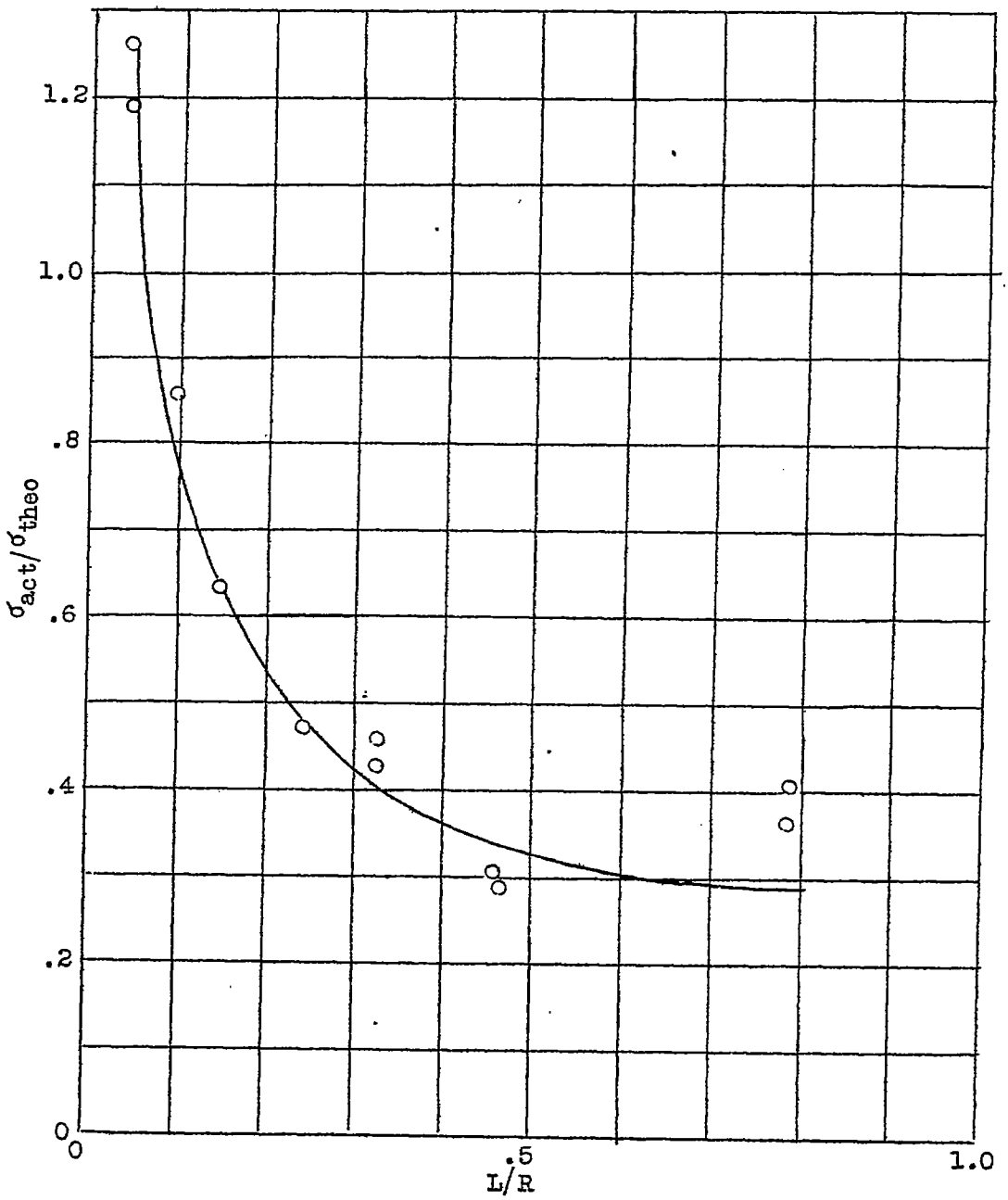

Figure 63.- Compression of circular cylinders length effect, $\sigma_{act}/\sigma_{theo}$ against L/R, R/t = 1081, radius = 6.375", material steel.

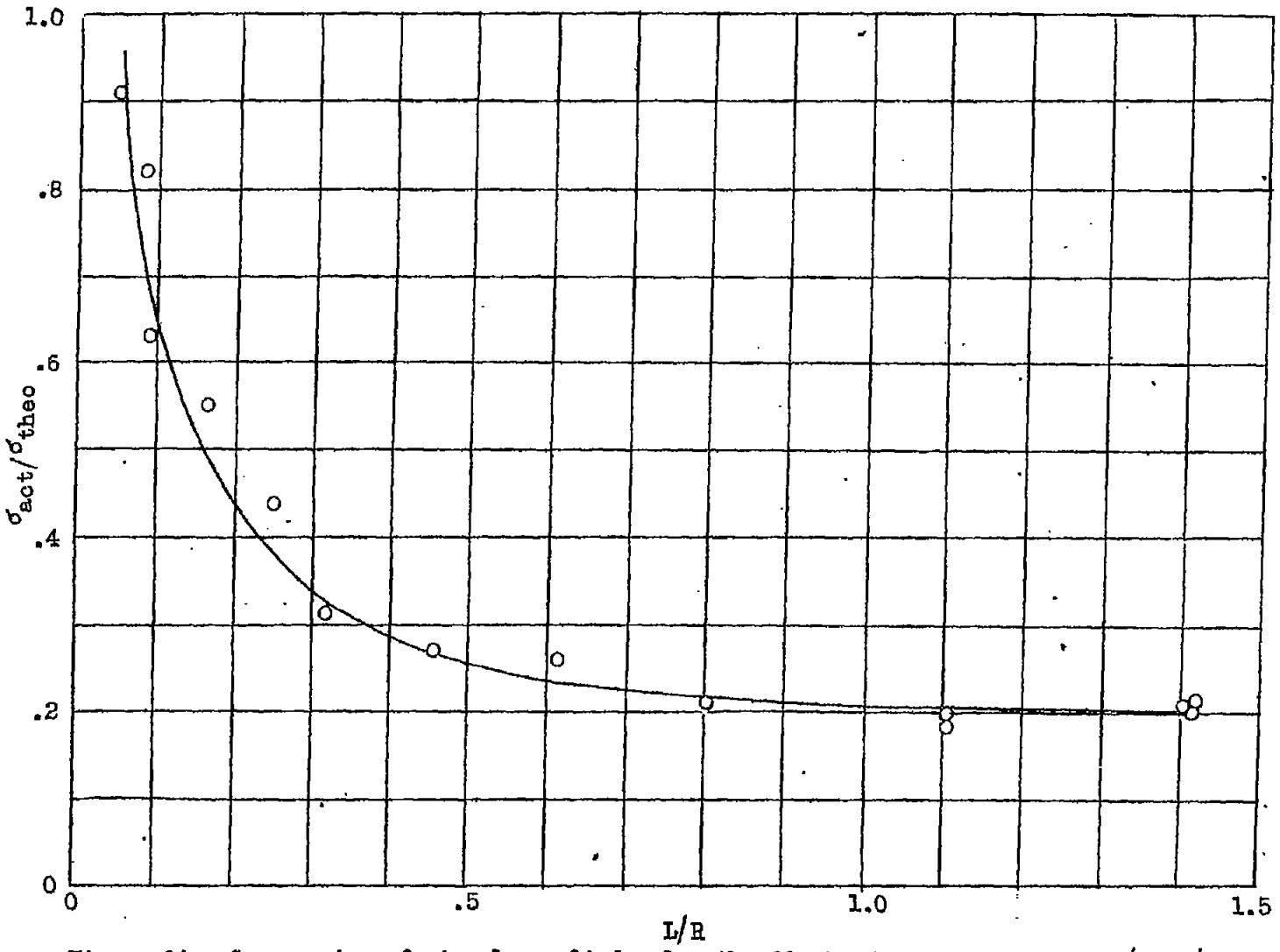

Figure 64.- Compression of circular cylinder length effect, $\sigma_{act}/\sigma_{theo}$ against L/R, R/t = 1150 to 1250, radius = 6.375", material steel.

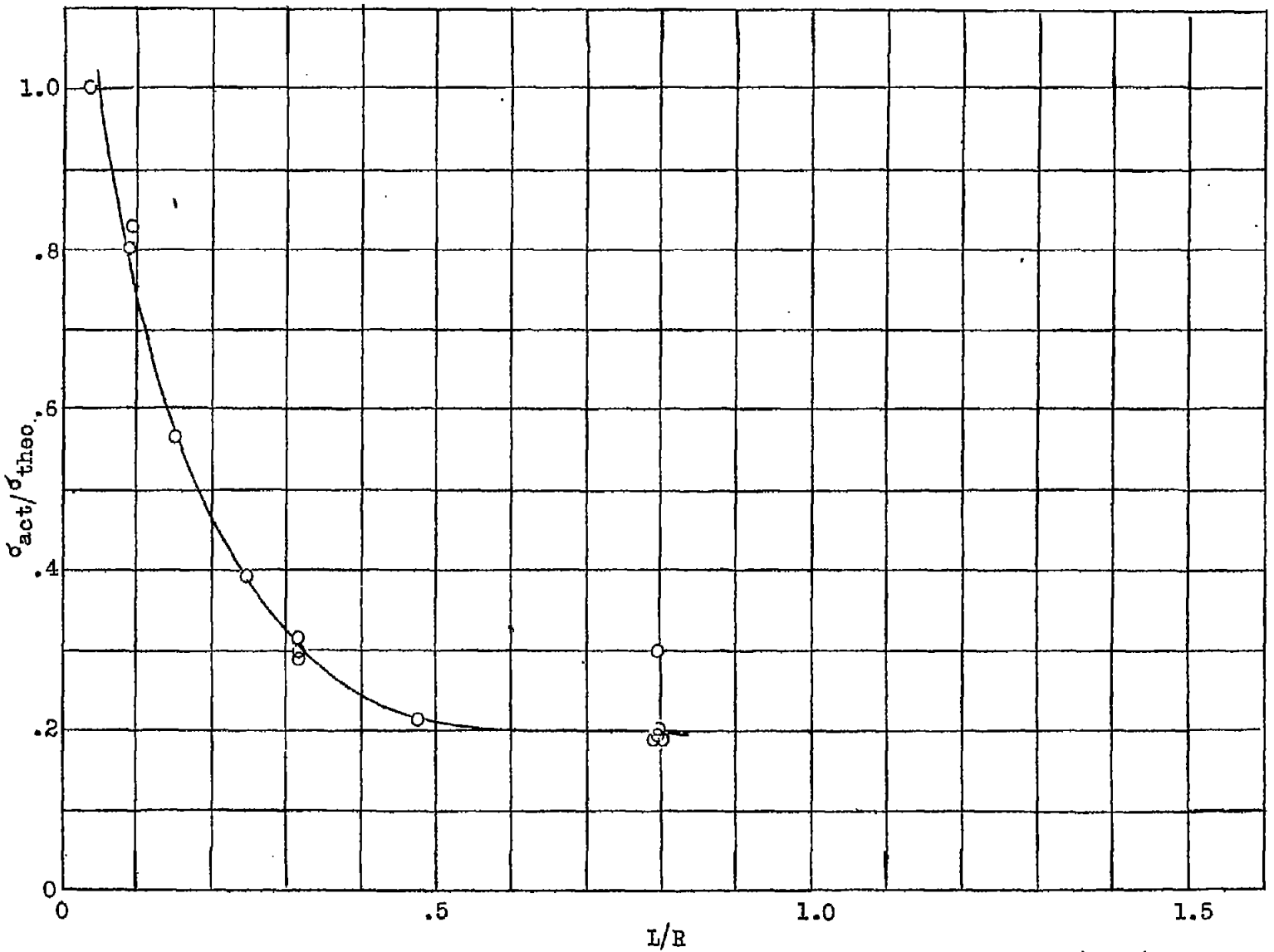

Figure 65.- Compression of circular cylinders length effect, $\sigma_{act}/\sigma_{theo}$ against L/R, R/t = 1550 to 1600, radius = 6.375", material steel.

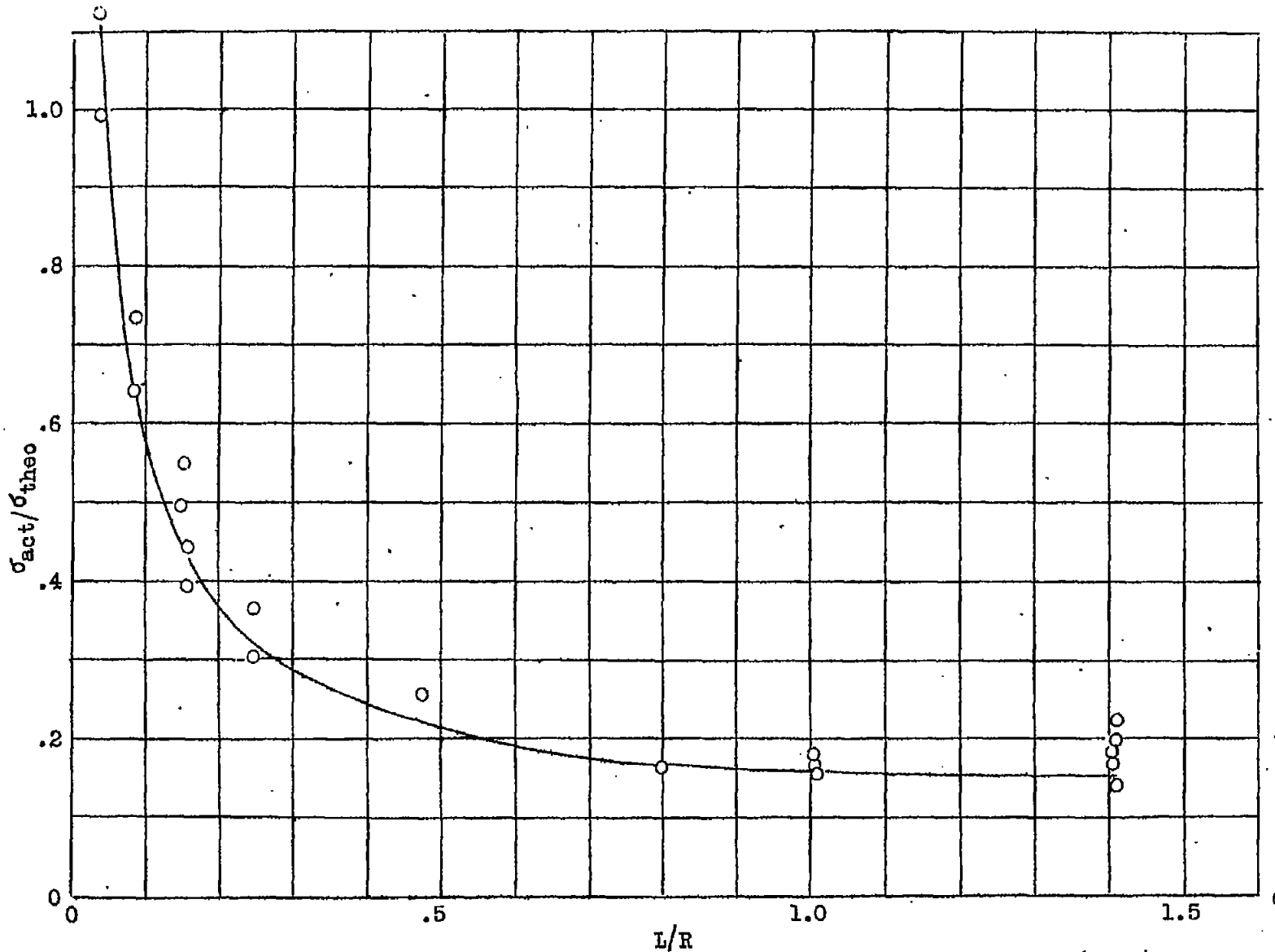

Figure 66.- Compression of circular cylinders length effect, $\sigma_{act}/\sigma_{theo}$ against L/R, R/t = 1850 to 2000, radius = 6.375", material steel.

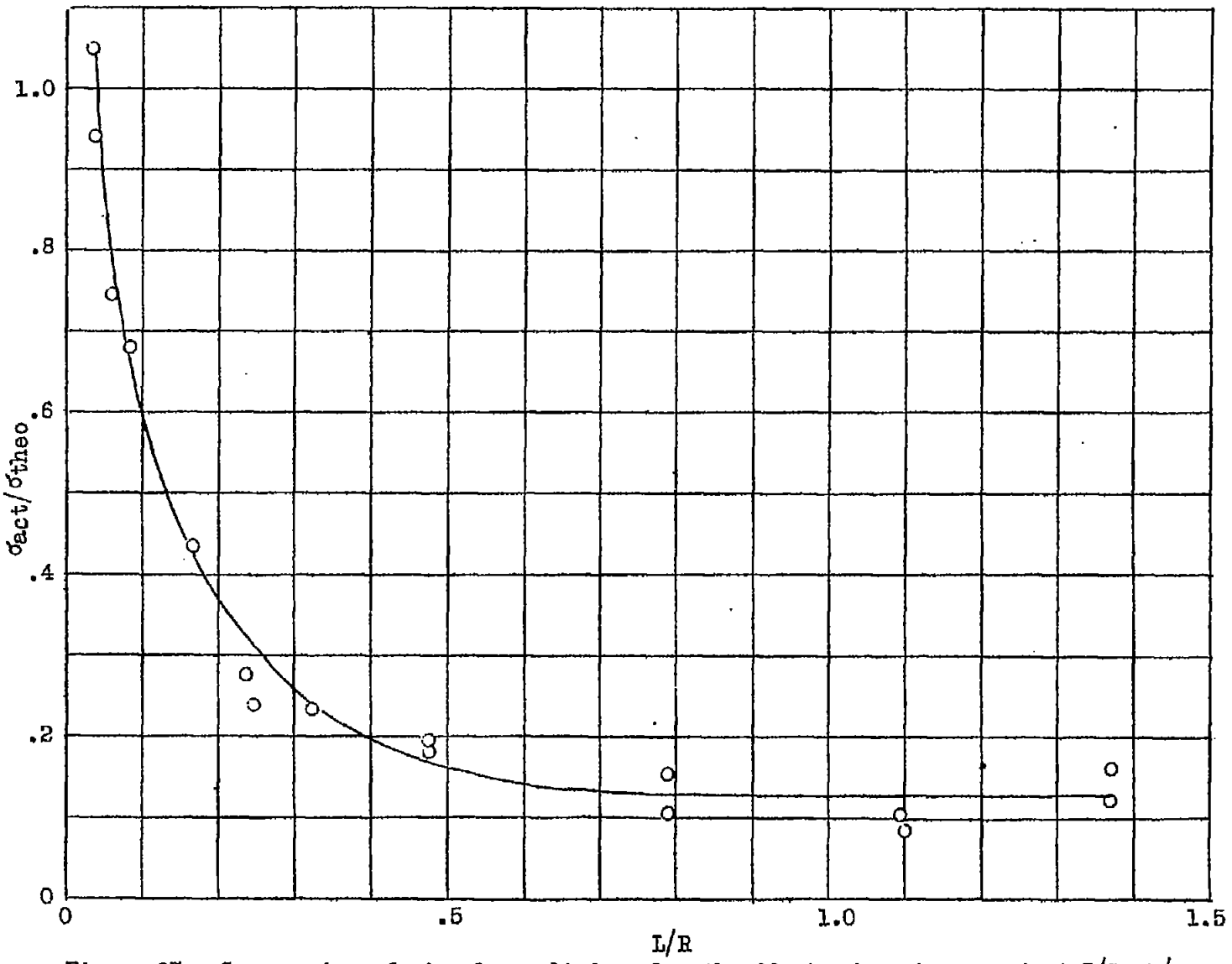

Figure 67.- Compression of circular cylinders length effect, $\sigma_{act}/\sigma_{theo}$ against L/R, R/t = 2600 to 3000, radius 6.375", material steel.

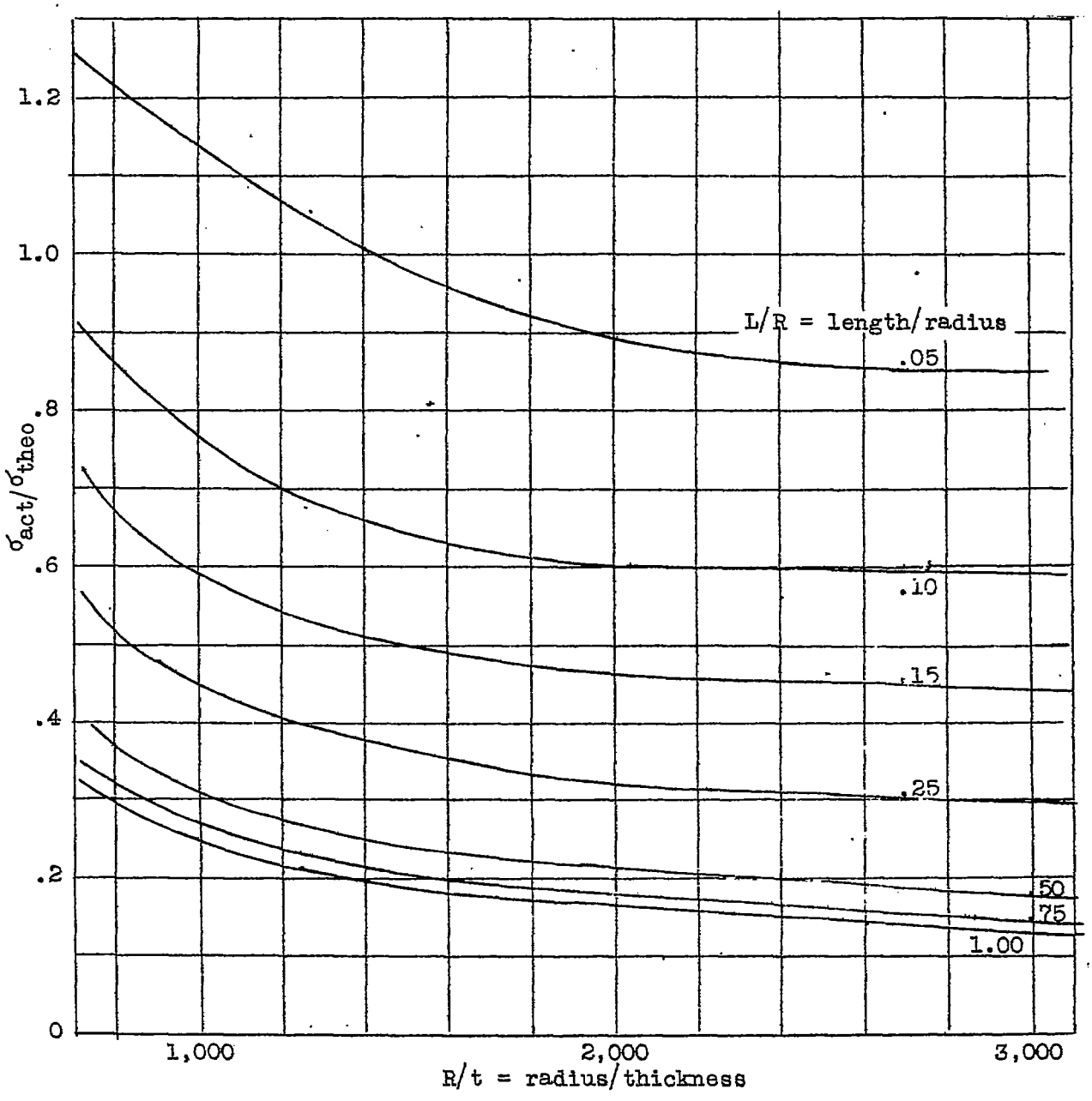

Figure 68.- Compression of circular cylinder length effect, $\sigma_{act}/\sigma_{theo}$ against R/t for constant L/R, radius 6.375", material steel.

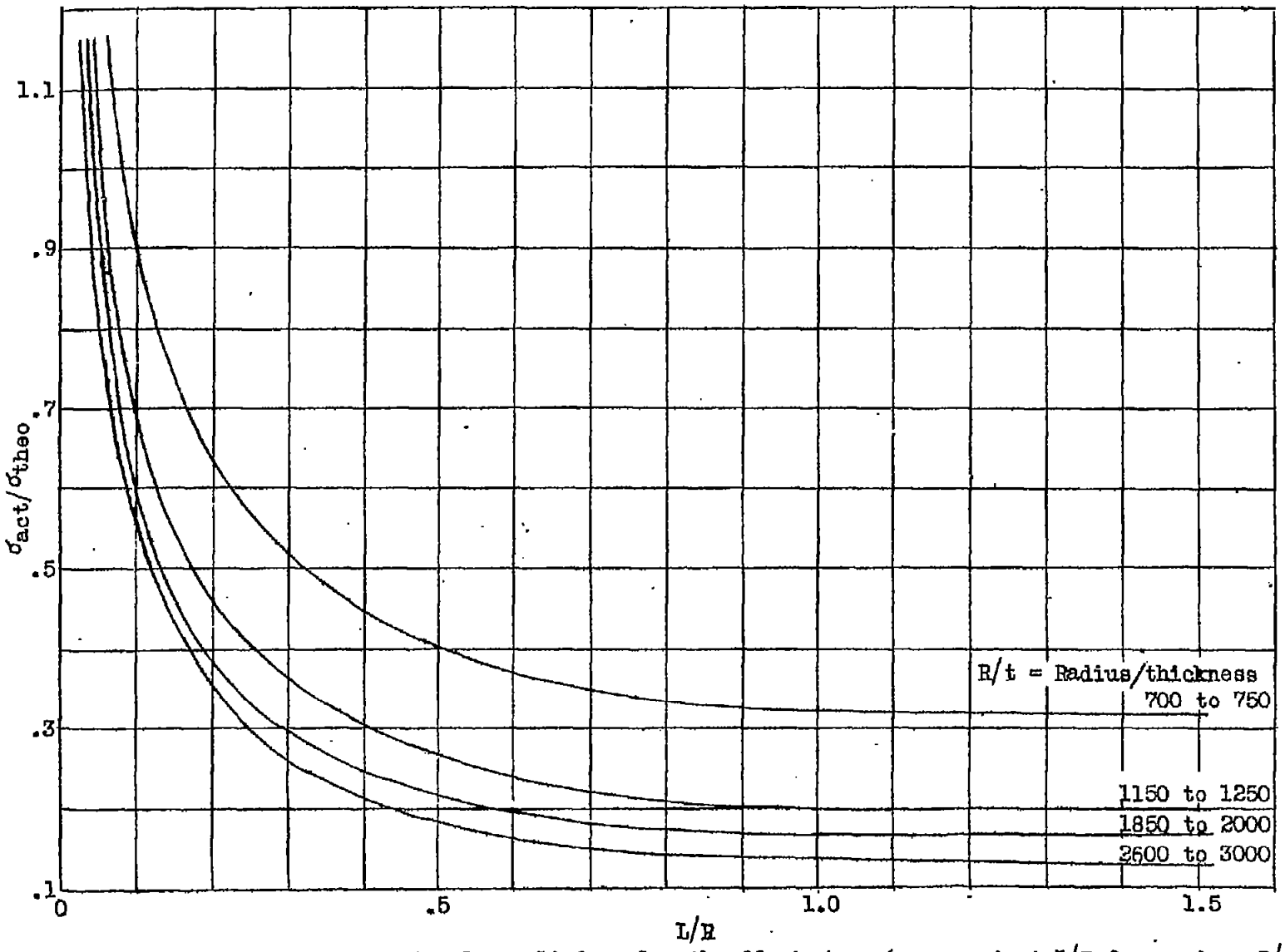

Figure 69.- Compression of circular cylinders length effect, $\sigma_{act}/\sigma_{theo}$ against L/R for various R/t, radius 6.375", material steel.

TITLE: Some Investigations of the General Instability of Stiffened Metal Cylinders - II - Preliminary Tests of Wire-Braced Specimens and Theoretical Studies

AUTHOR(S): (Not known)

ORIGINATING AGENCY: National Advisory Committee for Aeronautics, Washington, D. C.

PUBLISHED BY: (Same)

ATI- 8501

REVISION (None)

ORIG. AGENCY NO. TN-906

PUBLISHING AGENCY NO.

DATE	DOC. CLASS.	COUNTRY	LANGUAGE	PAGES	ILLUSTRATIONS
July '43	Unclass.	U.S.	Eng.	72	photos, tables, graphs, drwgs

ABSTRACT:

In the first part of the report, experimental investigations were made on the failure of stiffened metal cylinders, principles underlying the failure of thin shells, and the compressive failing stress of unstiffened circular cylinders. The second part of the report pertains to a discussion on the use of a wire network to provide shear stiffness. Results of the experiments showed that specimens of the type tested do not fail suddenly but tend to approach a maximum allowable bending moment in an asymptotic manner.

P 20/11

DISTRIBUTION: Request copies of this report only from Originating Agency

HEADINGS: Cylinders - Stiffened - Instability (28610); Cylinders - Stress analysis (28505)

240 400

AD-B805 288

INDEX

Wright-Patterson Air Force Base
Dayton, Ohio

Classification cancelled
or changed to _____

AUTH:

By _____

Date APR 29 1949

Classification cancelled per authority
of List NACA dd. 28 Sept 1945
George R. Jordan, USCO, 29 Apr 1949